University of Alberta

Radiolabelling and bio-evaluation of 2,4-difluoro-5-iodo-1-(2-deoxy-β-D-ribofuranosyl)benzene (5-IDFPdR)

by

Anke Stahlschmidt

A thesis submitted to the faculty of Graduate Studies and Research in partial fulfilment of the requirements for the degree of Master of Science

in

Pharmaceutical Sciences

Faculty of Pharmacy and Pharmaceutical Sciences

Edmonton, Alberta
Spring 2004

Library and
Archives Canada

Published Heritage
Branch

395 Wellington Street
Ottawa ON K1A 0N4
Canada

Bibliothèque et
Archives Canada

Direction du
Patrimoine de l'édition

395, rue Wellington
Ottawa ON K1A 0N4
Canada

Your file Votre référence
ISBN: 0-612-96550-3
Our file Notre référence
ISBN: 0-612-96550-3

The author has granted a non-exclusive license allowing the Library and Archives Canada to reproduce, loan, distribute or sell copies of this thesis in microform, paper or electronic formats.

The author retains ownership of the copyright in this thesis. Neither the thesis nor substantial extracts from it may be printed or otherwise reproduced without the author's permission.

L'auteur a accordé une licence non exclusive permettant à la Bibliothèque et Archives Canada de reproduire, prêter, distribuer ou vendre des copies de cette thèse sous la forme de microfiche/film, de reproduction sur papier ou sur format électronique.

L'auteur conserve la propriété du droit d'auteur qui protège cette thèse. Ni la thèse ni des extraits substantiels de celle-ci ne doivent être imprimés ou aturement reproduits sans son autorisation.

In compliance with the Canadian Privacy Act some supporting forms may have been removed from this thesis.

While these forms may be included in the document page count, their removal does not represent any loss of content from the thesis.

Conformément à la loi canadienne sur la protection de la vie privée, quelques formulaires secondaires ont été enlevés de cette thèse.

Bien que ces formulaires aient inclus dans la pagination, il n'y aura aucun contenu manquant.

Canada

Abstract:

The objectives were to synthesise and radiolabel the thymidine mimic 1-(2,4-difluoro-5-iodophenyl)-2'-deoxyribose (5IDFPdR), and to determine the pharmacokinetics (PK) and tissue biodistribution of 5-IDFPdR and its kinase bypass prodrug, (S_P)-*cyclo*(3-methylsaligenyl)-5'-O-[1'-(2,4-difluoro-5-iodophenyl)-2'-deoxy-β-D-ribofuranosyl]phosphate (*cycloSal*-5IDFPdR).

The radiolabelling was optimised for temperature, reaction time, concentration of precursor and concentration of NaOH, to obtain 85 % yields (0.14 mg precursor, 140 °C, 60 minutes).

The PK of ^{125}I-IDFPdR in Sprague-Dawley rats showed an elimination half-life of 0.51 h, a clearance of 0.75 L/kg/h and a distribution volume of 0.96 L/kg. *CycloSal*-5IDFPdR was cleared more slowly from blood. In mice, ^{125}I-IDFPdR accumulated in bile and bladder, whereas *cycloSal*-5IDFPdR accumulated in blood, lung, bile and bladder. The maximum tumour : blood ratio for ^{125}I-IDFPdR was 2.6, while that for *cycloSal*-5IDFPdR never exceeded 1.

The PK and biodistribution data for ^{125}I-IDFPdR suggest that a second metabolic pathway involving the liver and bile is operative. Neither 5-IDFPdR or *cycloSal*-5IDFPdR appear to be useful for applications in diagnostic oncology.

Acknowledgement:

This thesis research was performed during the period September 1998 to January 2004 in the Faculty of Pharmacy and Pharmaceutical Sciences at the University of Alberta and in the Department of Radiopharmacy at the University Hospital of Tübingen under the supervision of

Prof. Dr. L. I. Wiebe, Prof. Dr. E. E. Knaus and Prof. Dr. H.-J. Machulla.

My thanks are going to Prof. Dr. L. I. Wiebe, Prof. Dr. E. E. Knaus and Prof. Dr. H.-J. Machulla for their supervision and their continuous advice during my work.

For the support of my practical work I want to thank my colleagues in the laboratory of the Faculty of Pharmacy and Pharmaceutical Sciences at the University of Alberta, especially Dr. P. Khalili, Mrs. A. Zhou, Dr. Z.-X. Wang, Dr. W. Sun, Dr. P. Kumar and Dr. S. Moharram. Furthermore I would like to thank Dr. D. Abrams from the Cross Cancer Institute and Dr. T. Riauka from the Department of Nuclear Medicine. Also, I would like to thank my colleagues in the Department of Radiopharmacy at the University Hospital Tübingen, especially Mr. H. J. Rahm, Dr. G. Reischl and Dr. C. Solbach.

Table of contents

1. Introduction 1
  1.1 Emission tomography 2
    1.1.1 Single photon emission computer tomography (SPECT) 2
    1.1.2 Positron emission tomography (PET) 3
    1.1.3 Chemical and kinetic aspects of radiolabelling 5
  1.2 Radioiodination of organic molecules 6
    1.2.1 Direct electrophilic iodination 7
    1.2.2 Electrophilic demetallation 9
    1.2.3 Nucleophilic substitution 9
  1.3 Tracer for measuring tumour proliferation 10
    1.3.1 Nucleotides 10
      1.3.1.1 De novo synthesis 10
      1.3.1.2 Salvage pathway 10
      1.3.1.3 Replication of DNA 11
  1.4 Radiolabelled tracers for proliferation 11
2. Literature review of iodine radioisotope production 13
  2.1 Introduction 13
  2.2 Methods and materials 16
  2.3 Discussion: 18
  2.4 Isotopes used for life sciences 20
3. Rationale, Hypothesis and Objectives: 29
  3.1 Rationale 29
  3.2 Hypotheses 30
  3.3 Objectives 30
4. Production of iodine-124 31
  4.1 Materials and methods 31
  4.2 Results and Discussion 32
5. Production of the precursor 2,4-difluoro-5-iodo-1-(2-deoxy-β-D-ribofuranosyl)benzene (5-IDFPdR) for labelling with [^{124}I]iodide 34
  5.1 Synthesis of 2,4-difluoro-5-iodo-1-(2-deoxy-β-D-ribofuranosyl)benzene (5-IDFPdR) 34

5.1.1 Production of 2-deoxy-3,5-di-*O*-(*p*-chlorobenzoyl)-α-D-ribofuranosyl chloride (1) 36
5.1.2 Synthesis of 2,4-difluoro-5-iodobenzene (2) 36
5.1.3 Production of 2,4-difluoro-1-(2-deoxy-3,5-di-*O*-(*p*-chlorobenzoyl)-α-D-ribofuranosyl)benzene and 2,4-difluoro-1-((2-deoxy-3,5-di-*O*-(*p*-chlorobenzoyl)-ß-D-ribofuranosyl)benzene (3,4) 37
5.1.4 Epimerisation of 2,4-difluoro-1-(2-deoxy-3,5-di-*O*-(*p*-chlorobenzoyl)-α-D-ribofuranosyl)benzene 38
5.1.5 Production of 2,4-difluoro-5-iodo-1-(2-deoxy-3,5-di-*O*-(*p*-chlorobenzoyl)-ß-D-ribofuranosyl)benzene (5) 38
5.1.6 Production of 2,4-difluoro-5-iodo-1-(2-deoxy-β-D-ribofuranosyl)benzene (5-IDFPdR) (6) 39
5.1.7 Separation of 2,4-difluoro-1-(2-deoxy-3,5-di-*O*-(*p*-chlorobenzoyl)-α-D-ribofuranosyl)benzene and 2,4-difluoro-1-(2-deoxy-3,45-di-*O*-(*p*-chlorobenzoyl)-ß-D-ribofuranosyl)benzene via HPLC 40
6. Synthesis of 5-[^{124}I]iodo-2,4-difluoro-1-(2-deoxy-ß-D-ribofuranosyl)benzene 40
6.1 Materials and methods 40
6.1.1 Dependency of the reaction upon temperature 41
6.1.2 Dependency of the reaction upon the concentration of precursor 42
6.1.3 Dependency of the reaction upon the amount of sodium hydroxide 42
6.1.4 Time dependency 43
6.2. Results and discussion of the acquired reaction parameter data: 43
6.2.1 Temperature dependency 43
6.2.2 Dependency of the reaction on the amount of precursor 44
6.2.3 Dependency of the reaction upon amount of NaOH 45
6.2.4 Time dependency 46
7. Animal Experiments 51
7.1 Materials and methods 51
7.1.1 Tracer production for in vivo pharmacokinetic studies 51
7.1.2 Application of tracer for in vivo pharmacokinetic studies. 51
7.2 Results and Discussion 53
8. Biodistribution 58
8.1 Materials and methods 58

8.1.1 Tracer production for in vivo pharmacokinetic studies........58
8.1.2 Application of tracer for in vivo pharmacokinetic studies. 58
8.2 Results and discussion........58
9. Gamma camera images of 5-IDFPdR in vivo........66
9.1 Materials and methods........66
9.1.1 Tracer production for imaging studies with 5-[^{123}I]IDFPdR........66
9.1.2 Application of the tracer for imaging studies with 5-[^{123}I]IDFdR........67
9.2 Results and discussion........67
10. General discussion and conclusions........72
References........76
Appendix A: Quality and vendors of chemicals used in the studies described. 87
Appendix B: Tables........88
Appendix C: Detailed production parameters for producing iodine isotopes 104

List of tables

Table 1: Positron emitting isotopes of the elements carbon, oxygen and nitrogen, which are the most common elements in physiological effective substrates. 2

Table 2: All isotopes of iodine characterised on the chart of nuclides from Straßbourg 1992. [3] 15

Table 3: Most common nuclear reactions for production of [^{124}I]iodine. 25

Table 4: Pharmacokinetic parameters for 5-[^{125}I]IDFPdR following i.v. administration to rats, the data are for n = 3, ± S.D. 57

Table 5: Pharmacokinetic properties for unlabelled and labelled 5-IDFPdR in rats after i.v. bolus injection and for the unlabelled compound after oral dosing. The data are for n = 3, ± S.D. at least for the labelled compound. 57

Table 6: ^{124}I radioactivity recovered in 4 mM NaOH from a 300 mg target after 10 minutes irradiation with different beam currents 88

Table 7: Production yield of ^{124}I with a 300 mg target after 10 minutes irradiation with different beam currents 88

Table 8: Temperature dependency of the reaction of [^{123}I]I$^-$ with 5-IDFPdR with a reaction time of 2 hours 88

Table 9: Dependency of the reaction of [^{123}I]I$^-$ with 5-IDFPdR on the amount of 5-IDFPdR, reaction time was 2 hours, reaction temperature 120°C 89

Table 10: Dependency of the reaction of [^{123}I]I$^-$ with 5-IDFPdR on the mass of sodium hydroxide, reaction time was 2 hours, reaction temperature was 120°C 90

Table 11: Time dependency of the reaction of [^{123}I]I$^-$ with 5-IDFPdR at a temperature of 85°C 90

Table 12: Time dependency of the reaction of [^{123}I]I$^-$ with 5-IDFPdR at a temperature of 120°C 91

Table 13: Time dependency of the reaction of [^{123}I]I$^-$ with 5-IDFPdR at a temperature of 140°C 91

Table 14: Values for calculating the rate constant for the synthesis of 5-[^{123}I]IDFPdR at a temperature of 85°C 92

Table 15: Values for calculating the rate constant for the synthesis of 5-[^{123}I]IDFPdR at a temperature of 120°C 92

Table 16: Values for calculating the rate constant for the synthesis of 5-[^{123}I]IDFPdR at a temperature of 140°C 92

Table 17: Values for calculating the activation energy for the synthesis of 5-[^{123}I]IDFPdR 93

Table 18: Total radioactivity measured in 1 mL of plasma and its percentage applied to the injected dose of 5-IDFPdR into each rat 93

Table 19: Total radioactivity measured in 1 mL of plasma and its percentage applied to the injected dose of the *cycloSal* derivative into each rat 94

Table 20: Radioactivity [cpm] of 5-IDFPdR in 1 mL plasma and its percentile contribution to each fraction analysed on HPLC following injection of 5-[^{125}I]IDFPdR into rats via catheter. 95

Table 21: Radioactivity [cpm] of unchanged *cycloSal* compound in 1 mL plasma and its percentile contribution to each fraction analysed on HPLC, following injection of *cyclo*Sal-5-[^{125}I]IDFPdR into rats via catheter. 96

Table 22: Radioactivity [cpm] of metabolites from 5-IDFPdR in 1 mL plasma and their percentile contribution to each fraction analysed on HPLC following injection of 5-[^{125}I]IDFPdR into rats via catheter. 97

Table 23: Radioactivity [cpm] of metabolites from *cycloSal* derivative in 1 mL plasma and their percentile contribution to each fraction analysed on HPLC after injection of *cyclo*Sal-5-[^{125}I]IDFPdR into rats via catheter. 98

Table 24: In vivo biodistribution of 5-[^{125}I]IDFdR in mice following i. v. injection via tail vein, expressed as % I.D./g organ. 99

Table 25: In vivo biodistribution of 5-[^{125}I]IDFdR in mice following i. v. injection into tail vein, expressed as % I.D./total organ. 99

Table 26: In vivo biodistribution of 5-[^{125}I]IDFdR in mice following i. v. injection into tail vein, expressed as organ/blood ratio. 100

Table 27: In vivo biodistribution of *cyclo*Sal-5-[^{125}I]IDFdR in mice following i. v. injection into tail vein, expressed as % I.D./g organ. 100

Table 28: In vivo biodistribution of *cyclo*Sal-5-[^{125}I]IDFdR in mice following i. v. injection into tail vein, expressed as % I.D./total organ. 101

Table 29: In vivo biodistribution of *cyclo*Sal-5-[^{125}I]IDFdR in mice following i. v. injection into tail vein, expressed as organ/blood ratio. 101

Table 30: Evaluation of two to three ROIs of the static gamma camera pictures acquired using two male Sprague Dawley rats dosed with 5-[^{123}I]DFPdR after 70 minutes for rat #1 and after 60 minutes for rat #2 102

Table 31: Evaluation of two to three ROIs of the static gamma camera pictures taken in two male Sprague Dawley rats dosed with 5-[^{123}I]DFPdR after 100 minutes for rat #1 and after 90 minutes for rat #2 102

Table 32: Evaluation of two to three ROIs of the static gamma camera pictures taken in two male Sprague Dawley rats dosed with 5-[^{123}I]DFPdR after 130 minutes for rat #1 and after 120 minutes for rat #2 103

Table 33: Independent production cross section in (mb) for the reaction of ^{127}I with pions having the energy of 60-350 MeV to result in ^{117}I: [97] 113

Table 34: Independent production cross section in (mb) for the reaction of ^{127}I with pions having the energy of 60-350 MeV to result in ^{118}I: [97] 115

Table 35: Independent production cross section in (mb) for the reaction of ^{127}I with pions having an energy of 60-350 MeV to result in ^{119}I: [97] 117

Table36: Independent production cross section in (mb) for the reaction of ^{127}I with pions having an energy of 60-350 MeV to result in ^{120}I: [97] 119

Table 37: Independent production cross section in (mb) for the reaction of ^{127}I with pions having an energy of 60-350 MeV to result in ^{121}I: [97] 121

Table 38: Independent production cross section in (mb) for the reaction of ^{127}I with pions having an energy of 60-350 MeV to result in ^{122}I: [97] 122

Table 39: Independent production cross section in (mb) for the reaction of ^{127}I with pions having an energy of 60-350 MeV to result in ^{123}I: [97] 124

Table 40: Independent production cross section in (mb) for the reaction of ^{127}I with pions having an energy of 60-350 MeV to result in ^{124}I: [97] 126

Table 41: Independent production cross section in (mb) for the reaction of ^{127}I with pions having an energy of 60-350 MeV to result in ^{125}I: [97] 127

Table 42: Independent production cross section in (mb) for the reaction of ^{127}I with pions having an energy of 60-350 MeV to result in ^{126}I: [97] 129

List of figures

Fig. 1: Schematic data acquisition performed by a PET scanner.[5] 4

Fig. 2: Excitation functions for simultaneous reactions of protons with ^{63}Cu [36] 16

Fig. 3: Excitation function of the ^{122}Te(p,3n)^{120m,g}I process [39] 21

Fig. 4: Excitation functions of ^{120}Te(p,xn)^{120m,120g,119}I reactions. Experimental data (symbols) are from Hohn et al. and theoretical results (curves) from Sudar [40] 22

Fig. 5: Excitation curve for the ^{120}Te(d,xn)reactions leading to the formation of ^{121}I, ^{120m}I and ^{120g}I. The solid lines are eyeguides. There is no suitable energy range for the production of ^{120g}I. The shaded area simply describes an energy range where the yield of ^{120g}I could be maximum, but with large amount of the ^{121}I-impurity [38] 22

Fig. 6: Exitation functions for the ^{124}Te(p,n) and ^{124}Te(p,2n) reaction. [53] 26

Fig. 7. Structures of thymidine and 5-IDFPdR 29

Fig. 8. Structures of the two diastereomeres of *cycloSal*-5-IDFPdR 30

Fig. 9. Beam-current dependency of the [^{124}I]iodide production [kBq] on the PETtrace from General Electrics cyclotron at the PET-centre in Tübingen. The target was plated with 300 mg of a mixture of 94 % ^{124}TeO$_2$ and 6 % Al$_2$O$_3$ and irradiated for 10 minutes. The ^{124}I was recovered by dry distillation at 690 °C for 10 min. Each point represents 3 samples, ± S.D., linear regression was applied to fit the solid line. The slope is 502.4 and the correlation coefficient (r^2) is 0.99. 33

Fig. 10. Current dependency of the [^{124}I]iodide production [kBq/µAh] on the PETtrace from General Electrics cyclotron at the PET-centre in Tübingen. The target was plated with 300 mg of a mixture of 94 % ^{124}TeO$_2$ and 6 % Al$_2$O$_3$ and irradiated for 10 minutes. The ^{124}I was recovered by dry distillation at 690 °C for 10 min. Each point represents 3 samples, ± S.D, linear regression was applied to fit the solid line. The slope is 53.36 and the correlation coefficient (r^2) is 0.70. 33

Fig. 11. reaction scheme for producing 5-IDFPdR [67] 35

Fig. 12. Schematic depiction of the isotope exchange reaction in the system 5-IDFPdR/^{124}I 40

Fig. 13. Temperature dependency of the reaction of [^{123}I]I$^-$ with 5-IDFPdR, reaction time was 2 hours. The data are for n = 3; ± S.D. A Boltzmann fit from Origin 6.1 was applied to fit the solid line. 44

Fig. 14. Dependency of the reaction of [^{123}I]I$^-$ with 5-IDFPdR upon the concentration of 5-IDFPdR when the reaction time was 2 hours, and the reaction temperature was 120 °C. The data are for n = 3; ± S.D. A Boltzmann fit from Origin 6.1 was applied to fit the solid line. 45

Fig. 15. Dependency of the reaction of [^{123}I]I$^-$ with 5-IDFPdR upon the weight of NaOH when the reaction time is 2 hours, and the reaction temperature was 120 °C. The data are for n = 2; ± S.D. A Boltzmann fit from Origin 6.1 was applied to fit the solid line. 46

Fig. 16. Dependency of the reaction of [^{123}I]I$^-$ with 5-IDFPdR with respect to time at three different reaction temperatures (85 °C, 120 °C and 140 °C). The data are for n = 2; ± S.D. A Boltzmann fit from Origin 6.1 was applied to fit the solid lines. 46

Fig. 17. Linear functions for determination of the rate constants of the 5-[^{123}I]IDFPdR synthesis for three temperatures (⊗: 85 °C, T: 120 °C, ×: 140 °C). Linear regression was applied to fit the curves. 50

Fig. 18. Arrhenius plot for the 5-[^{123}I]IDFPdR synthesis. Linear regression was used to fit the curve. The slope is -11743.39. 51

Fig. 19. Plasma clearance of 5-[^{125}I]IDFPdR and *cycloSal*-5-IDFPdR as a function of time after i.v. bolus administration (• 5-[^{125}I]IDFPdR ■ *cycloSal*-5-IDFPdR). The data are for n = 3, ± S.D.. 54

Fig. 20. 5-[^{125}I]IDFPdR and its metabolites as a percent (%) of the total radioactivity in plasma analysed by HPLC. Rats received i.v. injections of 5-[^{125}I]IDFPdR via catheter. The data are for n = 3, ± S.D. (•: Metabolites of 5-[^{125}I]IDFPdR, ■: 5-[^{125}I]IDFPdR.) 55

Fig. 21. Radioactivity of *cycloSal*-5-IDFPdR as a percent (%) of the total radioactivity in plasma fractions analysed by HPLC. Rats received i.v. injections of *cycloSal*-5-[^{125}I]IDFPdR via catheter. The data are for n = 3, ± S.D. 56

Fig. 22. Biodistribution of 5-[^{125}I]IDFPdR in mice after i.v. bolus into tail vein at different time points. The data are for n = 3, ± S.D 59

Fig. 23. Biodistribution of *cycloSal*-5-IDFPdR in mice after i. v. bolus into tail vein at selected time points. The data are for n = 3 60

Fig. 24. Biodistribution of 5-[^{125}I]IDFPdR, and *cycloSal*-5-[^{125}I]IDFPdR, in the blood of mice after i.v. bolus into tail vein at preselected time intervals (■ 5-[^{125}I]IDFPdR, • *cycloSal*-5-IDFPdR). The data are for n = 3, ± S.D. 61

Fig. 25. Radioactivity, at preselected time points, in the thyroid of mice after i.v. bolus injection into tail vein of 5-[^{125}I]IDFPdR or *cycloSal*-5-[^{125}I]IDFPdR (■ 5-[^{125}I]IDFPdR, • *cycloSal*-5-IDFPdR. The data are for n = 3, ± S.D.. 62

Fig. 26. Radioactivity of 5-[^{125}I]IDFPdR, and *cycloSal*-5-[^{125}I]IDFPdR in the kidney of mice after i.v. bolus into tail vein at preselected time points (■ 5-[^{125}I]IDFPdR, • *cycloSal*-5-IDFPdR). The data are for n = 3, ± S.D.. 63

Fig. 27. Biodistribution of radioactivity, after i.v. bolus injection into tail vein of 5-[^{125}I]IDFPdR or *cycloSal*-5-[^{125}I]IDFPdR, in the lung of mice at preselected time points (■ 5-[^{125}I]IDFPdR, • *cycloSal*-5-IDFPdR). The data are for n = 3, ± S.D.. 64

Fig. 28. Biodistribution of 5-[^{125}I]IDFPdR and *cycloSal*-5-[^{125}I]IDFPdR, in the liver of mice after i.v. bolus into tail vein at preselected time points (■ 5-[^{125}I]IDFPdR, • *cycloSal*-5-IDFPdR). The data are for n = 3, ± S.D.. 65

Fig. 29. Biodistribution of 5-[^{125}I]IDFPdR and *cycloSal*-5-[^{125}I]IDFPdR, in the bile of mice after i.v. bolus into tail vein at preselected time points (■ 5-[^{125}I]IDFPdR, • *cycloSal*-5-IDFPdR). The data are for n = 3; ± S.D.. 65

Fig. 30. Biodistribution of 5-[^{125}I]IDFPdR and *cycloSal*-5-[^{125}I]IDFPdR in the tumour of mice after i.v. bolus into tail vein at preselected time points (■ 5-[^{125}I]IDFPdR, • *cycloSal*-5-IDFPdR). The data are for n = 3, ± S.D.. 66

Fig. 31. Dynamic and first static scans of rat #1, dosed with 3.9 MBq 5-[^{123}I]IDFPdR via tail vein injection. Counting time for each dynamic frame was 30 seconds. 69

Fig. 32. Three static scans of rat #1, dosed with 3.9 MBq 5-[^{123}I]IDFPdR via tail vein injection. The images were taken 70, 100 and 130 minutes after dosing. 70

Fig. 33. Dynamic and first static scans of rat #2, dosed with 3.6 MBq 5-[^{123}I]IDFPdR via tail vein injection. Counting time for each dynamic frame was 30 seconds. 71

Fig. 34. Three static scans of rat #2, dosed with 3.9 MBq 5-[^{123}I]IDFPdR via tail vein injection. The images were taken 70, 100 and 130 minutes after dosing. 72

Fig. 35. Schematic diagram showing the principle of recoil decay tagging. Prompt γ rays are recorded by Eurogam. Recoiling evaporation residues pass through a velocity filter with crossed electric (E) and magnetic (B) fields (Daresbury Recoil Separator) and are there dispersed according to their mass-to-charge ratio (A/q) before being implanted into the double sided silicon strip detector (DSSD) at position (x,y) at time t_0 with energy E_0. Within the same pixel (x,y) subsequent charged-particle radioactivity (decay at time t1 with energy E1) can be correlated with the initial implantation. [76] 105

Fig. 36. Decay scheme of both isomers of ^{114}I. 109

List of abbreviations

5-IDFPdR	2,4-difluoro-5-iodo-1-(2-deoxy-β-D-ribofuranosyl)benzene
β^-	Beta particle
β^+	positron
δ	chemical shift
ε	electron capture
Φ	flux of particles
σ	cross section
μAh	micro ampere hour
app.	approximately
AUC_{inf} [ng.min/ml]	area under the curve from the time of dose administration to time infinity
$[B_0]$	starting concentration of the radionuclide
Bq	becquerel
brd	broad doublet
[C]	concentration of product
Cl [ml/min]	clearance
cpm	counts per minute
cycloSal-5-IDFPdR	(S_P)-*cyclo*(3-methylsaligenyl)-5'-O-[1'-(2,4-difluoro-5-iodophenyl)-2'-deoxy-β-D-ribofuranosyl]phosphate
d	Deuterons
ddd	doublets of doublets of doublets
do	Doublet
EC	electron capture
EOB	end of bombardment
f	Fission
fig.	Figure

gs	Ground state
^{1}H-NMR	proton nuclear magnetic resonance
HPLC	high performance liquid chromatography
I	Isomer
i.d.%	percent of the injected dose
I.T.	isomeric transformation
J	coupling constant
k'	rate constant
keV	kilo-electron volt
m	Multiplet
MBq	megabecquerel
MHz	mega hertz
mM	millimolar
n	neutron (s)
n_{th}	thermal neutrons
p	proton (s)
PET	positron emission tomography
pm	pico meter
RCY	Radiochemical yield
s	Singlet
S.D.	standard deviation
spec	Specific
SPECT	single photon emission computer tomography
t	Triplet
$t_{1/2}$ [h]	biological elimination half life
$t_{1/2a}$	physical decay half-life of an isotope
Vss [l/kg]	steady state volume of distribution
$X_{1...9}$	experiment 1-9
Y	Radiochemical yield

1. Introduction

Experimental cancer research started with the beginning of the 20th century but a generally applicable and accepted cancer model was not established before 1964 (Boutwell 1964). Although many detailed questions about cancer are clarified, cancer is still an unpredictable disease which is often diagnosed too late and thus leads to death.

Better therapy methods, and in particular, more accurate diagnostic tools play an important role in fighting cancer. The earlier a tumour is found the broader is the range of therapeutic approaches for treatment of the tumour. Nuclear medical diagnostic tools like single photon emission computer tomography (SPECT) and positron emission tomography (PET) play a significant role in early diagnosis.

SPECT and primarily PET make it possible to see biochemical processes in vivo. They are based on the tracer technique developed in 1923 by Hevesy.[1] Physiological substrates are labelled with suitable radionuclides which emit radiation that can be measured outside of a patient's body. In this way the distribution of the substrate can be determined externally after administration of the labelled substrate. Suitable radionuclides must have similar or the same physical-chemical capacity, as the stable isotopes. They replace in the tracer molecule so that the chemical and biochemical properties of the labelled substance are only minimally changed. The best radionuclides for labelling physiologically effective substrates are isotopes of the elements carbon, hydrogen, oxygen, nitrogen, phosphorus or sulphur, that is, the *isotopic* radionuclides. But this suitability is restricted; as another necessity for radionuclides used in diagnostic applications is that they have suitable decay characteristics. This means:

- their radiation must be able to penetrate the body barrier as only γ-quants are able to do,
- they should not emit α or β^- particles as those particles are adsorbed inside the body and increase only the radiation dose without any practical use for the external registration,
- their half-life should be short enough to reduce the radiation dose for the patient. If the radiation dose is low enough it will also allow repeating measurements if

necessary. On the other side the half-life should be long enough, so that the physiological distribution of the labelled substrate can take place.

Therefore only a few radioactive nuclides are suitable. The typical "organic" radionuclides used in medicine are listed in Table 1: [2,3]

Table 1: Positron emitting isotopes of the elements carbon, oxygen and nitrogen, which are the most common elements in physiological effective substrates.

nuclide	$t_{1/2}$	type of decay (%)	maximum energy$_{\beta+}$ (keV)	rel. frequency (%)	main γ line (keV)	frequency (%)
^{11}C	20.4 min	β^+ (99.8) EC (0.2)	961	100	511	199.6
^{13}N	9.97 min	β^+ (100)	1190	100	511	200
^{15}O	2.04 min	β^+ (100)	1730	100	511	200

Those isotopes lead to unchanged biomolecules. However, their short half-lives restrict their use considerably. The time interval for production, synthesis, isolation, purification and administration to the patient should not exceed 2-3 half-lives of the radionuclide, as the radioactivity otherwise is to much decreased. For the above mentioned isotopes this is a time period in the range of approximately 4-60 minutes. Another possibility for labelling physiological substrates is to substitute hydrogen atoms or hydroxy or methyl groups by radiohalogens such as ^{18}F, $^{75,77}Br$, $^{123,124}I$ because of their steric similarity. However, the polarity of the bonds and the liphophilicity of the molecule can be changed drastically. Therefore it is necessary to evaluate the biodistribution, transport capacity, metabolism, enzyme activity and receptor affinity of such a labelled substrate.

1.1 Emission tomography

1.1.1 Single photon emission computer tomography (SPECT)

Radionuclides with a main gamma ray energy between 100-300 keV are used for SPECT. The emitted radioactivity is measured with a rotating detector. Then images of tissue layers can be reconstructed from the measured radioactivity with suitable mathematical models. Depending on the radionuclide used, a spatial resolution of 0.8-2 cm can be reached. The different tissue layers in the body of a patient show different absorption of the emitted irradiation, as different tissues have different densities. This moderation of the radiation in the body of the patient is difficult to correct. Therefore, the precision of quantification is restricted. The most commonly used radionuclide for SPECT today is technetium-99m. Its half-life of 6.02 hours and its γ energy of 140 keV are optimal for the measurement with SPECT. As a generator nuclide it is available at low costs and without any technical expenditure. ^{99m}Tc is a metal, which makes its intoduction into biomolecules difficult. It can be linked to an organic substrate only as a complex with high coordination numbers, which changes the steric properties of the substrate itself and usually leads to a change in physiological behaviour. To avoid these difficulties, other alternative radionuclides have been tried. One of these alternatives is iodine-123. Its half-life of 13 hours is still short enough to keep the radiation dose for the patient low, and long enough for the physiological distribution to take place. Its main γ-ray has an energy of 159 keV which is well suited for SPECT. The atomic radius of an iodine atom is nearly equivalent to the molecule radius of a methyl group. Therefore it can be used as a steric analogue of a methyl group without introducing a major change in the structure of the molecule. The electronegativity of iodine is very similar to the electronegativity of carbon, so that introduction of iodine into an organic substrate will not change the polarity of the bonding much. All in all the labelling of organic molecules with a radioactive iodine isotope will induce only minimal change in the physiological behaviour of this molecule.

1.1.2 Positron emission tomography (PET)

In PET it is possible to establish a linear correlation between the count density measured with PET and the concentration of the labelled substrate applied to the patient. The possibility of quantification is achieved by calibration measurements with a known source.

The detector of a PET camera is built using many small scintillation crystals in a circular arrangement. The crystals are connected in coincidence, which means that only if two opposite crystals detect a γ ray at the same time will this detection event be counted. By measuring two or more pairs of coincident γ quanta, the volume of decay can be localised. To achieve this, PET is based on the special decay of positron emitting (β^+) nuclides. The β^+ particle recombines, after loss of its kinetic energy, with an electron e^- particle. They form a short lived antiparticle particle pair (positronium), which destroys itself. [4] During the annihilation process two photons are formed which contain the rest mass of electron and positron in form of energy, 511 keV each. The photons are emitted at an angle of almost 180°. The deviation of the γ-photons from 180° is a result of the residual momentum of the β^+ particle and the e^- in the positronium. One detector in the ring of a PET camera is combined with a group of opposite detectors. That means the decay of positrons leads to the detection of parallel activity projections as illustrated in Fig. 1.[5]

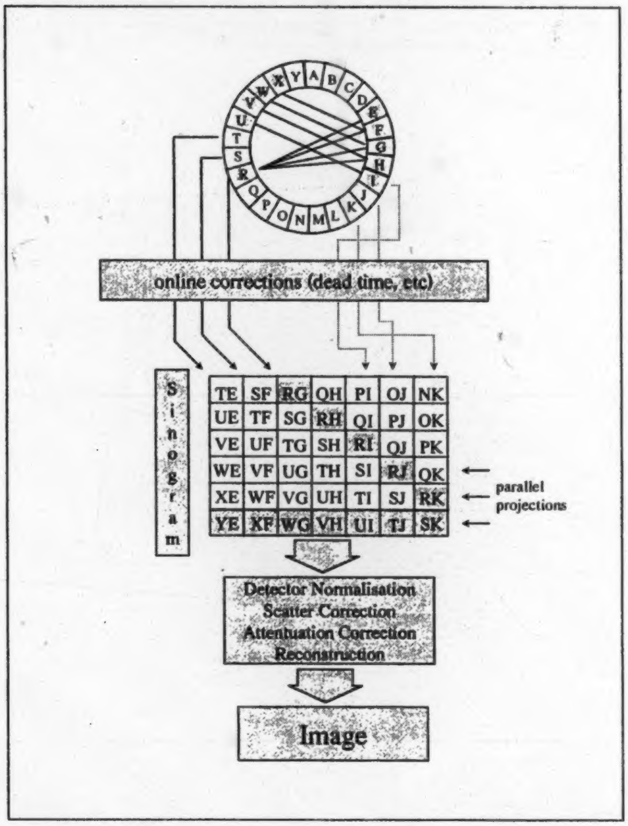
A
B
C
D
E
F
G
H
I
J
K
L
M
N
O
P
Q
R
S
T
U
V
W
X
Y
online corrections (dead time, etc)
Sinogram
TE SF RG QH PI OJ NK
UE TF SG RH QI PJ OK
VE UF TG SH RI QJ PK
WE VF UG TH SI RJ QK
XE WF VG UH TI SJ RK
YE XF WG VH UI TJ SK
parallel projections
Detector Normalisation
Scatter Correction
Attenuation Correction
Reconstruction
Image

Fig. 1: Schematic data acquisition performed by a PET scanner.[5]

As there are usually more than one circle of detectors in a PET camera the crystals of each circle are interconnected so that it is possible to measure activity projections in different spatial planes. The measured data are corrected online for random coincidences, deadtime, differences between the detectors, scatter and attenuation effects. From these projections the activity distribution can be reconstructed by mathematical models, for example the filtered back projection. The spatial concentration of the physiologically active compound can be quantified as the sum of the absorption probability for each photon pair. The resolution of an efficient tomograph can reach (4 x 6) mm. [6] Radionuclides used for PET are cyclotron produced neutron deficient nuclides. The most important nuclides are carbon-11, fluorine-18, nitrogen-13 and oxygen-15. Recently a different group of nuclides are finding an increasing interest in PET. These isotopes are iodine-124 and yttrium-86, as they can be used for therapy control by iodine-131 labelled therapy substrates like MIBG or iodide itself, or [^{90}Y]-labelled antibodies.

1.1.3 Chemical and kinetic aspects of radiolabelling

For the reaction between a radionuclide and an appropriate substrate the specific activity is a critical aspect. A synthesis can be classified as either no-carrier added, carrier-free or carrier added. Carrier in a labelling synthesis is a stable isotope of the radionuclide used for the labelling. A carrier will decrease the specific radiochemical yield of a synthesis. The specific activity is defined as the activity per mass substance:

$$A_{spec} = \frac{A}{mass}$$

A_{spec} = specific activity **formula 1.1.3-1**
A = Amount of radioactivity [Bq]
m = mass

In practice, every labelling reaction is a no-carrier-added reaction because of the universal occurrence of all natural elements. A no-carrier-added synthesis is performed without addition of isotopes of the radionuclide used for labelling. The isotopic impurity of the synthesis is based on isotope impurities in the chemicals used for the synthesis or the natural occurrence of those isotopes in the surrounding sphere like [^{12}C]carbon from CO_2 as the natural isotope impurity for [^{11}C]carbon labelling reactions. A carrier-free reaction is only possible by labelling with radionuclides, which are completely artificial like technetium or astatine. Carrier-added reactions are reactions where another isotope of the radionuclide used for labelling is added to the reaction to increase the yield or as a reactant of the reaction as in many iodination reactions (see chapter 1.2.1). Another type of reaction, which is carrier-added, is an isotope exchange reaction. Here the stable isotope of the radionuclide used for labelling is used as a leaving group during the reaction. The radioisotope exchanges the stable isotope. This type of reaction is frequently used as an iodination reaction. The covalent radius of iodine-127 is 133 pm. It is the biggest of the stable halogens. Therefore its 5p-electrons are low in energy. The electron affinity and the electronegativity for iodine are low in comparison to bromine, chlorine and fluorine so that the energy of covalent binding for iodine is very low, which makes iodine a good leaving group.

The conditions established for most organic synthesis reactions cannot be directly transferred to labelling reactions. The amount of radioisotope is usually low in comparison to all other reactants of the reaction. This can lead to surprising effects, e.g. the radionuclide can react primarily with an impurity of the chemicals used or the radionuclide can be absorbed on the surface of the reaction vessel. The exchange capacity of a glass surface is approximately 10^{-10} mol/cm^2, which can be higher than the concentration of the radionuclide. To avoid this absorption effect, special materials can be used for the reaction vessel like quartz glass, glass carbon, platinum or special synthetic materials. The kinetics of labelling reactions are usually given as pseudo first order. This is also based on the fact that the concentration of the radionuclide is low in comparison to all other reactants. The concentration of the other reactants can be viewed as constant during the labelling process. For a simple bimolecular reaction in the form of A + B gives C, the equation for the increase in product [C] with constant concentration of adduct [A] is given as:

$[C] = [B_0]*(1-e^{-k't})$ **formula: 1.1.3-2**

$[C]$ = concentration of product
$[B_0]$ = starting concentration of the radionuclide
k' = rate constant
t = reaction time

1.2 Radioiodination of organic molecules

As aromatic iodination is more stable in-vivo than aliphatic iodinations, the aromatic iodination reactions are the better examined ones. There are 3 major labelling routes for radioiodination of aromatic systems:

a) direct electrophilic substitution: a positively charged iodine species is reacted with an activated aromatic ring,

b) electrophilic demetallation: a metal organic compound reacts with iodonium,

c) nucleophilic substitution with copper catalysts: the iodide replaces an easily removable group on the aromatic ring. Usually copper ions are used as catalyst to polarize the bond between aromatic system and leaving group.

1.2.1 Direct electrophilic iodination

The direct electrophilic substitution of hydrogen on an organic molecule by radioactive iodine is only possible at strongly activated positions of the molecule. Easily available radioiodide is oxidised in situ to a positively charged or positively polarised iodine species. It is necessary to control the reaction parameters diligently as, for example, protic solvents with an pH ≤ 7 will lead to the formation of iodine hydride which reacts as a reductant. Therefore an oxidizing agent or a buffer system is used as an acceptor of iodine hydride. A number of labelling techniques were developed using different oxidising agents. Here the principal effect of only the most commonly used oxidising agents will be described.

a) Iodine monochloride [7-9]

The active species is formed by the reaction between commercially available iodine monochloride (ICl) and radioactive iodide. The iodine in ICl is much more reactive than molecular iodine, as the electronegativity of chlorine is higher than of iodine. Therefore, the iodine in ICl is more positively polarised than in I_2. The disadvantage is the addition of carrier iodine to the labelling reaction, which will reduce the specific activity of the labelled product.

b) Iodate [IO_3^-]

The main disadvantage here is also the carrier addition to the labelling process. On the other side, iodate is a very mild oxidising agent. Therefore it is suitable for the labelling of sensitive compounds. It was used for example in the labelling of 3-[*I]-α-methyltyrosine before a labelling procedure with Iodogen™, which leads to a no carrier added product was developed. [10-14]

c) Chloramine-T and derivatives

Chloramine-T (N-chloro-4-methyl benzene sulphonamide sodium salt) is one of the most frequently used oxidising agents. In water it hydrolyses and releases sodium hypochlorite which is an effective oxidising agent. However, its oxidising potential is so high it might lead to many by-products such as diiodination or chlorination of the precursor, or to denaturation of proteins. To avoid these reactions usually the reaction time, the concentration of reagent and the temperature are kept low. [7,15,16] The reaction is usually quenched by addition of sodium metabisulphite. [17] Chloramine-B (N-chloro-benzene sulphonamide sodium salt), dichloramine-T (N-dichloro-4-methyl benzene sulphonamide sodium salt) and Iodobeads™ belong to the same class of oxidising agents. For the latter compound, the Chloramine-B is covalently linked to small beads of polystyrene. In this way it is easy to quench the reaction just by filtration of the reaction mixture.

d) Iodogen™

Iodogen™ belongs to the class of N-chlorinated urea derivatives and is the trade name for 1,3,4,6-tetrachloro-3α,6α-diphenylglycouril. It is used mainly for the labelling of proteins as it is a mild oxidising agent. As it is not soluble in water the reaction vial is precoated with Iodogen™ prior to the reaction by dissolving it in chloroform, adding a portion of this solution to the vial and removing the chloroform under reduced pressure. The reactions are usually performed at room temperature in aqueous solutions. After the reaction is complete it can be stopped by simply removing the reaction solution from the vial.

e) Others

There are still many other oxidising agents like N-halogen-succinimides, peroxoacids, enzymes (lactoperoxidase), electrolytic oxidation or direct radiochemical reactions *via* the ^{123}Xe decay to ^{123}I. Here the iodine created in situ has a high recoil energy so that it is highly reactive. These reactions play a minor role compared to the above-mentioned methods.

1.2.2 Electrophilic demetallation

The above described electrophilic substitution reactions are easily applied methods. Because of the usually short reaction times and the ease of carrying out the reaction they are useful as kit reactions. To exploit these methods for electron-poor (non-activated) aromatic systems organo-metallic derivatives of these compounds have been developed. They also allow for regio-selective labelling reactions. The metals of the IV main group of the periodic system are used most frequently, in addition to mercury and boron. The most applicable metal is tin. The labelling of the organo-metallic precursors follows the above described methods. The polarisation of the organo-metallic bond with carbon showing a negative polarisation is responsible for the reactivity of the electrophilic substitution.

1.2.3 Nucleophilic substitution

During the nucleophilic substitution reaction of aromatic compounds the iodide reacts as anion. This reaction is difficult because the π electron cloud of the aromatic system rejects the electron rich nucleophile and a delocalisation and therefore stabilisation of the negative charge during the reaction is not possible. These effects can be compensated by strong electron withdrawing groups in the aromatic system. Substitution in ortho and para position are favoured as the negative charge can be distributed, helped by the first substituent, over the whole molecule by mesomeric effects. Nevertheless direct nucleophilic substitution on aromatic systems are not easily performed and only possible under harsh reaction conditions. [18, 19] However, with suitable catalysts the nucleophilic aromatic substitution is also possible under mild conditions. Most of all, the halogen substitution catalysed by copper ions are of great importance. [20-22] In these reactions the d-electrons of copper form a stable complex with either the halogen or the π-electrons of the aromatic system and polarize its complex partner. The mechanism of the reaction goes through the building of a tetrahedral complex of the copper ion in two steps. First the radioiodide is linked to the complex via ligand exchange reaction. Then the aromatic compound is linked to the complex via its halogen. At the same time the bond between radiodiode and the aromatic compound and the bond between the halogen and copper is formed. The nucleophilic aromatic substitution reaction is usually performed in buffered water or strong protic solvents like acetone or water/ethanol mixtures.

1.3 Tracer for measuring tumour proliferation

1.3.1 Nucleotides

Nucleic acid is of central importance for reproduction of life. It stores genetic information and transmits or transfers its content. Nucleic acid is built of nucleotides. They are derivatives of aromatic purine or pyrimidine as bases bonded to C-1 of ribose or 2-deoxyribose moieties, which are linked as phosphodiesters *via* the hydroxy groups on C-5 or C-3 of the sugar moieties. Nucleotides are essential to life. Cells usually produce their own nucleotides, but under special conditions, they may take them from their surrounding medium through complex processes.

1.3.1.1 De novo synthesis

The production of new nucleotides needs very high amounts of energy and is a complex procedure for the cell. The nucleobase, the sugar moiety and the phosphate components are synthesised step by step. For this procedure the cell needs amino acids like aspartate, glutamide and glycine, and other substrates like formate and hydrogen carbonate. The starting material for the synthesis is activated ribose-5-phosphate. From there the nucleobase is consequently constructed onto C-1 of this activated ribose derivative. Afterwards the various mono-, di - and -triphosphates are synthesised with the assistance of a multitude of enzymes like kinases or phosphotransferases. For production of 2-deoxy-ribonucleotides the ribonucleotides are reduced by reductases rather than produced de novo from deoxyribose-containing precursors.

1.3.1.2 Salvage pathway

In this process existing or similar nucleotide frameworks from catabolic processes are taken and incorporated into nucleic acid reproduction. This process is faster and less energy consumptive for the cell than de novo synthesis if enough intracellular resources are available. The most important enzymes in this process besides HGPRT (Hypoxanthine-guanine phosphoribosyltransferase) and APRT (adenine phosphoribosyltransferase) are nucleoside kinases, which phosphorylate extra cellular nucleosides in cytoplasm to nucleotide monophosphate. Nucleotide monophosphate can than be used for metabolism again.

1.3.1.3 Replication of DNA

The main parts of the deoxynucleotides are used for duplicating DNA during the S-phase of the cell cycle. This process is catalysed by DNA -directed DNA polymerases, using appropriate deoxynucleoside triphosphates to build new strands of DNA along single stranded template from the parental DNA. To form a double helix with the template strand the new DNA is build from nucleoside triphosphates, which are able to form Watson-Crick base pairs with the template DNA. The direction of replication is almost always in 5' ⟶ 3' direction.

1.4 Radiolabelled tracers for proliferation

Nucleoside derivatives play an important role in oncology. The aim of using these tracers is either therapeutic or as proliferation markers in diagnosis. They must be stable in vivo, their organ toxicity must be low and it should be possible to label them easily. One of the first compounds investigated, as a radiolabelled proliferation tracer was ^{11}C-thymidine. It can be labelled either in the ring or in the methyl group of thymine. Both varieties, however, are liable to catabolism started by cleavage of the N-glycosidic bond in vivo. A large variety of radiohalogenated compounds followed, many of them investigated and used in connection with gene therapeutic approaches, like IVFRU, FIRU, FIAU, and BVDU. [23-26] There are many possibilities for labelling nucleosides. They can be changed in many different ways with many different effects. Some of these changes are substitution of the hydrogen or hydroxy group at C-2', C-3' or C-5' in the base, of the whole base or a combination of these changes. Some of the disadvantages and advantages of these changes are:

- Substitution in the base of the nucleoside alone is usually not very effective, as nucleosides undergo fast metabolism in blood. Thymidine or 5-iodo-deoxyuridine are metabolised in blood by pyrimidine phosophorylases up to 90%.[27,28,29] For iodinated compounds there is also deiodination after the breakdown of the C-N glycosidic bond. Therefore, only a minimum of compound reaches the target tissue. Furthermore, the measuring signal is composed of all radioactive labelled metabolites, no matter if they are occurring from blood metabolism or from cell metabolism. Therefore it is not possible to say which parameter has been measured.

- Substitution at C-2' stabilises the C-N bond between base and sugar moiety as was shown by Lu et al., [30] but the metabolism can be changed in away that the nucleoside derivative becomes toxic to the organism to which it is applied.
- Substitution at C-3' will block the DNA polymerase, as the 3'-OH is necessary to form the phospho ester link in DNA. A missing OH group in this position will lead to chain termination. The blockage in metabolism can be useful in a radiopharmaceutical concept for measuring single metabolic steps, but which step is measured must be clarified. [31]
- Substitution at C-5' will block the kinases in the DNA replication process, as the 5' hydroxy group is the group which is phosphorylated by pyrimidine kinases. Therefore it will not be a direct marker for proliferation, as it is not incorporated into DNA. [37]
- Substitution of the complete base leading to a stable carbon-carbon bond between sugar and base which will decrease the metabolism in blood. This will increase the lipophilicity of the compound which might lead to a different behaviour in vivo, e.g. those compounds might be able to cross the blood-brain-barrier.

As can be seen above, different radiopharmaceutical approaches are possible to prevent cleavage of the glycosidic bond. One possibility to prevent this cleavage is the introduction of a fluorine atom at C3' in the sugar moiety as was used in the application of 3'-FLT. [31] One other possibility is the introduction of a carbon-carbon bond between sugar moiety and the base of the nucleoside. Kool et al (1994) developed a new non-polar isostere of thymidine. They replaced thymine by a substituted aromatic ring. [32-35] The sp2 hybridised carbon atoms replaced the nitrogen and fluorine took the place of oxygen. The electrostatic potential and the chemical structure are almost identical to those of thymidine. This compound was developed to examine the importance of the hydrogen bonding during DNA replication. Kool et al could show that the Klenow fragment of polymerase I of *Escherichia coli* inserted the triphosphate of this compound into DNA opposite of adenine. They also could show that it was incorporated with almost the same efficiency as thymidine. By replacing the 5-methyl group of thymidine with the structure analogue iodide it would be possible to produce a precursor for an easy radioactive labelling procedure, which should be incorporated into DNA as a tracer for proliferation. The iodine label should be stable in vivo as it is bonded to an aromatic system. Also the introduction of a lipophilic benzene ring should increase the lipophilicity of the compound so that it might be able to cross the brain-blood-barrier in vivo.

2. Literature review of iodine radioisotope production

2.1 Introduction

There is only one naturally occurring iodine isotope, iodine-127. However, 32 artificial radioactive iodine isotopes have been produced and identified via nuclear reactions. Another 23 isotopes have been predicted and their properties have been calculated via mathematical modelling procedures. These isotopes are used for basic research, as tracer atoms in natural sciences, in health care as diagnostic or therapeutic tools and in many other realms of our life.

The table below shows an overview over the isotopes, produced and identified, including their decay characteristics and their half-lives. More detailed information about their decay characteristics is given in Appendix C where the isotopes are discussed individually.

These isotopes are produced either by fission or fusion reactions. These global groups of reactions can be differentiated into the following subtypes:

Fusion:	Heavy ion fusion
	Fusion of light ions with heavy elements
	Substitution reactions
Fission:	Classical fission
	Fragmentation
	Spallation

The differentiation between those reactions is very small. Producing isotopes via heavy ion fusion means two heavy elements of approximately the same weight are fused together to produce one new element. Only small particles such as protons, neutrons, electrons or α-particles are leaving the new nucleus. In the fusion reaction of light ions with heavy elements the same thing happens except that the two reacting species differ greatly in weight. Substitution reactions are not really fusion reactions. Here a target element fuses with light particles such as protons, neutrons, deuterons or α-particles to form a new nucleus, which then releases light particles. Producing isotopes via fission reactions is the opposite way to fusion reactions. Here one very heavy nucleus is bombarded with either small ions or light particles and gives at least two smaller new nuclei. The difference between classical fission and the other two fission reactions is that classical fission gives two new elements of approximately the same weight (reverse reaction to heavy ion fusion) and a few light particles while fragmentation will give a series of new lighter elements and light particles and spallation will give one slightly lighter new element and a series of light particles. These reactions are performed either in an accelerator or in a reactor. The nucleus to be transformed is placed into a beam of the particles used for the transformation. The chamber containing the element, which is bombarded, is called target. Each target can react in different ways with the particles used for bombardment depending on their energy, which means that different isotopes will be produced at different energy levels.

To predict the course of a reaction it is necessary to find out the cross section (σ in cm^2 or barn, which is equivalent to 10^{-24} cm^2) for the particle that is used on a given target and the flux (Φ in particles $*s^{-1}*cm^{-2}$) of these particles (usually the unit barn is used for the cross section and will be used in this paper exclusively). For an experimental evaluation of the cross section the yield of a nuclear reaction is determined as a function of the energy of the particles used for the bombardment. The yield of the produced isotopes is measured by γ spectroscopy. The energy dependency of the cross section of a given reaction is also called excitation function. In a diagram of this energy dependency of the cross section is shown that with low energy the cross section is very small or zero as the bombarding particles need enough energy to cross the potential barrier of the nucleus which is bombarded. With higher energies there will be maximums, so called resonance zones. In these zones of resonance the kinetic energy of the particles is identical to preferred excitation energies.

Table 2: All isotopes of iodine characterised on the chart of nuclides from Straßbourg 1992. [3]

Isotope	Form of decay	Half life time	Comments
I-108	α	≤ 10 ms	
I-109	p	109 µs	
I-110	β^+, α, $\beta\alpha$, βp	0.65 s	
I-111	ε, β^+,γ, α	2.5 s	
I-112	ε, β^+,γ, α, $\beta\alpha$, βp	3.42 s	
I-113	ε, β^+,γ, α, $\beta\alpha$	6.3 s	
I-114	ε, β^+,γ	2.1 s	
I-115	ε, β^+,γ	1.3 min	
I-116	ε, β^+,γ	2.91 s	
I-117	ε, β^+,γ	2.25 min	
I-118	ε, β^+,γ, ε, β^+,γ	8.5 m, 14.2 m	
I-119	ε, β^+,γ	19.1 min	
I-120	ε, β^+,γ, ε, β^+, γ	53 min, 1,35 h	Will be evaluated for use in medicine (diagnostic)
I-121	ε, β^+,γ	2.12 h	
I-122	ε, β^+,γ	3.58 min	
I-123	ε,γ,	13.14 h	Used in medicine (diagnostic)
I-124	ε, β^+,γ	4.18 days	Used in medicine (diagnostic)
I-125	ε, γ	59.4 days	Used in biology and medicine (therapeutic and diagnostic)
I-126	β^-, γ, ε, β^+,γ	13 days	
I-127	No decay	stable	
I-128	β^-, γ, ε, β^+,γ	24.99 min	
I-129	β^-, γ	$1.6*10^7$ a	Used as a standard
I-130	Isomeric transition, β^-, γ, β^-, γ	9 min, 12.36 h	
I-131	β^-, γ	8.067 days	Used in medicine and biology (therapeutic)
I-132	Isomeric transition, β^-, γ, β^-, γ	83.6 min,2.285 h	
I-133	Isomeric transition, β^-, γ	9 s, 20.8 h isomer, ground state	Short half life for isomeric transition
I-134	Isomeric transition, β^-, γ	3.53 min, 52.6 min isomer, ground state	Short half life for isomeric transition
I-135	β^-, γ	6.57 h	
I-136	β^-, γ	46 s, 1.39 m isomer, ground state	Both decays with β^- and γ-particle
I-137	β^-, γ, delayed particle, γ	24.5 s	
I-138	β^-, γ, delayed particle, γ	6.49 s	
I-139	β^-, γ, delayed particle, γ	2.29 s	
I-140	β^-, γ, delayed particle	860 ms	
I-141	β^-, γ, delayed particle	430 ms	
I-142	β^-	0.2 s	

The nuclear reaction will run with especially high yields in these zones. With even

The nuclear reaction will run with especially high yields in these zones. With even higher energy (= higher velocity) the cross section will decrease as the velocity of the bombarding particle is too high for a nuclear reaction or other reactions will become predominant. An example of such a diagram is given in figure 2. [36] With these excitation functions the most effective energy for a given reaction can be estimated so that the desired isotope will be produced in as high yield as possible and as pure as possible. As most nuclear reactions for a given target nuclide and a given particle of bombardment will compete with each other the desired product will contain one or more impurities either an isotopic impurity which can not be easily separated or a non isotopic impurity which can then be separated chemically from the product isotope.

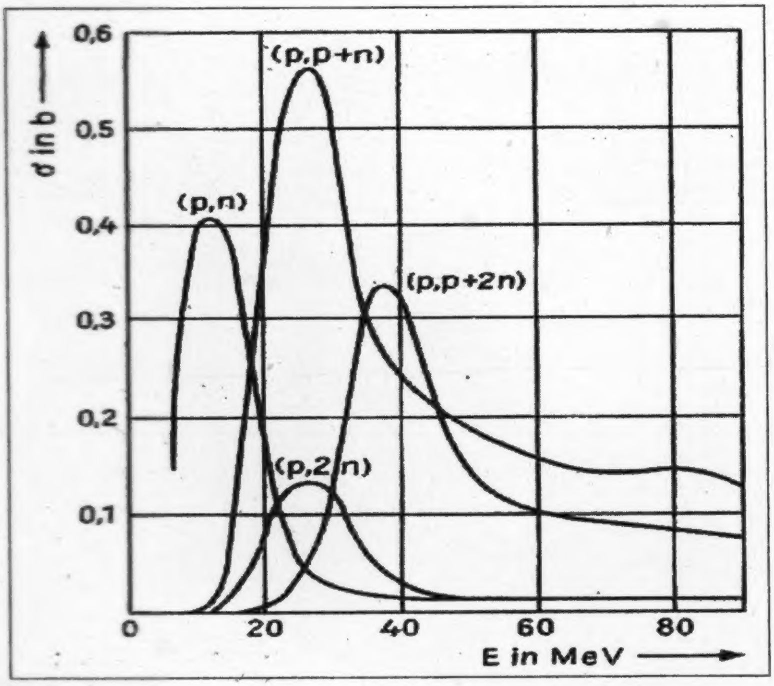

Fig. 2: Excitation functions for simultaneous reactions of protons with ^{63}Cu [36]

2.2 Methods and materials

$^{108-115}$I

These isotopes are generally produced via heavy ion fusion reactions. Used are ^{63}Cu, $^{58/60}$Ni or ^{54}Fe targets which are bombarded with either ^{58}Ni^{3+} or ^{58}Ni^{5+} ions. 200-250 MeV are typical beam currents. The purification is performed via mass analyser.

These reactions usually will give a mixture of all isotopes mentioned above with varying compositions depending on the target material and beam current. The purification and identification is performed immediately at the target. More detailed information about production parameters, purification and physical characteristics is given in Appendix C. The isotopes produced have short half-lives and the yield is usually low. They are used for basic research only.

$^{115\text{-}123,125,127}$I:

These isotopes can be produced by bombarding heavy elements with light ions. Used are target materials such as cadmium, silver, palladium or molybdenum which are bombarded with ions like lithium, boron, carbon and others. Beam currents are usually between 30 to

100 MeV. Purification is mostly performed via mass analyser. More detailed information about production parameters, purification and physical characteristics is given in Appendix C.

$^{120,121,123\text{-}131,136}$I:

These isotopes can be produced via substitution reactions. Used is tellurium, antimony, xenon or stable iodine as target materials. They are bombarded with protons, neutrons, deuterium or α-particles with varying energies. Purification is performed either via chemical separation techniques or via dry distillation procedures. More detailed information about production parameters, purification and physical characteristics is given in Appendix C and for some of these isotopes in the discussion.

$^{113\text{-}124}$I:

These isotopes can be produced via fragmentation reactions. Xenon or cerium is used as target materials. They are bombarded with protons or aluminium ions with high energies. Purification is performed via mass analyser. More detailed information about production parameters, purification and physical characteristics is given in Appendix

C and for some of these isotopes in the discussion.

^{116,118,120,122}I:

These isotopes can be produced via spallation reactions. Lanthanum is used as target material. It is bombarded with high energetic protons. Purification is performed via mass analyser. More detailed information about production parameters, purification and physical characteristics is given in Appendix C.

$^{118,127,129,131-143}$I:

These isotopes can be produced via classical fission reactions. Uranium, californium, curium or gold are used as target materials. They are bombarded with thermal neutrons or with carbon ions. More detailed information about production parameters, purification and physical characteristics is given in Appendix C.

2.3 Discussion:

An isotope used as tracer element especially in life sciences must have an appropriate type of decay. A β^- decay or α-particles are not easily detected. If the isotope is used for human diagnostics these types of decay cannot be detected at all as they do not escape from the body. They will add to the radiation dose without being of any practical value. In animals, cell studies or in natural sciences it might be possible to use these types of decay as it is possible to use special detection procedures such as radiography or scintillation counting techniques. They can also be used as therapeutic isotopes as these decay types have short ranges inside of material and they will do a lot of damage as they are particle decays. To be effective as therapeutic isotopes they will need a half life in the range of several days so that the radiation dose is not to high for healthy tissues but the time of irradiation is not too short to do enough damage to the target tissue.

Auger electrons emitted following electron capture decay have the same particle characteristics. In therapy they are useful because of their short range of a few nanometers and as they are charged particles capable of causing tissue damage. Auger electrons add high radiation doses without any value (for the same reasons for which they are useful for therapy) as they are absorbed within a few nanometers of the atom from which they are emitted.

Furthermore it should be possible to produce and purify an isotope which will be used as a tracer in natural sciences or life sciences in an appropriate amount in a time which is not longer than three half-lives of this isotope. In practice it is not useful to irradiate longer than 3 half-lives of the isotope because 87.5% of the theoretical possible yield is reached. A long purification time for the isotopes leads to losses in yield by decay and to reduced specific activity.

Most of the isotopes of iodine have either a too short half life or an inappropriate decay type to be useful in life sciences. Especially the isotopes 108-119, 122, 134 and 136-142 have half-lives ranging from a few micro seconds up to a few minutes. They are used only for basic research. Furthermore their production, their separation and purification is rather difficult. The isotope ^{121}I has an β^+ decay of only 14% which is too low for diagnostic purposes while the major emission from this material is Auger electrons which will add a high dose without any use for diagnostic. But for therapy, for which the Auger electrons could be used the half-life of ^{121}I is too short. ^{126}I is produced via a (n,γ) reaction or via a $(n,2n)$ reaction. The (n,γ) reaction will lead to high levels of ^{125}I impurities while the $(n,2n)$ reaction will lead to high levels of ^{127}I impurities. Both will decrease the specific activity in especially the ^{127}I. A high specific activity can be needed for diagnostic. Also the long half-life of 13 days and its decay form, mainly β^- makes it not suitable for diagnostic. Furthermore the ^{125}I will increase the radiation dose because of its long half-life and the Auger electrons. Because of the high levels of impurity it is also not suitable for therapy. ^{128}I was used in nuclear medicine during 1934 to 1936 as it was the first radioactive isotope produced. Because of its short half-life it was thought unsuitable for medical purposes. Therefore it was replaced by ^{131}I after it was produced and identified in 1936. Today the β^- decay of ^{128}I is the main reason for not using it in diagnostic applications as it will increase the radiation dose. The half-life is to short for therapy. The half-life of ^{129}I is with $1.6*10^7$ years too long for any medical purpose. It is mainly used as a standard of measuring devices, in waste management or material testing. The β^- energy of the isotopes 130,132, 133, and 135 are mainly high energetic. High β^- energies means these particles have a long range in tissue so that their therapeutic value is rather low and the radiation dose of these isotopes is high.

Only a few isotopes are useful for life sciences. These isotopes are ^{120}I, ^{123}I, ^{124}I, ^{125}I and ^{131}I. These isotopes will be discussed in detail. The production routes and detailed information about production parameters, purification and physical characteristics for all produced isotopes are given in Appendix C.

2.4 Isotopes used for life sciences

^{120}I:

^{120}I is an isotope which exists in a ground state and in an isomeric state. The ground state (^{120g}I) has 46% β^+ decay but with a high maximum beta energy. Its half-life is 1.35 h, which is sufficient for labelling, purification and measuring metabolic processes. The isotope is evaluated as tracer for PET (positron emission tomography). The high maximum beta energy of 4 MeV is not ideal because of the decreased resolution but acceptable. Also the isomeric state (^{120m}I) may cause some disturbances. ^{120m}I has a slightly shorter half-life than ^{120g}I, namely 53 min. Its main decay form is also β^+ with a maximum beta energy of 3.75 MeV. Due to the production route the impurity of ^{120m}I and of ^{121}I can be kept quite low. The main production routes for ^{120}I are:

a) $^{127}\text{I}\ (p, 8n)\ ^{120}\text{Xe} \xrightarrow[40\ \text{min}]{\beta^+,\ \text{EC}} {}^{120g}\text{I}$

b) $^{122}\text{Te}\ (p, 3n)\ ^{120g}\text{I}$

c) $^{120}\text{Te}\ (p, n)\ ^{120g}\text{I}$

d) $^{120}\text{Te}\ (d, 2n)\ ^{120g}\text{I}$

e) $^{nat}\text{Sb}\ (\alpha, x)\ ^{120m}\text{I}$

More reaction routes and more detailed information about production parameters, purification, cross sections and physical characteristics will be given in Appendix C.

Reaction a) usually gives a low yield which is sufficient for spectroscopy only. The main advantage of this reaction is the absence of ^{120m}I.[38]

Reaction b) gives high ^{120g}I yields. The disadvantage is the high level of ^{120m}I and ^{121}I impurities. Also a medium sized cyclotron is needed as a proton energy of 32 to 37 MeV will give a maximum yield. The target costs are moderate. [38]

Reaction c) will give slightly lower yields than reaction b). Also a cyclotron with low energy is sufficient for the production. The level of impurities is clearly lower than in reaction b). However the target costs are rather high. [39]

Reaction d) will give very low yields with high levels of ^{120m}I (up to 68%) and is therefore unsuitable for the production purpose. [38]

Figures 3,4 and 5 give the excitation functions for reaction b), c) and d) from reference 38- 40.

Reaction e) will give only ^{120m}I. As ^{120g}I is the desired product for medical purposes this reaction is unsuitable.

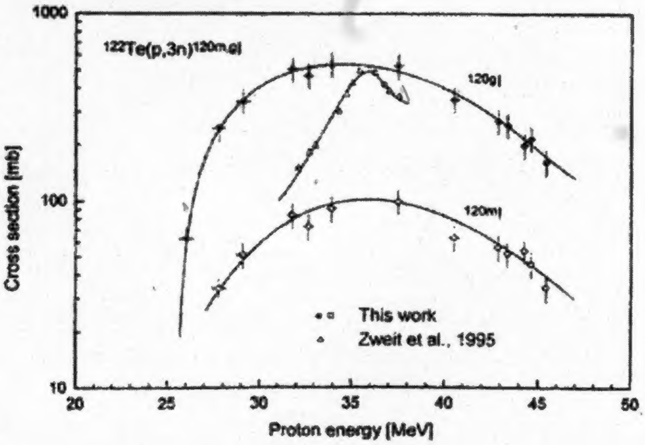

Fig. 3: Excitation function of the ^{122}Te(p,3n)^{120m,g}I process [39]

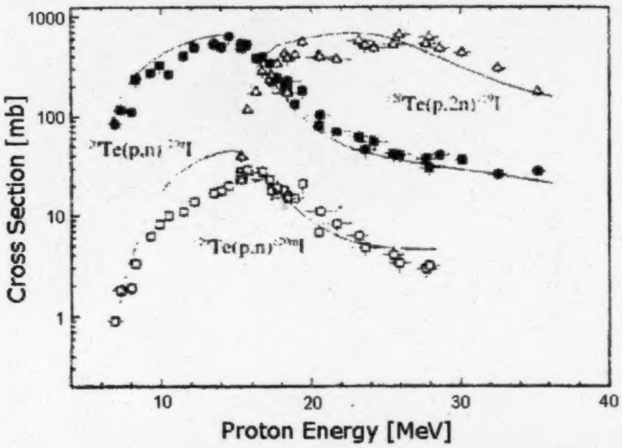

Fig. 4: Excitation functions of ^{120}Te(p,xn)^{120m,120g,119}I reactions. Experimental data (symbols) are from Hohn et al. and theoretical results (curves) from Sudar [40]

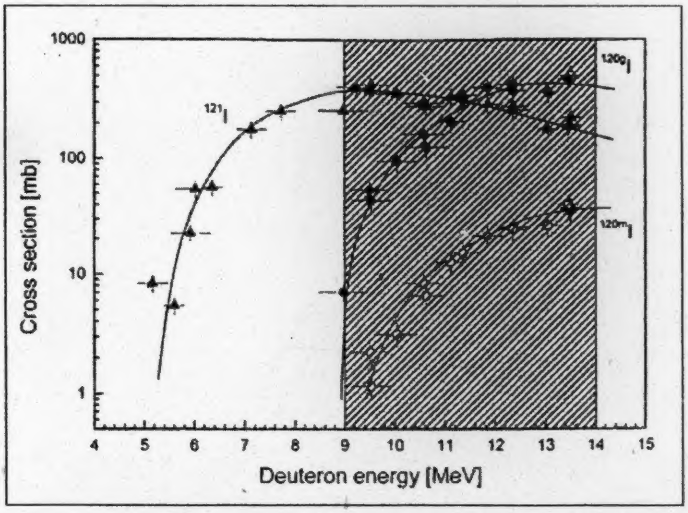

Fig. 5: Excitation curve for the ^{120}Te(d,xn)reactions leading to the formation of ^{121}I, ^{120m}I and ^{120g}I. The solid lines are eyeguides. There is no suitable energy range for the production of ^{120g}I. The shaded area simply describes an energy range where the yield of ^{120g}I could be maximum, but with large amount of the ^{121}I-impurity [38]

So the production route depends on the cyclotron available and the amount of money that can be spent on the production and the amount of time. The purest ^{120g}I will come from reaction

a) but with very low yield. For medical purposes reaction b) and c) are the only ones viable where reaction c) will give the better quality with higher costs while reaction b) gives the higher quantity at lower costs.

^{123}I:

^{123}I is an isotope with a half-life of 13 hours with an electron capture decay and a main γ emission at 159 keV. The γ energy makes it suitable for diagnostics via gamma camera or single photon emission computer tomograph (SPECT). Its half-life of 13 hours is more than sufficient for production, labelling and purification. Even a transportation of labelled compounds and their medical application in a radius of a few 100 km is possible. On the other side the Auger electrons of ^{123}I will increase the radiation dose for patients. But because of its half-life this increase is still acceptable. ^{123}I is produced mainly via the following reactions:

a) ^{124}Te(p,2n)^{123}I

b) ^{123}Te(p,n)^{123}I

c) ^{122}Te(d,n)^{123}I

d) $^{124}\text{Xe}(p, 2n)^{123}\text{Cs} \longrightarrow {}^{123}\text{Xe} \longrightarrow {}^{123}\text{I}$

e) $^{127}\text{I}(p,5n)\ ^{123}\text{Xe} \longrightarrow {}^{123}\text{I}$

More reaction routes and more detailed information about production parameters, purification, cross sections and physical characteristics will be given in Appendix C.

Reaction a) is the most commonly used production route for ^{123}I from the direct production routes. Costs for target material are reasonable and the handling of targeting and purification of the product is easy. The reaction and various purification methods have been studied extensively and are very well known. A cyclotron that is capable of producing protons with an energy of 25-30 MeV is needed. In literature impurity levels of ^{124}I ranging from 1% up to 3.8% are given for this reaction. Yields of 370 MBq/µAh are possible.

Reaction b) will give ^{123}I with ~98% purity. ^{124}I with ~2% will appear as impurity.

Other impurities have not been measured. A small cyclotron with proton energies of 15 MeV is sufficient. The yield of ^{123}I is low with only ~111 MBq/μAh. [41]

Reaction c) is a low yield reaction. It will give not only ^{124}I as impurity, even if it is only 0.4%, but also ^{126}I (0.3%), ^{130}I (1.4%) and ^{131}I (0.4%). [42] All impurity data are given for 30h after EOB. The impurities arise from the isotopic impurities in the target material. The reaction will yield ~74 MBq/μAh of ^{123}I. A medium sized cyclotron with deuteron energies of 16 MeV is necessary. [41]

Reaction d) will give a high purity product. Impurities are ^{125}I and ^{124}I in the range of 10^{-5} to 10^{-7} at 24 h after EOB. [43] This reaction is used for routine production of commercially used ^{123}I. The disadvantage of this reaction is the high cost of the target material as ^{124}Xe is present only at 0.1% in natural xenon gas and must be enriched. The target design and construction to prevent losses of gas is complicated and expensive. Therefore only commercially orientated application is practical where a reliable and reproducable production is absolutely necessary. Also a medium sized cyclotron is necessary as the protons used for bombardment need an energy of 30 MeV.

Reaction e) will give a high purity product. Its only contamination is 0.13-0.7% ^{125}I from ^{125}Xe which is produced via the ^{127}I(p, 3n) reaction and decays with a half life of 17h to ^{125}I. [44] The target material is very inexpensive as it consists of natural iodine. However the complicated design and construction of the target according to the aggressive target material and the high energy of the protons needed for irradiation (~60 MeV) make this reaction suitable only for specialised cyclotron sides.

^{124}I:

^{124}I is an isotope with a half life of 4.18 days with a decay of 25% β^+ and 75 % electron capture. The β^+ decay makes it suitable for PET applications. However its long half life and the high amount of Auger electrons, due to the electron capture, lead to high radiation doses. Therefore it would be more suitable for therapy. On the other hand the long half life makes it suitable for transporting labelled compounds even to destinations very far away. Iodine-124 was first produced in 1938 by bombarding antimony with α-particles. [45] In the beginning it was viewed as a by product in the production of ^{123}I. [41, 46-48] Today it is produced and evaluated as a suitable PET isotope. [49-52] The most commonly used reactions for the production of ^{124}I are summarised in table 3 below.

Table 3: Most common nuclear reactions for production of [^{124}I]iodine.

Reaction	Energy range [MeV]	Byproducts	Literature
^{124}Te(p,n)^{124}I	13-9	41% ^{123}I	53
	12-8	1% ^{123}I	
^{124}Te(d,2n)^{124}I	15-8	0.8% ^{125,126,131}I	54
^{124}Te(d,2n)^{124}I	15-0	^{123,125,126}I	55
^{124}Te(d,2n)^{124}I	16-6	^{123,125,126}I	56
^{125}Te(p,2n)^{124}I	21-15	^{123,125}I	57
	21-17	^{123,125}I	
^{126}Te(p,3n)^{124}I	36.8-33.6	^{125,126}I	58

More reaction routes and more detailed information about production parameters, purification, cross sections and physical characteristics will be given in Appendix C.

Nowadays [^{124}I]iodine is produced mostly by the following nuclear reaction: ^{124}Te(d,2n)^{124}I. [54-56, 59-61] This reaction produces ^{124}I in high yields. But a major drawback of this reaction is the building of ^{125}I. Both, the long half life of 60.14 days and the high amount of Auger electrons which occur during decay of ^{125}I are increasing the radiation dose during usage of ^{124}I considerably. Other impurities due to isotope impurities of the target material or due to side reactions, e.g. (d,n) reactions are ^{123}I, ^{126}I, ^{130}I and ^{131}I. [44] Another drawback is the necessity of a medium sized cyclotron, which is able to produce deuterons with an energy of 14 MeV. The highest yield is given with the ^{125}Te(p,2n)^{124}I reaction. [57, 58] Here also the by production of ^{125}I is the major problem. Also the relatively high energies of the protons from 21 MeV necessitate a bigger cyclotron for production. The production of ^{124}I from ^{126}Te by a (p,3n) reaction gives high yields of ^{124}I. But besides ^{125}I also ^{126}I is produced as a by-product and the energy needed for production is about 37 MeV, even higher than for the ^{125}Te(p,2n) reaction. The highest purity of ^{124}I with approximately 99% radiochemical purity is given by two reaction routes: ^{124}Te(p,n) and ^{123}Te(d,n). The second reaction route gives only low yields of ^{124}I with a high amount of ^{123}I. For both reactions a thin layer of highly enriched ^{124}TeO$_2$ is molten onto a platinum/iridium base. [62] A thin layer of the target material will improve the cooling possibilities, which will allow higher beam currents. To increase the effective beam length the target plate is usually placed at an angle of 10-15 degrees into the target chamber. For the ^{124}Te(p,n) reaction a small cyclotron with proton energies of 12-8 MeV is sufficient. The main impurity is ^{123}I which is formed by the (p,2n) reaction at higher proton energies. Figure 6 shows the excitation functions for the ^{124}Te(p,n) and (p,2n) reactions from reference [53].

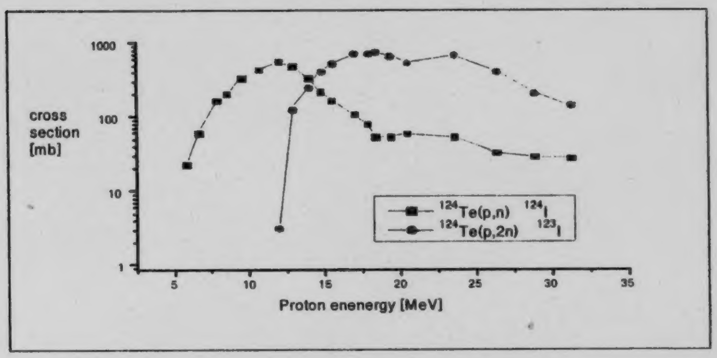

Fig. 6: Exitation functions for the ^{124}Te(p,n) and ^{124}Te(p,2n) reaction. [53]

^{125}I:

^{125}I is an isotope with a half-life of approximately 60 days with a decay of 100% electron capture. It is not suitable for diagnostic use as the energy of the γ rays are too low to cross the body barrier and a high flux of Auger electrons are emitted. ^{125}I is mostly used for in vitro diagnostics, in vitro or ex vivo tracer experiments and sometimes in therapy. The low energy of Auger electrons leads to a very short range in tissue. This range is usually only a few nanometers. Brought into a cell into DNA or near DNA the Auger electrons will lead to strand or even double strand breaks, which will kill the cell. This feature makes ^{125}I inserted into an appropriate compound very useful for therapy. Its long half-life will lead to very high radiation doses. ^{125}I is produced mainly via the following reaction: [63]

a) $^{124}\mathrm{Xe}(n,\gamma)^{125}\mathrm{Xe} \xrightarrow{\text{E.C}} {}^{125}\mathrm{I}$

More reaction routes and more detailed information about production parameters, purification, cross sections and physical characteristics will be given in Appendix C.

Reaction a) will give a high quality product with up to 99.5%. The main impurity is ^{126}I which will form through neutron reactions with the primarily formed ^{125}I because of long irradiation times. As ^{126}I has a shorter half life than ^{125}I it will decrease after EOB via decay. The main disadvantage of the reaction is the high cost of the target material as ^{124}Xe occurs only to 0.1% in natural xenon gas. Furthermore a reactor is necessary for the production. Nevertheless most manufacturers will use this process as it gives good quality product with high yields.

^{131}I:

^{131}I is an isotope with a half-life of 8.067 days with 86% β- decay of an energy of 0.6065 MeV as main decay. This decay form will be absorbed in tissue after ~0.4 cm which is nearly optimal for therapy. The long half-life on the other side leads to a high radiation dose. It would be desirable to have an isotope with the same decay and a slightly shorter half-life (1-2 days). ^{131}I also has a γ emission at 364 keV with intensity of 100% which can be used for diagnostic purposes accompanying a therapy. ^{131}I is produced mainly via the following routes:[64]

a) $^{130}\mathrm{Te}(n,\gamma)^{131m}\mathrm{Te} \xrightarrow[30\ \mathrm{hr}]{\mathrm{I.T.}} {}^{131}\mathrm{Te} \xrightarrow[25\ \mathrm{min}]{\beta\text{-},\ \gamma} {}^{131}\mathrm{I}$

b) $^{235}\mathrm{U}(n_{th},f)\ ^{131}\mathrm{I}$

More reaction routes and more detailed information about production parameters, purification, cross sections and physical characteristics will be given in Appendix C.

Both reactions are performed in a reactor. Reaction a) will give a nearly carrier free product while reaction b) usually contains ^{127,129}I as impurities.

Reaction a) can be performed either with elemental enriched ^{130}Te or with natural TeO_2. An elemental tellurium target necessitates a chemical purification procedure with various steps which makes it difficult to handle. The iodine from a tellurium dioxide target on the other side can be recovered by dry distillation which is quite easy. This will give some non-isotopically impurities like lead, selenium and tellurium.

Reaction b) necessitates also a chemical work up. Another disadvantage is the necessity of handling gaseous by-products such as xenon gas. Their handling is difficult and necessitates special equipment.

Nevertheless both reactions are used for routine production of ^{131}I as both reactions will give high yields.

3. Rationale, Hypothesis and Objectives:

3.1 Rationale

5-IDFPdR was designed as a replacement for thymidine, on the finding that the 5-methyl-5'- triphosphate analogue of this compound was incorporated into DNA with almost the same efficiency as thymidine itself. [34]

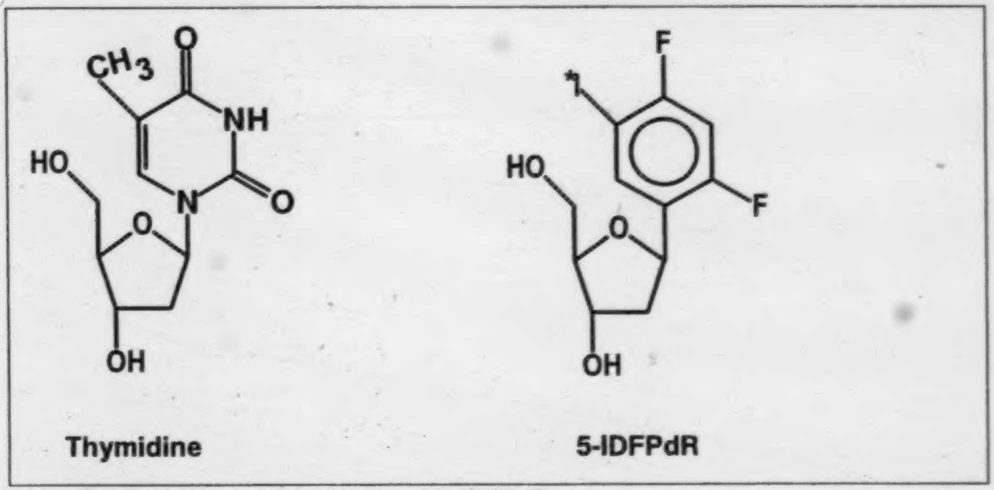

Fig. 7. Structures of thymidine and 5-IDFPdR

Since iodine is a bioisostere for a methyl group, it was expected that 5-IDFPdR would behave similarly to the 5-methyl derivative. If this were to be the case, 5-IDFPdR might be a useful anticancer or antiviral agent. At the same time, 5-IDFPdR offers a simple possibility of labelling by an isotope exchange reaction which might lead to a new agent to image in vivo cellular proliferation. Therefore, a labelling procedure was developed and optimised with regard to temperature, amount of precursor, amount of sodium hydroxide and time. The chemical synthesis of unlabelled 5-IDFPdR was performed following the procedures published by Z.-X. Wang et al. [68] The labelling procedure was to be performed with ^{124}I so that it would be possible to use the labelled compound with PET. As ^{124}I is not commercially available, it was to be produced using the cyclotron at the PET centre in Tübingen. A beam-current dependency curve was experimentally derived to determine the best production parameters. Finally, as the labelled compound might be a useful anti-cancer or anti-viral agent and /or a useful tool for imaging proliferation in vivo, its pharmacokinetic properties and its biodistribution parameters were determined. Some preliminary cell culture experiments suggested that 5-IDFPdR might not be a substrate for thymidine kinase [Ebenhahn et al.,unpublished data]. Therefore, a masked 5'-mono phosphorylated compound, (S_P)-*cyclo*-(3-methylsaligenyl)-5'-*O*-[1'-(2,4-difluoro-5-iodophenyl)-2'-deoxy-*β*-D-ribofuranosyl]phosphate (*cycloSal*-5-IDFPdR), which would diffuse across cell membranes because it is highly lipophilic, was synthesised. Thus, the pharmacokinetic data and the biodistribution of *cycloSal*-5-IDFPdR were to be established.

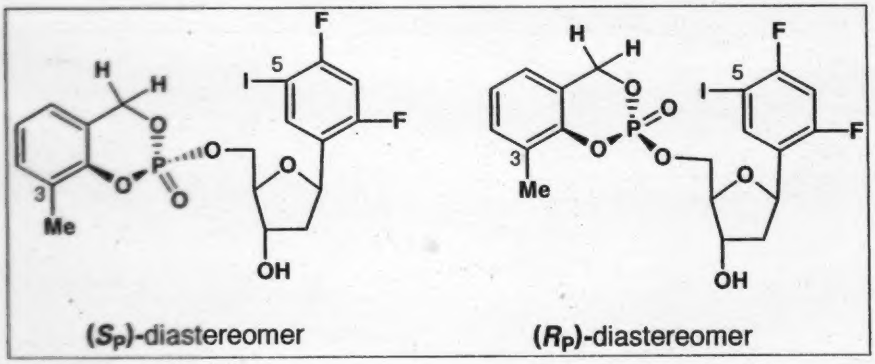

Fig. 8. Structures of the two diastereomeres of *cycloSal*-5-IDFPdR

3.2 Hypotheses

The development of radiotracers is based on both scientific principles and technical resources. In this case, the objectives are based on available technological resources and specific hypotheses, which exploit this technology. These hypotheses include:

1. Production of $[^{124}\text{I}]\text{I}^-$ is possible with a small sized cyclotron.
2. The labelling of 5-IDFPdR with $[^{124}\text{I}]\text{I}^-$ is a facile procedure.
3. Radiolabelled 5-IDFPdR is stable in vivo and will not undergo metabolic deiodination.
4. *cycloSal*-5-IDFPdR is a possible prodrug of the 5'-monophosphorylated 5-IDFPdR.
5. Radiolabelled 5-IDFPdR is a good imaging agent.

3.3 Objectives

The overall objectives of this work were to optimize the radioiodination procedure for 5-IDFPdR and *cycloSal*-5-IDFPdR, and to then determine the biodistribution of these compounds in an animal model. Specific objectives were to:

1. Determine the production parameters for ^{124}I, particularly the beam-current dependency.
2. Develop procedure for labelling 5-IDFPdR with ^{124}I.
3. Delineate the pharmacokinetics of 5-^{125}IDFPdR and *cycloSal*-5-IDFPdRin rats.
4. Determine biodistribution of 5-^{125}IDFPdR and *cycloSal*-5-IDFPdR.
5. Evaluate the usefulness of 5-^{123}IDFPdR as an imaging agent.

4. Production of iodine-124

4.1 Materials and methods

Iodine-124 was produced with a solid target constructed at the PET-centre in Tübingen, Germany. The target consisted of a mixture of 94 % tellurium dioxide and 6 % aluminium oxide that was melted onto a platinum/iridium plate. This plate was placed into the target at a 10° angle relative to the direction of the particle beam. [65] In this arrangement the effective beam length on the target material is increased by a factor of 4 in comparison to a 90° angle. Thus, the layer of the target material can be much thinner, which allows better cooling possibilities. The nuclear reaction for producing Iodine-124 from tellurium dioxide is a (p,n) or (d,2n) reaction. The energy of the deuterons should be 15 MeV and the energy of the protons should be 13 MeV. [54] Since the PETtrace^{TM} (General Electric) cyclotron in Tübingen produces deuterons up to an energy of 8 MeV and protons up to an energy of 16.5 MeV, only the (p,n) reaction was feasible. Iodine-123, formed via the (p,2n) reaction at energies higher than 13 MeV, is a by product of this process because of the slightly higher energy of the protons (16.5 MeV instead of 13) in PETtrace™. To reduce the amount of Iodine-123 produced, a thick aluminium foil can be used at the beam entry position, which will lower the energy of the protons. First of all, the current dependency for the production of ^{124}I was determined. Therefore, the target mixture (94% tellurium dioxide and 6% aluminium oxide; 300 mg) was melted onto a target plate with a density of approximately 200 mg/cm^2. To check the beam position inside the target chamber, aluminium foils were attached to an empty target plate and irradiated before and after every irradiation in place of the real target. The aluminium foils were then measured in a digital radiograph (Instant Imager, Canberra) and the images acquired were analysed with regard to the planar distribution of the radioactivity. When the beam spot was not centred on the foil, the target chamber was moved up or down to accommodate the beam shift. The tellurium targets were then irradiated for 10 minutes at different beam currents. The beam current was set and checked by the cyclotron itself and also monitored with an external ammeter.

Thirty minutes after irradiation, the iodine was recovered from the target by dry distillation. [63] The target was placed into an oven at 690 °C, and the gaseous iodine was trapped in a capillary which was precoated with a 4 mM sodium hydroxide solution. The radioactivity could then be transferred into 200 μL of the same sodium hydroxide solution simply by washing the capillary several times with the sodium hydroxide solution. The ^{124}I radioactivity of the sample was then determined by γ-ray spectroscopy. This was necessary because of the ^{123}I impurity.

4.2 Results and Discussion

The beam-current dependency curve for the irradiation of ^{124}Te with protons was found to be linear over a 5-13 μA range, with a calculated regression line having a slope of 502.4 and a correlation coefficient (r^2) of 0.99. The yield, displayed in Figure 9, applies to the yield of a 10 minute beam with changing currents. The value used to describe the efficiency of a target is defined as the amount of radioactivity that is produced during a one hour irradiation with a beam current of 1 μA. This curve, displayed in Fig. 10, has a minimal positive slope of 53.36, f(0) = 2660 and a correlation coefficient of 0.70. The radioactivity formed per μAh should be independent of the beam current. Therefore, the curve in Figure 8 should have a vertical course. The positive slope of the curve here can be attributed to the radioactivity values measured after the irradiation of the target with 5 μA. Usually the cyclotron has a beam current range from 0 to 75 μA. The optimum beam current range for irradiations is between 35 to 50 μA. A beam current of 5 μA is very low for the cyclotron and the variation in beam current during the beam time is usually high. Therefore, this value has a relatively high uncertainty. In addition, the slope (53.36) of the curve is only a very small fraction of standard deviation, which lies between 606 and 120. Therefore, the curve can be viewed as vertical and the formed radioactivity as independent of beam current.

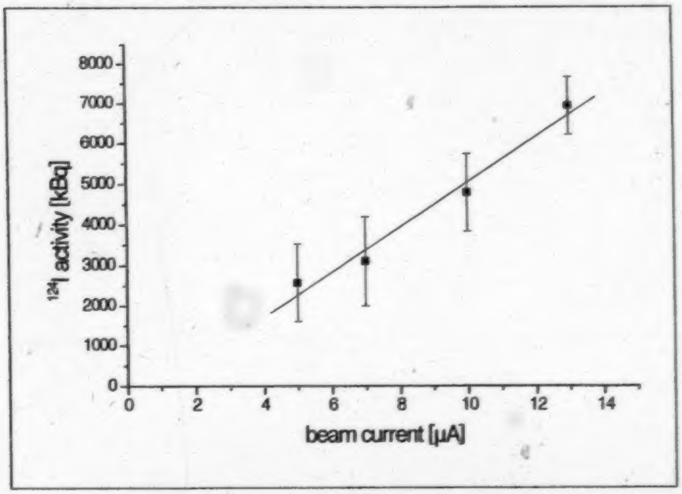

Fig. 9. Beam-current dependency of the [^{124}I]iodide production [kBq] on the PETtrace from General Electrics cyclotron at the PET-centre in Tübingen. The target was plated with 300 mg of a mixture of 94 % $^{124}TeO_2$ and 6 % Al_2O_3 and irradiated for 10 minutes. The ^{124}I was recovered by dry distillation at 690 °C for 10 min. Each point represents 3 samples, ± S.D., linear regression was applied to fit the solid line. The slope is 502.4 and the correlation coefficient (r^2) is 0.99.

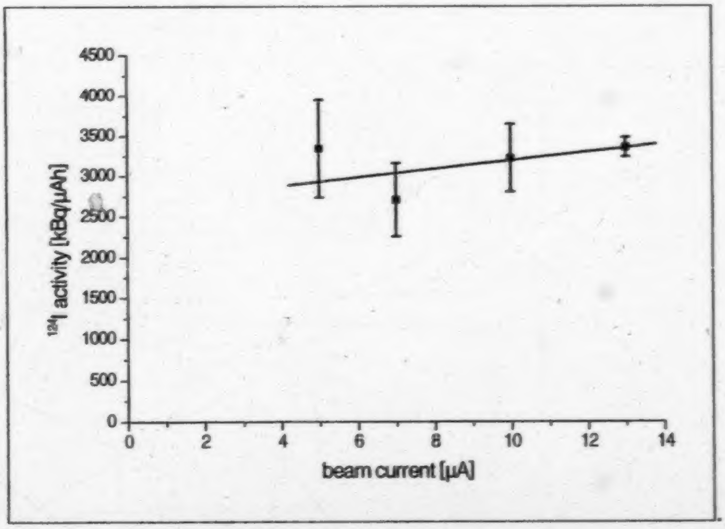

Fig. 10. Current dependency of the [^{124}I]iodide production [kBq/µAh] on the PETtrace from General Electrics cyclotron at the PET-centre in Tübingen. The target was plated with 300 mg of a mixture of 94 % $^{124}TeO_2$ and 6 % Al_2O_3 and irradiated for 10 minutes. The ^{124}I was recovered by dry distillation at 690 °C for 10 min. Each point represents 3 samples, ± S.D, linear regression was applied to fit the solid line. The slope is 53.36 and the correlation coefficient (r^2) is 0.70.

Nevertheless, the yield of the iodine production is low compared with literature data. The latest data published were in 2002 from Qaim et al., who reported a value of approximately

6 MBq/μAh for the ^{124}Te(p,n) reaction.[66] The reason for the low yield here is attributed to the small amount of target material used during irradiation. A comparison between the beam spot determined from the irradiated aluminium foils and the area coated with target material on the target approximately showed that the beam area was 3 times larger than the area coated with the Tellurium target material. Based on this knowledge, an increase in target material should increase the production yield of ^{124}I. Some preliminary experiments with a target plate coated with 600 mg target material on a surface of approximately 3 cm^2 showed a doubling in yield for a beam current of 10 μA. The table of results for the irradiation of both targets can be found in Appendix B.

5. Production of the precursor 2,4-difluoro-5-iodo-1-(2-deoxy-β-D-ribo furanosyl)benzene (5-IDFPdR) for labelling with [^{124}I]iodide

5.1 Synthesis of 2,4-difluoro-5-iodo-1-(2-deoxy-β-D-ribofuranosyl)benzene (5-IDFPdR)

The synthesis of 5-IDFPdR was performed in 5 steps following a method described in the literature. [67] The reaction sequence consisted of the synthesis of a protected chloro-sugar, the production of an iodinated aromatic system, the coupling, deprotection and iodination at C-5 in the aromatic ring. Each synthetic step is described in detail below.

General Methods: ^{1}H-NMR spectra were measured in $CDCl_3$ on a Brucker 250 MHz spectrometer. Proton chemical shifts (δ) are listed relative to the internal reference TMS (0.00 ppm). Silica gel 60 (40-60 μ) from Merck Co. was used for silica gel flash chromatography purification; all chemicals used were from Merck in p.a. quality if not mentioned otherwise.

A structural diagram for this series of reactions is provided in figure 11 on the next page.

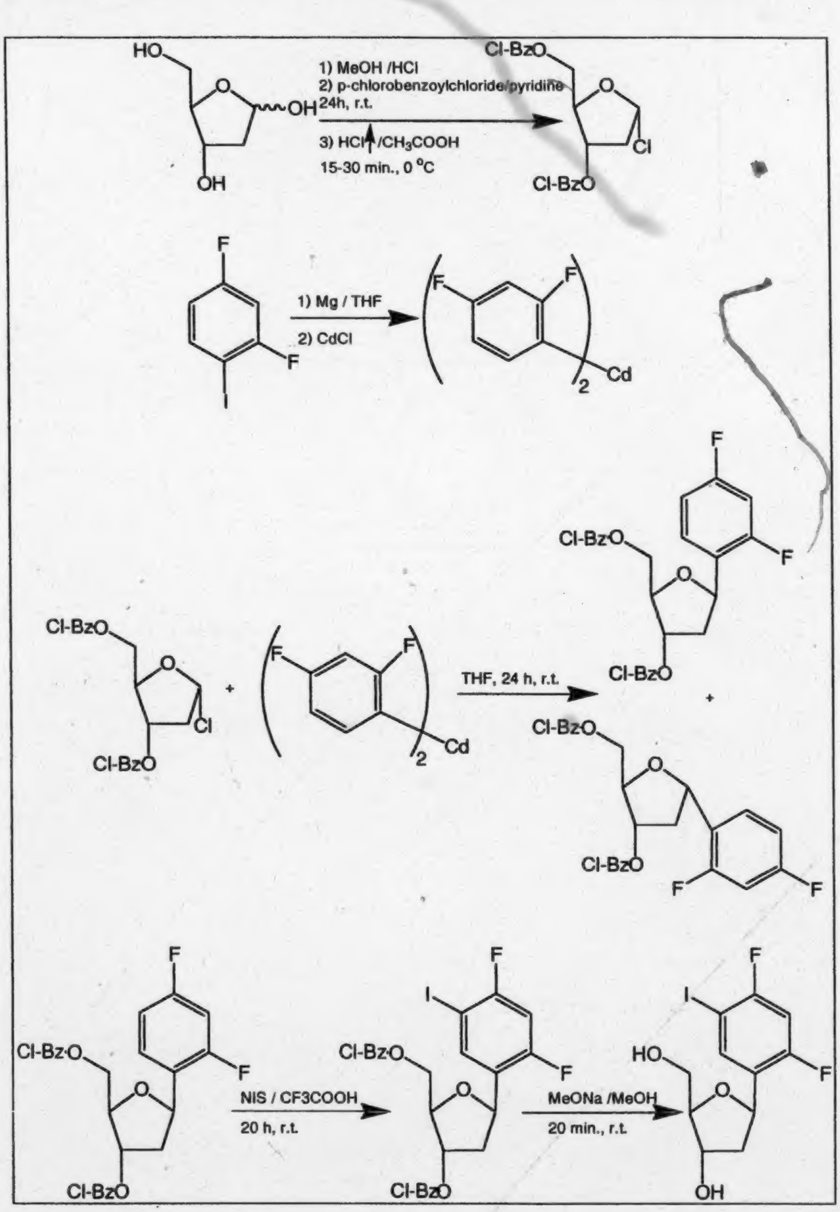
HO
OH
1) MeOH /HCl
2) p-chlorobenzoylchloride/pyridine
24h, r.t.
3) HCl↑/CH3COOH
15-30 min., 0 °C
Cl-BzO
Cl
F
I
1) Mg / THF
2) CdCl
Cd
2
THF, 24 h, r.t.
+
NIS / CF3COOH
20 h, r.t.
MeONa /MeOH
20 min., r.t.

Fig. 11. Reaction scheme for producing 5-IDFPdR [67]

5.1.1 Production of 2-deoxy-3,5-di-*O*-(*p*-chlorobenzoyl)-α-D-ribofuranosyl chloride (1)

Ten grams (0.075 mol) of deoxyribose were dissolved in 150 mL methanol. Acetyl chloride (0.5 mL) was added, and the resulting solution was stirred for 40 minutes at room temperature. Pyridine (10 mL) was added to quench the reaction and the solvent was removed under reduced pressure to remove all traces of HCl. The oil obtained was dissolved in 30 mL pyridine and a catalytic amount of DMPU (1,3-dimethyltetrahydro-2(1*H*)-pyrimidone) was added. The solution was cooled on ice before *p*-chlorobenzoyl chloride (14 mL) was added. The resulting mixture was stirred for another 30 minutes at ice-bath temperature before it was allowed to warm up to room temperature. The reaction was allowed to proceed with stirring overnight. The reaction was quenched with
100 mL of water, and 120 mL of CH_2Cl_2 were added. The organic phase was separated and the aqueous phase was extracted again with dichloromethane. The combined organic phases were washed consecutively with two times 100 mL saturated sodium hydrogen carbonate, two times with 100 mL sulphuric acid (15%), water, and then with brine. The organic phase was dried over sodium sulphate, filtered, and the solvent was removed under reduced pressure. The residue was dissolved in ether and the solids were removed by filtration. The solvent was removed under reduced pressure. To remove all residual pyridine, toluene (50 mL) was added and evaporated again. The resulting oil was dissolved in ether and cooled on ice. Meanwhile, 50 mL acetic acid which contained 5 mL HCl was saturated with gaseous HCl, on ice. The ether solution was added to the acetic acid and the HCl gas was passed through until white crystals were formed. The crystals were filtered off and washed with a cold mixture of 50 % ether and 50 % hexane, and dried in vacuo in the presence of P_2O_5 to give 9.29 g (0.021 mol, 28 %) of product.

5.1.2 Synthesis of 2,4-difluoro-5-iodobenzene (2)

In a dry three-neck round bottom flask 1,3-difluorobenzene (1.9 g, 16.67 mmol) was added to trifluoroacetic acid (5 mL) under an atmosphere of argon. The flask was placed into an ice bath and 3.9 g (17 mmol) of *N*-iodosuccinimide was added in small aliquots. After approximately 30 minutes, the ice-bath was removed, the reaction mixture was stirred over night at room temperature, and then the reaction mixture was poured onto ice (50 mL). The product was extracted with hexane (3 x 30 mL), and the combined organic fractions were washed with an aqueous saturated sodium hydrogen sulphite solution and then with brine. The resulting clear and colourless hexane extract was dried over sodium sulphate and the solvent was evaporated under vacuum to give two products. ^{1}H-NMR showed a mixture of 2,4-difluoro-5-iodobenzene and 2,4-difluoro-1,5-diiodobenzene. The mixture could be separated by HPLC on a Nucleosil C-18 column, (250*4.6) mm, water:acetonitrile 30:70 v/v, 2 mL/min. Since the desired compound (2,4-difluoro-5-iodobenzene) is commercially available, this separation was not performed.

^{1}H-NMR (mixture of 2 and 2,4-difluoro-1,5-diiodobenzene): δ 8.09 (t, $J = 7$ Hz, 1 H), 7.68 (ddd, $J = 0.92$; 7.93; 8.55 Hz 1 H), 6.83 (m, 2 H), 6.7 (ddd, $J = 1.22$; 2.75; 7.93 Hz, 1H)

5.1.3 Production of 2,4-difluoro-1-(2-deoxy-3,5-di-*O*-(*p*-chlorobenzoyl)-α-D-ribofuranosyl)benzene and 2,4-difluoro-1-((2-deoxy-3,5-di-*O*-(*p*-chlorobenzoyl)-ß-D-ribofuranosyl)benzene (3,4)

2,4-Difluoro-5-iodobenzene (5 g, 0.04 mol) was added dropwise to a mixture of 0.972 g (0.04 mol) magnesium and one iodine crystal in 75 mL dry THF, while stirring under argon. The resulting mixture was stirred for another hour at 40 °C to allow the formation of the Grignard reagent to complete. Then, 3.665 g (0.02 mol) of dried, ground cadmium chloride was added to the light brown solution. The resulting mixture was heated under reflux for 1 hour. After cooling this solution to room temperature, 10.72 g (0.025 mol) 2-deoxy-3,5-di-*O*-(*p*-chlorobenzoyl)-α-D-ribofuranosyl chloride (1) was added over 1 hour. The reaction mixture was stirred over night at room temperature, quenched by adding an aqueous solution of ammonium chloride, and the reaction mixture was extracted with ether (3 x 50 mL). The combined organic phases were washed with water, brine, and dried over solid sodium sulphate. After filtration, the solvent was removed under reduced pressure, and the residue was purified via flash chromatography with hexane/ethyl acetate (18:1 v/v) as eluent to give 2,4-difluoro-1-(2-deoxy-3,5-di-*O*-(*p*-chlorobenzoyl)-α-D-ribofuranosyl)benzene (7.3 g) and 2,4-difluoro-1-(2-deoxy-3,5-di-*O*-(*p*-chlorobenzoyl)-ß-D-ribofuranosyl]}benzene (900 mg). The α-compound was epimerised after purification to obtain more of the β-compound.

^{1}H-NMR ($CDCl_3$):

α-compound: δ 8.02, 7.69, 7.43, 7.35 (do, *J* = 8.5Hz, 2H each), 7.55 (td, *J* = 8.6, 6.4 Hz, 1H), 6.90 (dd, *J* = 8.8, 7.9 Hz, 1H), 6.82 (ddd, *J* = 11.0, 8.8, 2.6 Hz, 1H), 5.60 (ddd, *J* = 6.4, 3.4, 3.0 Hz, 1H, [H-3']), 5.54 (dd, *J* = 7.0, 4.9 Hz, 1H, [H-1']), 4.70 (td, *J* = 5.2, 3.0 Hz, 1H, [H-4']), 4.61 (dd, *J* = 11.6, 5.2 Hz, 1H, [H-5'a]), 4.55 (dd, *J* = 11.6, 5.2, 1H, [H-5'b]), 2.96 (ddd, *J* = 14.0, 7.0, 6.4 Hz, 1H, [H-2'a]), 2.31 (ddd, *J* = 14.0, 4.9, 3.4 Hz, 1H, [H-2'b]).

β-compound: δ 7.95, 7.89, 7.39, 7.33 (do, *J* = 8.5 Hz, 2H each), 7.40 (m, 1H), 6.80-6.70 (m, 2H), 5.53 (br d, *J* = 6.4 Hz, 1H, [H-3']), 5.37 (dd, *J* = 10.7, 5.2 Hz, 1H, [H-1']), 4.62 (dd, *J* = 11.9, 4.4 Hz, 1H, [H-5'a]), 4.56 (dd, *J* = 11.9, 4.3 Hz, 1H, [H-5'b]), 4.44 (m, 1H, [H-4']), 2.58 (br dd, *J* = 13.7, 5.2 Hz, 1H, [H-2'a]), 2.09 (ddd, *J* = 13.7, 10.7, 6.4 Hz, 1H, [H-2'b]).

5.1.4 Epimerisation of 2,4-difluoro-1-(2-deoxy-3,5-di-*O*-(*p*-chlorobenzoyl)-α-D-ribofuranosyl)benzene

The α-anomer (2.2 g) was dissolved in 21 mL of nitroethane and 2 mL of boron trifluoride diethyl oxide were added under an atmosphere of argon. The resulting solution was stirred for 45 minutes at 110-120 °C. After cooling, the solution was poured into 11 mL cold water and neutralized with saturated, aqueous sodium hydrogen carbonate. The mixture was extracted with ether (3 x 11 mL), the combined organic fractions were washed with water and brine, and the organic fraction was dried over solid sodium sulphate. After filtering, the solvent was removed under reduced pressure and the residue was purified via flash chromatography to give 950 mg of the β-anomer, 520 mg of the α-anomer, and the rest which was a mixture of both anomers.

5.1.5 Production of 2,4-difluoro-5-iodo-1-(2-deoxy-3,5-di-*O*-(*p*-chlorobenzoyl)-ß-D-ribofuranosyl)benzene (5)

Compound 4 (140 mg, 0.31 mmol) was dissolved in trifluoroacetic acid (5 mL) and cooled in an ice-bath. *N*-Iodosuccinimide (140 mg, 0.62 mmol) was added in aliquots over 10 minutes, and the resulting red solution was stirred for 20 h at room temperature. After the reaction was finished, the reaction mixture was poured into 20 mL cold water and extracted with ether (3 x 20 mL). The combined organic extracts were neutralised with 20 mL of saturated aqueous $NaHCO_3$ solution (2 times), reduced with 20 mL of a saturated aqueous $Na_2S_2O_5$ solution (2 times), and washed with brine before drying over anhydrous sodium sulphate. After filtration, the solvent was removed under reduced pressure and the residue was purified via column chromatography using hexane/ether (5:1 v/v) as eluent. Removal of the solvent gave a yellow oil (166 mg, 261 μmol) which was recrystallised from ether-hexane to give **5** as white needles with a melting point of 104 ± 2 °C.

^{1}H-NMR ($CDCl_3$): δ 8.02, 7.99, 7.47, 7.43 (do, J = 8.5 Hz, 2H each), 7.90 (t, J = 7.5 Hz, 1H), 6.80 (dd, J = 9.8, 7.8 Hz, 1H), 5.59 (br d, J = 6.1 Hz, 1H, [H-3']), 5.40 (dd, J = 10.7, 5.2 Hz, 1H, [H-1']), 4.74 (dd, J = 11.9, 4.3 Hz, 1H, [H-5'a]), 4.66 (dd, J = 11.9, 4.0 Hz, 1H, [H-5'b]), 4.52 (ddd, J = 4.3, 4.0, 2.1 Hz, 1H, [H-4']), 2.64 (br dd, J = 14.0, 5.2 Hz, 1H, [H-2'a]), 2.10 (ddd, J = 14.0, 10.7, 6.1 Hz, 1H, [H-2'b]).

5.1.6 Production of 2,4-difluoro-5-iodo-1-(2-deoxy-β-D-ribofuranosyl)benzene (5-IDFPdR) (6)

Compound **5** (140 mg, 0.24 mmol) was dissolved in methanol (5 mL), 47 mg (0.87 mmol) of sodium methoxide was added, and the resulting solution was stirred for 20 minutes at room temperature. This reaction mixture was quenched with solid ammonium chloride, the solvent was removed under reduced pressure, and the residue was extracted with ethyl acetate. After filtration, the solvent was removed under reduced pressure, and the residue was purified via flash chromatography using hexane:ethyl acetate (1:1-1:1.5 v/v) as eluent to give **6** as a white solid (55 mg, 0.15 mmol) with a melting point of 70 ± 2 °C.

^{1}H-NMR ($CDCl_3$): δ 7.83 (t, J = 7.4 Hz, 1H), 6.83 (dd, J = 10.1, 7.6 Hz, 1H), 5.29 (dd, J = 10.1, 5.8 Hz, 1H, [H-1']), 4.47 (ddd, J = 6.4, 3.0, 1.8 Hz, 1H, [H-3']), 4.02 (ddd, J = 4.9, 4.3, 3.0 Hz, 1H, [H-4']), 3.86 (dd, J = 11.6, 4.3 Hz, 1H, [H-5'a]), 3.79 (dd, J = 11.6, 4.9 Hz, 1H, [H-5'b]), 2.33 (ddt, J = 13.4, 5.8, 1.8 Hz, 1H, [H-2'a]), 1.99 (ddd, J = 13.4, 10.1, 6.4 Hz, 1H, [H-2'b]), 1.89 (br s, 2H, OH)

5.1.7 Separation of 2,4-difluoro-1-(2-deoxy-3,5-di-*O*-(*p*-chlorobenzoyl)-α-D-ribofuranosyl)benzene and 2,4-difluoro-1-(2-deoxy-3,45-di-*O*-(*p*-chlorobenzoyl)-ß-D-ribofuranosyl)benzene via HPLC

A mixture of 2,4-difluoro-1-(2-deoxy-3,5-di-*O*-(*p*-chlorobenzoyl)-α-D-ribofuranosyl)benzene and 2,4-difluoro-1-(2-deoxy-3,5-di-*O*-(*p*-chlorobenzoyl)-ß-D-ribofuranosyl)benzene (270 mg) were dissolved in a small volume of ethyl acetate. An Econosil silica column, length 250 mm, inner diameter 10 mm was used for separation. The separation was performed using 91 % hexane and 9 % ethyl acetate as eluent with a flow of4 mL/min.. The separation was performed repeatedly with small volumes of the mixture. Under these conditions the ß-product has a retention time of 7.8 to 9 minutes and the α-product has a retention time of 9.2 to 11 minutes. Both fractions were collected and the solvents were removed under reduced pressure to yield 100 mg of pure α-product as a clear oil and 25 mg of pure ß-product as white crystals. Separation of the entire mixture was not completed.

6. Synthesis of 5-[^{124}I]iodo-2,4-difluoro-1-(2-deoxy-ß-D-ribofuranosyl)benzene

6.1 Materials and methods

The labelling of 5-iodo-2,4-difluoro-1-(2-deoxy-ß-D-ribofuranosyl)benzene (5-IDFPdR) with [^{124}I]iodine was performed as an isotope exchange reaction. The reaction procedures used are illustrated in the following scheme:

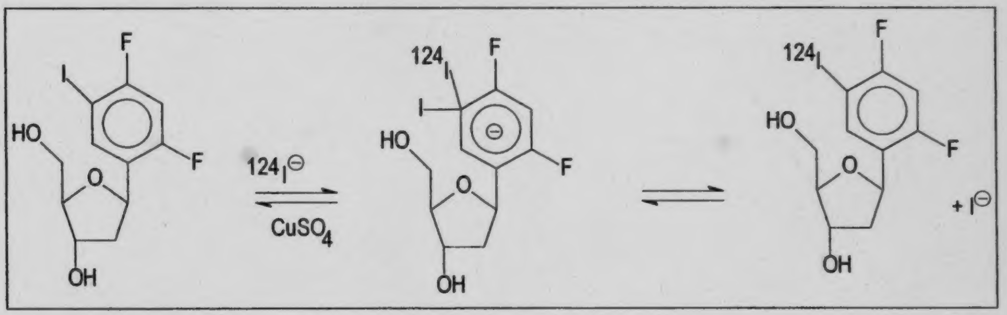

Fig. 12. Schematic depiction of the isotope exchange reaction in the system 5-IDFPdR/^{124}I

5-IDFPdR was dissolved in methanol. Copper sulphate, in water, ammonium sulphate, in water, and the required amount of [^{124}I]iodine in sodium hydroxide was added. This reaction mixture was heated in a closed reaction vial attached to a syringe filled with activated carbon for ventilation. C-18 cartridges from Waters were used to purify the product. These cartridges are short reversed phase columns, which can be used to purify small sample volumes without huge technical equipment. The filling material is prepared for separation by passing a small volume of methanol (10 mL) slowly through the cartridge. Then the cartridge is washed with a small volume of water (10 ml). After that the cartridge is ready to be used. The purification was checked via high performance chromatography to ensure the purity of the product and to ensure no product was lost during the washing procedure of the cartridge.

This methodology is similar to a typical isotope exchange reaction described in the literature for isotope exchange on aromatic systems. [69] To optimise the radiochemical yield, the reaction procedure was examined by varying reaction parameters that included temperature, concentration of the precursor, concentration of NaOH, and reaction time.

6.1.1 Dependency of the reaction upon temperature

The reaction was performed as follows:

5-IDFPdR (14 mg) was dissolved in 1 mL methanol. Aliquots of this solution (100 μL) were placed in separate reaction vials. To these solutions were added 100 μL $CuSO_4$ solution [0.36 mM in water], 100 μL $(NH_4)_2SO_4$ solution [3.6 mM in water] and the appropriate amount of [^{123}I]NaI in 0.004 M NaOH (total volume for each reaction 20 μL) each. The reaction vials (1 mL volume) were closed, the radioactivity was measured and the solvent was evaporated under a stream of dry nitrogen. The radioactivity was checked again to determine if any radioactive iodine had evaporated during the drying procedure. The vials were heated at different temperatures for 2 hours. The reaction vials were attached to syringes filled with activated carbon to trap any gaseous radioactivity. Radioactivity trapped in the syringe is due to the formation of [^{123}I]I_2 which sublimes even at room temperature, or [^{123}I]HI, which is highly volatile. Separation was performed via C-18 cartridges.

The cartridge was activated with 10 mL methanol and afterwards washed with 10 mL of water. Then the reaction solution was added and the cartridge was first flushed with 10 mL of water and then eluted with 4 mL of methanol, and air (10 mL) was passed through the cartridge. The water fraction contained iodide while the methanol fraction contained the labelled product, which was determined via HPLC using the following HPLC conditions:

- Solvent: water:methanol (45:55 v/v)
- Column: Partisil ODS 3, 10 μM, (50 X 8) cm
- Flow (mL/min): 4

The product peak was detected via UV at 254 nm and a radioactivity detector (NaI crystal 2 inches). The retention time of the product peak was 6.89 min while iodide eluted after 2 minutes.

6.1.2 Dependency of the reaction upon the concentration of precursor

The reaction was performed as follows:

5-IDFPdR (14 mg) was dissolved in 1 mL of methanol. From this solution, 10 to 100 μL aliquots were placed in separate reaction vials. All vials were adjusted to a total volume of 100 μL. To these solutions were added 100 μL $CuSO_4$ solution [0.36 mM in water], 100 μL $(NH_4)_2SO_4$ solution [3.6 mM in water], and the appropriate amount of [^{123}I]NaI in 0.004 M NaOH (total volume for each reaction 20 μL) each. The reaction vials (1 mL volume) were closed and the radioactivity was measured. During all reactions, the reaction vials were ventilated by syringes filled with activated carbon. The vials were heated to 120 °C for 2 hours prior to separation performed via C-18 cartridges as described previously (see temperature dependency).

6.1.3 Dependency of the reaction upon the amount of sodium hydroxide

The reactions were performed as follows:

5-IDFPdR (14 mg) was dissolved in 1 mL methanol. From this solution, 100 μL aliquots were placed in separate reaction vials. To each vial was added 100 μL $CuSO_4$ solution [0.36 mM in water], 100 μL $(NH_4)_2SO_4$ solution [3.6 mM in water], and the appropriate amount of [^{123}I]NaI in 0.004 M NaOH (total volume for each reaction 20 μL) each. Also various volumes of a 0.01 M NaOH solution were added. Since all reaction mixtures became dry during the course of the reaction, it was not necessary to adjust the reaction vials to the same volume. The reaction vials (1 mL volume) were closed and the radioactivity was measured. During all reactions the reaction vials were ventilated by syringes filled with activated carbon. Each vial was heated to 120 °C for 2 hours. Separations were performed via C-18 cartridges as described previously (see temperature dependency).

6.1.4 Time dependency

The reaction scheme for the synthesis of 5-[^{124}I]IDFPdR is displayed in Figure 12.

The reaction was performed as follows:

To a solution of 5-IDFPdR (100 µl of a solution containing 14 mg / 1 mL methanol) was added 100 µL $CuSO_4$ solution [0.36 mM in water], 100 µL $(NH_4)_2SO_4$ solution [3.6 mM in water], and the appropriate amount of [^{124}I]NaI in 0.004 M NaOH. The reaction vial (1 mL volume) was closed and the radioactivity was measured. For ventilation, a syringe filled with activated carbon was attached to the lid of the reaction vessel. Vials were then heated to 140 °C, 120 °C and 85 °C for different time periods. The time periods were from 5 to 240 minutes. The product was purified via C-18 cartridges.

6.2. Results and discussion of the acquired reaction parameter data:

6.2.1 Temperature dependency

The dependency of the radiochemical yield of the reaction system 5-IDFPdR/^{123}I with respect to temperature is displayed in Figure 12. The radiochemical yield was calculated using the following formula:

Y = (radioactivity of the product at the end of the reaction / total amount of radioactivity at the beginning of the reaction)* 100

Usually both activities used in the formula need to be corrected for decay. When the time interval between the two measurements is short compared to the half-life of the nuclide used in the reaction, the decay correction can be ignored. A table showing the results for the temperature dependency of the iodination reaction is provided in Appendix B.

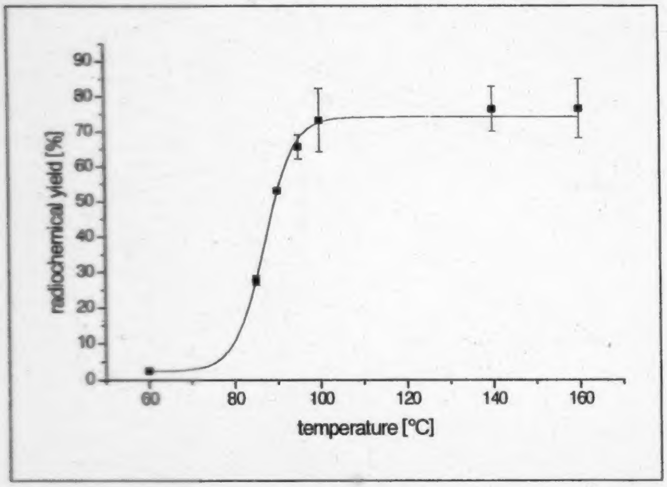

Fig. 13. Temperature dependency of the reaction of $[^{123}I]I^-$ with 5-IDFPdR, reaction time was 2 hours. The data are for n = 3; ± S.D. A Boltzmann fit from Origin 6.1 was applied to fit the solid line.

The results show that the radiochemical yield at 60 °C is only 2.4 %. The radiochemical yield increases slowly up to a temperature of 80 °C at which time it increases rapidly until a plateau of about 76 % radiochemical yield is reached at a temperature of 100 °C. Increasing the temperature to 160 °C did not increase the radiochemical yield. These data indicate the highest radiochemical yields under the chosen conditions require a minimum temperature of 100 °C since temperatures below 80 °C provide very low radiochemical yields. The temperature parameter selected for the following experiments was 120 °C to insure that the reactions were performed in an optimum temperature range.

6.2.2 Dependency of the reaction on the amount of precursor

The curve determined for the radiochemical yield of the reaction of $[^{123}I]I^-$ with 5-IDFPdR at a temperature of 120 °C and a reaction time of 2 hours as a function of the dependency on the amount of precursor (5-IDFPdR) is displayed in Figure 14. The radiochemical yield increases very rapidly even for low amounts of the precursor. The radiochemical yield reaches a plateau at about 66 %, where the precursor amount is about 0.5 µmol (0.17 mg). Accordingly, a precursor weight of 1.4 mg was chosen as the precursor weight parameter to insure that the reactions were performed in an optimum range of precursor concentration. A table showing the results for the dependency of the reaction on the amount of the precursor is presented in Appendix B

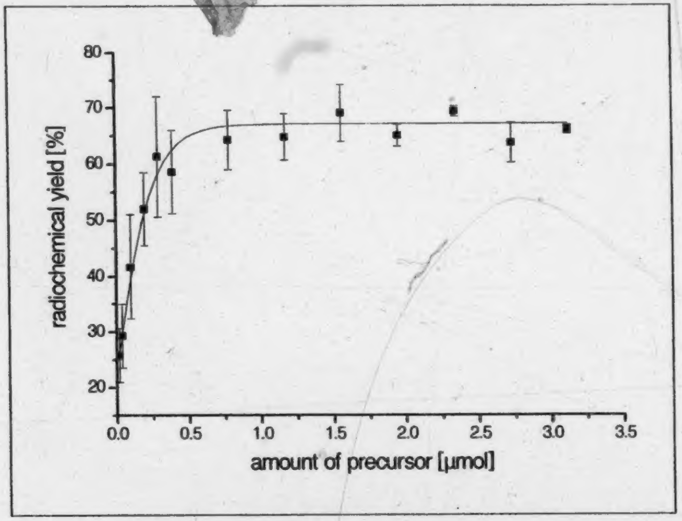

Fig. 14. Dependency of the reaction of $[^{123}I]I^-$ with 5-IDFPdR upon the concentration of 5-IDFPdR when the reaction time was 2 hours, and the reaction temperature was 120 °C. The data are for n = 3; ± S.D. A Boltzmann fit from Origin 6.1 was applied to fit the solid line.

6.2.3 Dependency of the reaction upon amount of NaOH

The radiochemical yield for the reaction of $[^{123}I]I^-$ with 5-IDFPdR at a temperature of 120 °C and a reaction time of 2 hours with respect to the dependency of the amount of sodium hydroxide in the reaction vessel during the reaction is displayed in Figure 15. The curve shows that the radiochemical yield is not influenced by NaOH up to an amount of about 20 µg. When the weight of sodium hydroxide is higher than 20 µg, the radiochemical yield decreases rapidly. When 43 µg of sodium hydroxide is present in the reaction mixture, very little iodine-exchange labelling occurs. Therefore, controlling the amount of sodium hydroxide during the reaction is very important. With higher amounts of sodium hydroxide, which can happen if another iodine isotope is used (e.g. $^{131}I^-$ from Amersham in 0.1M NaOH), the radiochemical yields can decrease drastically. To avoid such a decrease in radiochemical yield, more buffer is needed or the reaction needs to be optimised with another, stronger buffer system (e.g. $(NH_4)HSO_4$.[69]). A table showing the results for the dependency of the iodination reaction upon the amount of NaOH is attached in Appendix B.

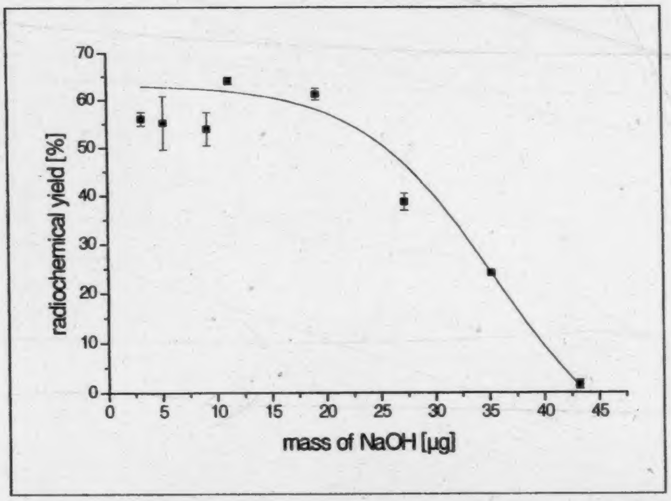

Fig. 15. Dependency of the reaction of $[^{123}\text{I}]\text{I}^-$ with 5-IDFPdR upon the weight of NaOH when the reaction time is 2 hours, and the reaction temperature was 120 °C. The data are for n = 2; ± S.D. A Boltzmann fit from Origin 6.1 was applied to fit the solid line.

6.2.4 Time dependency

The dependency of the radioactive yield with respect to reaction time for the iodine-exchange reaction 5-IDFPdR/^{124}I is displayed in Figure 16. The tables of results for the time dependency of the iodination reaction are attached in Appendix B.

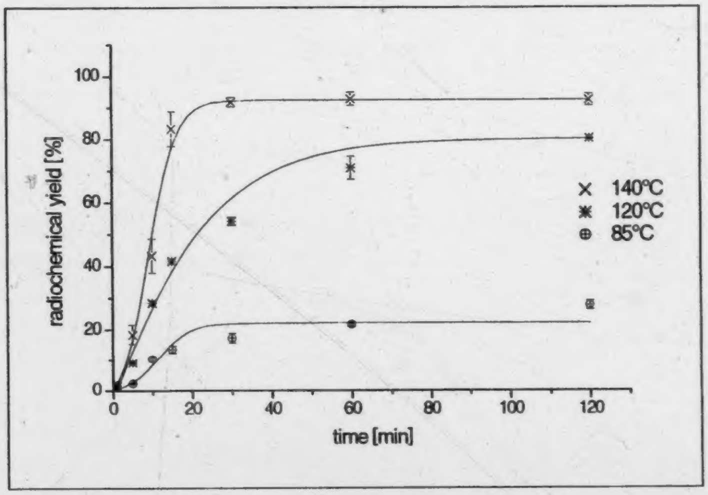

Fig. 16. Dependency of the reaction of $[^{123}\text{I}]\text{I}^-$ with 5-IDFPdR with respect to time at three different reaction temperatures (85 °C, 120 °C and 140 °C). The data are for n = 2; ± S.D. A Boltzmann fit from Origin 6.1 was applied to fit the solid lines.

The results show that there is a fast increase in radiochemical yield during the first 10 minutes for the 140 °C reaction temperature. After 20 minutes, a plateau is reached at about 90 % radiochemical yield. The radiochemical yield here is higher than in the temperature dependency curve for 140 o C. This is to bee seen in the influence of sodium hydroxide on the radiochemical yield. The experiments for the temperature dependency curve were performed with a slightly higher amount of sodium hydroxide than the time dependency curves. When the reaction temperature is 120 °C, the curve increases more slowly and the radiochemical yield, even at longer reaction times, is lower than for a reaction temperature of 140 °C. A plateau at about 75 % radiochemical yield is reached after 60 minutes. For a temperature of 85 °C, the curve increases even more slowly and the radiochemical yield is still lower. Nevertheless, a plateau at about 22 % radiochemical yield is reached after 60 minutes. From these radiochemical yield curves, it is possible to determine the activation energy of this reaction. An isotope exchange reaction follows first-order kinetics (see chapter 1.1.3). The equation for the speed of such a reaction is equivalent to:

$[C] = [B_0]*(1-e^{-k't})$ **formula: 1.1.3-2**

$[C]$ = concentration of product
$[B_0]$ = starting concentration of the radionuclide
k' = rate constant
t = reaction time

Formula 1.1.3-2 can therefore be illustrated as:

$\ln ([^{123}I]/[^{123}I_0]) = k'*t$ **formula: 6.2.4-1**

$[^{123}I]$ = concentration of ^{123}I at time point t
$[^{123}I_0]$ = starting concentration of ^{123}I

for the labelling of 5-IDFPdR with n.c.a ^{123}I.

The concentration of ^{123}I at time point t is equivalent to:

$[^{123}I] = [^{123}I_0] - [C]$ **formula: 6.2.4-2**

The insertion of formula 6.2.4-2 into formula 6.2.4-1 gives:

$\ln([^{123}I_0] - [C])/[^{123}I_0] = k'*t$ or **formula: 6.2.4-3**

$\ln(1 - [C]/[^{123}I_0]) = k'*t$ **formula: 6.2.4-4**

which is equivalent to:

$\ln(1 - \text{radiochemical yield}) = k'*t$ **formula: 6.2.4-5**

A graph of ln (1 - radiochemical yield) plotted against the reaction time will lead to a linear function with the slope of -k'. The temperature dependency of the reaction speed is given by the temperature dependency of the rate constant. The rate constant increases exponentially with increasing temperature. This is expressed usually by the following formula:

$k = A * e^{-b/T}$ **formula: 6.2.4-6**

A and b are empirically determined constants.

According to Arrhenius, the constant b can be replaced by $-E_A/R$. E_A is equivalent to the activation energy and R is equivalent to the general gas constant
($R = 8.314$ J/[°K mol]).
Therefore, formula 6.2.4-6 gives:

$k = A * e^{-E_A/(R * T)}$ **formula: 6.2.4-7**

Finding the logarithm of formula 6.2.4-7 it leads to:

$\ln k = \ln A - E_A/(R * T)$ **formula: 6.4-8**

The graph showing a plot of ln k against 1/T will lead to a linear function with the slope of $-E_A/R$. The activation energy can be determined graphically in this way. With two rate constants for one reaction, measured for different temperatures, the activation energy can be determined by the following formulae:

For T_1 : $\ln k_1 = \ln A - E_A/(R * T_1)$ **formula: 6.2.4-9**

For T_2: $\ln k_2 = \ln A - E_A/(R * T_2)$ **formula: 6.2.4-10**

Subtraction of formula 6.2.4-10 from formula 6.2.4-9 leads to:

$$\ln (k_1/k_2) = E_A/R * (1/T_2 - 1/T_1)$$ **formula: 6.2.4-11**

or rather

$$E_A = R * T_1 * T_2/(T_1 - T_2) * \ln (k_1/k_2)$$ **formula: 6.2.4-12**

To determine the rate constants of the reaction, the average of the radiochemical yield for one temperature at the same time point is used with formula 6.2.4-5. Then ln (1-Y) is displayed against time to give a linear function with the slope of -k. In Figure 17 the linear functions for the temperatures of 85 °C, 120 °C and 140 °C are displayed. The parameters of these linear functions were calculated by linear regression:

T (95 °C):

$\ln(1-y/100) = -0.02885 - 0.00108 * t$

T (120 °C):

$\ln(1-y/100) = -0.16326 - 0.00485* t$

T (140 °C):

$\ln(1-y/100) = 0.04597 - 0.03994 * t$

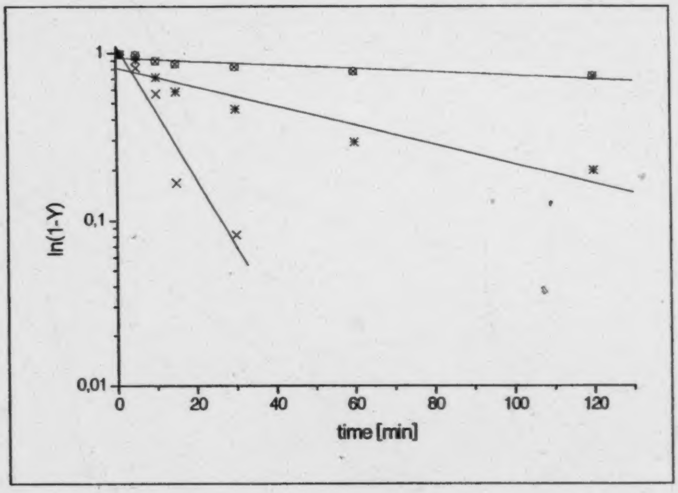

Fig. 17. Linear functions for determination of the rate constants of the 5-[^{123}I]IDFPdR synthesis for three temperatures (⊗: 85 °C, T: 120 °C, ×: 140 °C). Linear regression was applied to fit the curves.

According to Arrhenius, the activation energy can be determined by having the reaction going at two or more different temperatures. In this work three temperatures are used. Thus rate constants for three temperatures are obtained and the activation energy can be calculated using the rate constants in formula 6.2.4-12 for all possible combinations of the three values. The mean value for the activation temperature is:

$$EA = 105.37 \text{ kJ/mol}$$

A graphical solution for determining the activation energy is to plot ln k against the absolute temperatures. This leads to a linear function with the slope of - E_A/R. Multiplying the slope of the linear function with $R = 8.314$ J/(K mol) gives the activation energy.

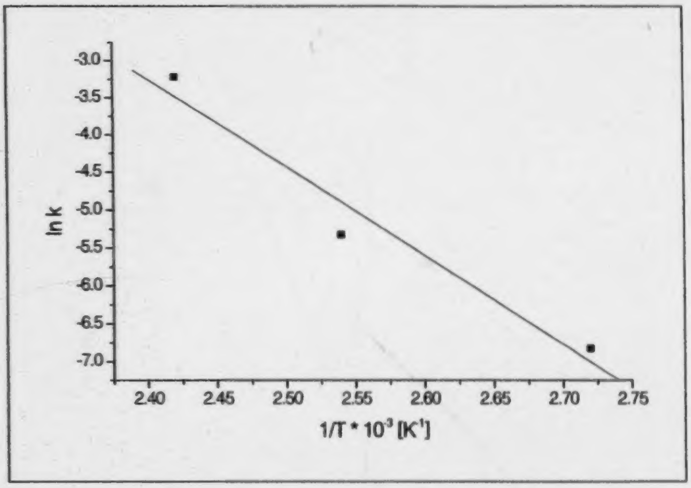

Fig. 18. Arrhenius plot for the 5-[^{123}I]IDFPdR synthesis. Linear regression was used to fit the curve. The slope is -11743.39.

The plot of the rate constants (as ln k) against the reciprocal temperature (in K) for the isotope exchange reaction is given in Figure 18. From the slope of the curve, the activation energy can be calculated by multiplying it by the general gas constant 8.314 J/(K mol). The slope is given by the linear regression:

$$\ln k = 24.94 - 11743.39 * 1/T$$

and

$$E_A = 11743.39 * 8.314 = 97.63 \text{ kJ/mol}$$

7. Animal Experiments

7.1 Materials and methods

7.1.1 Tracer production for in vivo pharmacokinetic studies

The labelling of 5-IDFPdR and *cycloSal*-5-IDFPdR with ^{125}I$^-$ was done by William Sun. The reaction was performed as a copper catalyzed isotope exchange reaction in a buffered system.

7.1.2 Application of tracer for in vivo pharmacokinetic studies.

Adult male Sprague Dawley rats (Health Sciences Laboratory Animal Services, University of Alberta) were used for the pharmacokinetic studies. The rats were handled in accordance with guidelines established by the Canadian Council of Animal Care. The experimental and surgical protocols were approved by the University of Alberta Health Sciences Animal Welfare and Policy Committee. For the studies, external right jugular vein cannulae were implanted one day before dosing the animals with either 5-[^{125}I]-5-IDFPdR)or with (S$_P$)-*cyclo*-(3-methylsaligenyl)-5'-*O*-[1'-(2,4-difluoro-5-iodophenyl)-2'-deoxy-*β*-D-ribo-furanosyl]phosphate (*cyclosal*-5-IDFPdR). Implantation of the cannulae into the animals was performed by Dr. P. Khalili. The animals were dosed with 46.8 μg/kg of 5-[^{125}I]IDFPdR and 55.09 mg/kg of the *cycloSal* derivative, respectively. The catheter was washed with 150 μL blood previously taken from the rat and with 300 μL saline solution after dosing. Following a protocol from earlier experiments with cold compound, blood samples were taken after 1, 5, 10, 15, 30, 45, 60, 90, 120, 150 and 180 minutes from the first animal. This time study showed that samples should be collected more frequently at early time points. Therefore in the following experiments samples were taken after 1, 3, 5, 7, 10, 15, 30, 45, 60, 90, 120, 180 and 1440 minutes. After collection of each sample, the catheter was washed with 300 μL saline solution. The samples were stored on ice prior to work up. The urine and the faeces of the animals were collected for 24 hours (metabolic cages). After 24 hours, the animals were sacrificed, 50 μL of each blood sample was taken for counting, and 200 μL of the blood was added to 650 μL of ice-cold acetonitrile to precipitate proteins and macromolecules from blood. The samples were centrifuged and the supernatant was filtered through a 0.45 μ syringe filter. An aliquot of serum (50 μL) was taken for counting, and an aliquot (100 μL) of the serum was used for HPLC analyses. HPLC conditions for 5-IDFPdR analyses were:

- column: reverse phase Radial-Pak™ cartridge column (8NVC184μ, Nova-Pak, C-18; Waters) with guard column of the same material;
- flow: 1 mL/min;
- solvent system: 45: 55 water: acetonitrile v/v.

The retention time for the unchanged labelled 5-IDFPdR was 12.5 minutes. A broad iodide peak was eluted just before the labelled 5-IDFPdR peak. Fractions during each run were collected according to the UV absorption peaks on the HPLC chromatogram.

The volume of the collected urine was measured and documented, and 3 samples of urine collected (50 μL each) were taken for counting. Two samples, 25 μL each were subjected to HPLC analysis. The conditions for separation were identical to those described for the serum samples.

HPLC conditions for *cycloSal*-5-IDFPdR were:

- column: reverse phase Radial-Pak^{TM} cartridge column (8NVC184μ, Nova-Pak, C-18; Waters) with guard column of the same material;
- flow: 1 mL/min;
- solvent system: 48: 52 water: acetonitrile v/v.

The retention time of labelled *cycloSal*-5-IDFPdR was 27-29 minutes. A broad radioactive peak was observed from 2-10 minutes, probably the labelled monophosphorylated 5-IDFPdR and iodide. Labelled 5-IDFPdR had a retention time of 13-15 minutes. This metabolite was identified by co-injection with unlabelled 5-IDFPdR. Fractions during each HPLC analysis were collected. The fractions were collected that coincided with the UV absorption peaks present in the HPLC chromatogram. The volume of the collected urine was measured and documented, and 3 samples of urine (50 μL each) were taken for counting. Two samples (25 μL each) were analyzed by HPLC. The conditions for separation were identical to those described previously for the serum samples.

7.2 Results and Discussion

The ~~mean~~ plasma levels of 5-[^{125}I]IDFPdR and *cycloSal*-5-IDFPdR (% i.d./mL plasma), as a function of time after i.v. bolus injection to rats, are plotted in Figure 19. Following the dosing, the levels of radioactivity of 5-[^{125}I]IDFPdR are rapidly decreasing in the first five minutes to a level below 1 % of the injected dose. For *cycloSal*-5-IDFPdR, the radioactivity level in plasma, after i.v. bolus injection, decreased rapidly from approximately 8 % after one minute to a level of approximately 4 % after 5 minutes. After 5 minutes the radioactivity level decreased slowly with approximately 0.5 % of the injected dose remaining in plasma at 24 hours. On average about 56 % of the administered 5-[^{125}I]IDFPdR radioactivity was recovered in urine collected over 24 hours, and another 3 % of the injected dose was found in faeces collected over 24 hours. On average about 25 % of the administered dose of *cycloSal*-5-IDFPdR radioactivity was recovered in urine collected over 24 hours, and another 2 % of the injected dose was recovered in faeces collected over 24 hours.

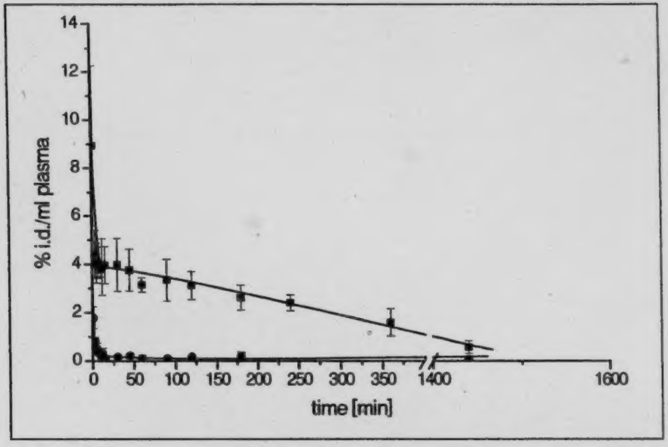

Fig. 19. Plasma clearance of 5-[^{125}I]IDFPdR and *cycloSal*-5-IDFPdR as a function of time after i.v. bolus administration (•:5-[^{125}I]IDFPdR ■: *cycloSal*-5-IDFPdR). The data are for n = 3, ± S.D..

The plasma samples collected after administration of both compounds were analysed to quantitate the amount of unchanged compound. The radioactivity of 5-[^{125}I]IDFPdR (%) and its metabolites referring to the total radioactivity of each HPLC fraction as a function of time is plotted in Figure 20. These data clearly show that the percentile amount of the unchanged compound in plasma decreases rapidly in the first hour from approximately 87 % down to 11 %, and that this decline is followed by an increase where the percentage of radioactivity has returned to the original amount after 24 hours. Naturally, the radioactivity relative to the total injected dose after 24 hours is much lower than at the beginning, but the amount of unchanged compound in this last HPLC fraction was as high as 78 % relative to the total radioactivity present in this plasma fraction. This observation could be due to hepato-biliary recirculation. In a paper published in 2002 by P. Khalili et al., cold 5-IDFPdR was evaluated in rats. [70] Preliminary results from this study suggested that one route of excretion of the intact compound is via bile after i.v. and oral dosing (53.4 mg/kg) of the animals. These data support the theory of hepato-biliary recirculation. The metabolites present in the HPLC chromatogram were all more polar than the parent compound as indicated by their shorter retention times on HPLC under the conditions used for separation. Two radioactive metabolites were found. These metabolites were not identified. The first metabolite eluting from the HPLC column could be free iodide. However, free iodide would accumulate in thyroid tissue. Biodistribution studies in mice showed only low radioactivity concentration in thyroid tissue of mice for labelled 5-IDFPdR as did gamma camera imaging of rats. These results would exclude free iodide as a metabolite in vivo. In an in vitro study of deiodination, this metabolite accounted for about 7 % of the radioactivity when 5-[^{125}I]IDFPdR was added to rat plasma; surprisingly, this amount did not change over approximately 3 weeks.

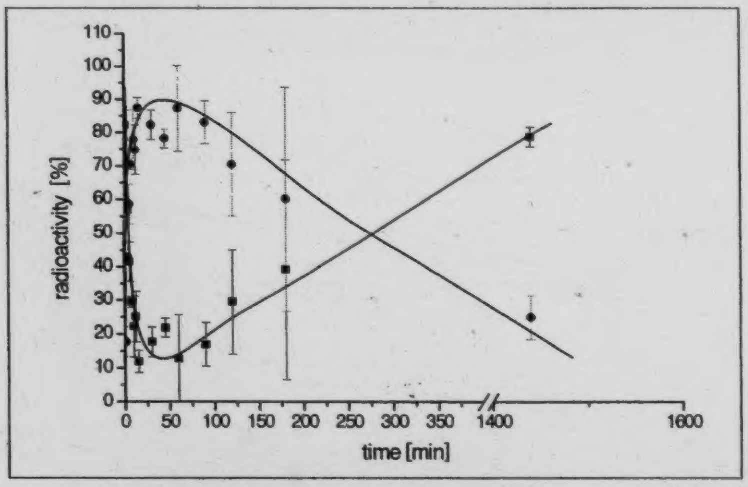

Fig. 20. 5-[^{125}I]IDFPdR and its metabolites as a percent (%) of the total radioactivity in plasma analysed by HPLC. Rats received i.v. injections of 5-[^{125}I]IDFPdR via catheter. The data are for n = 3, ± S.D. (●: Metabolites of 5-[^{125}I]IDFPdR, ■: 5-[^{125}I]IDFPdR.)

The radioactivity of the metabolite fraction in plasma is opposite to the radioactivity due to unchanged 5-[^{125}I]IDFPdR. For example, when the amount of unchanged compound (5-[^{125}I]IDFPdR)is decreasing, the relative amount of metabolites is increasing.

The radioactivity of *cycloSal*-5-IDFPdR (%) relative to the total radioactivity of each HPLC fraction as a function of time is plotted in Figure 21. The injected compound vanishes completely from plasma within the first 5 minutes, only to reappear after 2 hours. Following this time, the radioactivity due to *cycloSal*-5-IDFPdR increases once again, reaching approximately 12 % after 24 hours. Once again, this could be an indication of hepato-biliary recirculation or absorption and desorption processes in fatty tissue, since the *cycloSal* compound is even more lipophilic than 5-IDFPdR.

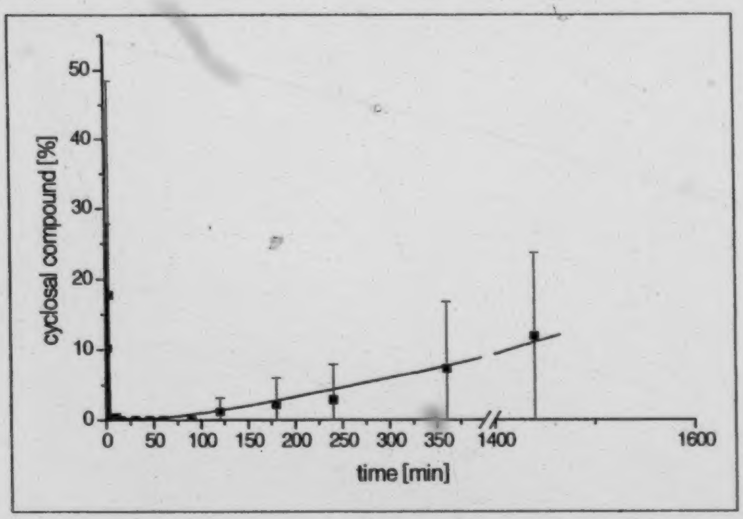

Fig. 21. Radioactivity of *cycloSal*-5-IDFPdR as a percent (%) of the total radioactivity in plasma fractions analysed by HPLC. Rats received i.v. injections of *cycloSal*-5-[^{125}I]IDFPdR via catheter. The data are for n = 3, ± S.D.

During HPLC analysis of plasma, three (3) radioactive metabolites were found, all of which were more polar than the parent *cycloSal* compound. The first metabolite eluted from the HPLC column as a broad peak, over several minutes. The second metabolite that eluted was identified as 5-[^{125}I]IDFPdR by co injection of this fraction with unlabelled 5-IDFPdR, both with the same retention time of approximately 13 minutes. The first and third metabolites eluted could not be identified. It is plausible that the first metabolite eluted may be the mono phosphorylated 5-IDFPdR derivative, but this could not be confirmed since an authentic sample for use as a standard reference compound was not available for comparison of their retention times. It also might be that this metabolite is free iodide. However biodistribution studies in mice showed relative low accumulation of radioactivity in thyroid tissue. If this metabolite is free iodide one would expect higher accumulations of radioactivity in thyroid tissue. Furthermore, different HPLC separation conditions would have been necessary for identification of this peak, which was tailing badly as it eluted from the column. The pharmacokinetic parameters acquired in this study are summarised in Table 4. The data were analysed by a non-compartmental model using WinNonlin version 1.1™.

Table 4: Pharmacokinetic parameters for 5-[^{125}I]IDFPdR following i.v. administration to rats, the data are for n = 3, ± S.D.

Parameter	Intravenous dosing, average of 3 animals	Standard deviation
$t_{1/2}$ [h]	0.51	0.14
AUC_{inf} [ng.min/mL]	3689.3	429.8
Cl [mL/min]	0.75	0.12
Vss [L/kg]	0.96	0.18

The elimination half-life after i.v. injection of 5-[^{125}I]IDFPdR was relatively long, the distribution volume is greater than the average total body water in rats (0.7 L/kg), and clearance was low compared with literature data for the unlabelled compound.[70] The large volume of distribution for 5-[^{125}I]IDFPdR suggests that the labelled compound is likely distributed intracellularly. Data reported in the literature were obtained for a relatively high dose of 53.6 mg/kg compared to the low dose that was used in this study (48.7 µg/kg). Selected pharmacokinetic data from the literature and from this study for 5-IDFPdR are summarised in Table 5. The data for the medium doses of 5 mg/kg and 15 mg/kg were obtained using a different model than was used in this work. The data for the medium doses were modelled using a two-compartment model whereas the data for the radioactive compound and the data for the dose of 53.6 mg/kg were modelled using a non-compartmental model. The two-compartment model used to calculate the data for the medium doses of 5 mg/kg and 15 mg/kg did not fit the data obtained for the radioactive compound.

Table 5: Pharmacokinetic properties for unlabelled and labelled 5-IDFPdR in rats after i.v. bolus injection and for the unlabelled compound after oral dosing. The data are for n = 3, ± S.D. at least for the labelled compound.

Parameter	5[^{125}I]IDFPdR (48.7 ug/kg i.v.)	5IDFPdR[113] (5 mg/kg i.v.)	5IDFPdR[113] (15 mg/kg i.v.)	5IDFPdR[70] (53.6 mg/kg i.v.)	5IDFPdR[70] (53.6 mg/kg oral)
$t_{1/2}$ [h]	0.51 (0.14)	0.14 (0.01)	0.13 (0.01)	0.15 (0.02)	0.25 (0.00)
Cl [L/kg/h]	0.75 (0.12)	1.72 (0.06)	1.93 (0.23)	1.23 (0.17)	1.10 (0.01)
Vss [L/kg]	0.96 (0.18)	0.30 (0.03)	0.33 (0.02)	0.34 (0.04)	0.34 (0.03)

A calculation of these parameters for the *cycloSal* derivative with WinNonlin version 1.1^{TM} was not possible by any of the offered methods.

8. Biodistribution

8.1 Materials and methods

8.1.1 Tracer production for in vivo pharmacokinetic studies

The labelling of 5-IDFPdR and cycloSal-5-IDFPdR with $^{125}I^-$ was done by William Sun. The reaction was performed as a copper catalyzed isotope exchange reaction in a buffered system.

8.1.2 Application of tracer for in vivo pharmacokinetic studies.

For biodistribution studies EMT6 tumour cells were injected subcutaneously under the left front leg of male Balb/C mice (20-24 g) (Health Sciences Laboratory Animal Services, University of Alberta) one week prior to injection of labelled 5-IDFPdR or *cycloSal*-5-IDFPdR. Animals were handled in accordance with guidelines established by the Canadian Council of Animal Care. The experimental and surgical protocols were approved by the University of Alberta Health Sciences Animal Welfare and Policy Committee. The handling of the animals was performed by Mrs. Aihua Zhou. After the tumour grew to an appropriate size (0.7 – 1 cc) to carry out the distribution studies, the labelled compound was injected into the tail vein of mice. Following the preselected times after dosing, mice were sacrificed. Three (n = 3) mice were used for each time point. Tissues and/or organs were removed by dissection, their weight was recorded and the amount of radioactivity present was measured. The biodistribution of the radioactivity in the tissues/organs collected was calculated as a % of the injected radioactive dose per gram of tissue or organ.

8.2 Results and discussion

An overview of the biodistribution of 5-[^{125}I]IDFPdR in mice is shown in Figure 22. These data show that the main localization of radioactivity occurred in bile and bladder. Accumulation of radioactivity in the bile indicates a second pathway for elimination of the compound, passing through the liver prior to accumulation in bile fluid and excretion into the intestine. This theory is supported by pharmacokinetic studies data published in 2002. [70] The tumour shows approximately the same concentration of radioactivity as thyroid. There is no real accumulation visible in tumour tissue. The maximum accumulation in tumour was approximately 5 % i.d./g after one hour. The tumour to blood ratio of 2.6 is relatively low. The high levels of radioactivity in stomach (13 % i.d./g), bile (20 % i.d./g) and bladder (16 % i.d./g) during the entire time interval would result in a high background which is undesirable for imaging tumour uptake.

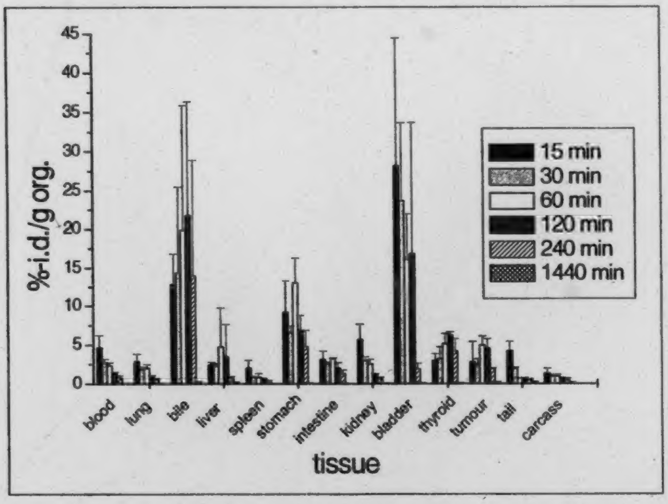

Fig. 22. Biodistribution of 5-[^{125}I]IDFPdR in mice after i.v. bolus into tail vein at different time points. The data are for n = 3, ± S.D

A similar overview for the biodistribution of *cycloSal*-5-IDFPdR shows that radioactivity localised primarily in blood, lung, bile and bladder. Tumour uptake of *cycloSal*-5-IDFPdR is even lower than that observed for 5-[^{125}I]IDFPdR. The high radioactivity level in blood (up to 17 % i.d./g after 15 minutes) resulted in a low tumour to blood ratio that is clearly below 1 for the entire observation interval. The high radioactivity levels in lung, bile and bladder would increase the background radioactivity level that is relevant to imaging studies. Furthermore, the high radioactivity level in lung tissue would deliver a high irradiation dose to the patient. Accordingly, these properties make this *cycloSal* compound unsuitable for diagnostic imaging purposes. Some of the more interesting tissue biodistribution data are discussed separately below. Tables summarising all of the results for the biodistribution study are provided in Appendix B.

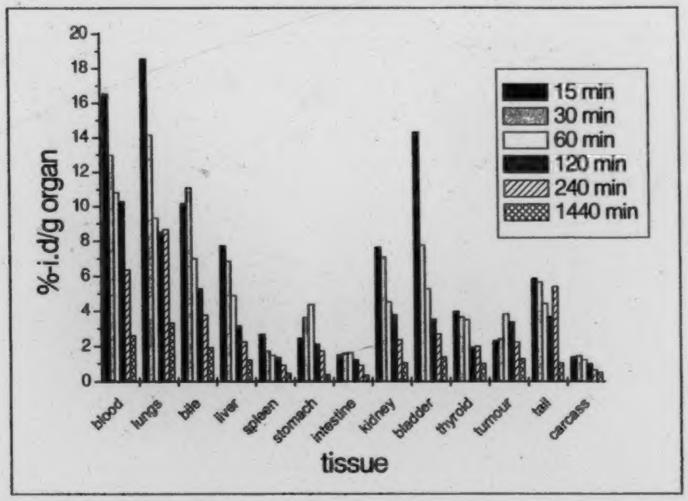

Fig. 23. Biodistribution of *cycloSal*-5-IDFPdR in mice after i. v. bolus into tail vein at selected time points. The data are for n = 3

The blood time curve of 5-[^{125}I]IDFPdR shows a rapid clearance. Within 15 minutes after dosing, only 5 % of the injected dose remains in blood, after 2 hours only 1 % of the injected dose can be measured, and after 24 hours nearly all radioactivity is absent. However, the *cycloSal* derivative shows high radioactivity levels in blood from the beginning. After 15 minutes there is still nearly 17 % of the injected dose in blood, and even after 24 hours there is still 2.6 % of the injected dose in blood. These values indicate that there is strong irreversible binding of the compound to proteins in blood.

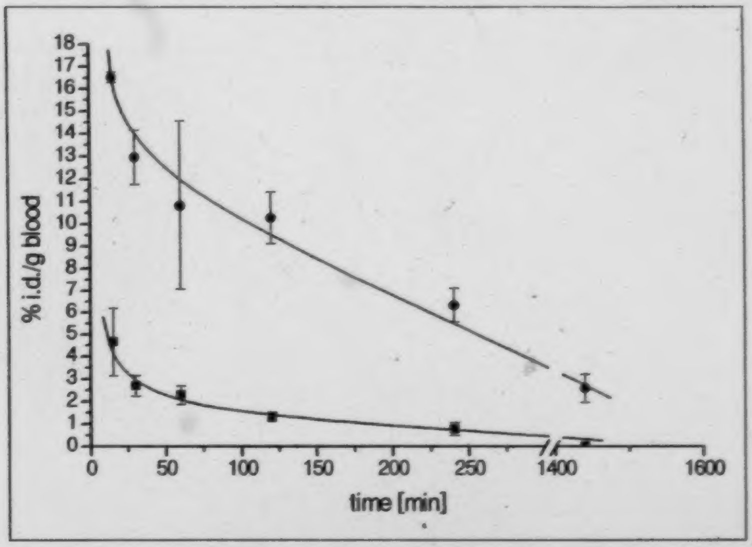

Fig. 24. Biodistribution of 5-[^{125}I]IDFPdR, and *cycloSal*-5-[^{125}I]IDFPdR, in the blood of mice after i.v. bolus into tail vein at preselected time intervals (■:5-[^{125}I]IDFPdR, •: *cycloSal*-5-IDFPdR). The data are for n = 3, ± S.D.

The radioactivity level in thyroid shows an influx of radioactivity two hours after injection of 5-[^{125}I]IDFPdR, which is eliminated during the remainder of the observation interval. One possible explanation for this is deiodination in blood. Irrespective of the mechanism, the level of radioactivity in thyroid did not exceed 6.5 % of the injected dose. This low level of thyroid radioactivity indicates that 5-[^{125}I]IDFPdR has good in vivo stability. On the other hand, this observed wash out of the radioactivity is not characteristic for iodine. Therefore, the radioactivity accumulation might indicate a direct interaction of the labelled compound with thyroid. *cycloSal*-5-[^{125}I]IDFPdR showed no accumulation in thyroid. The course of the time curve follows a typical blood curve which indicates a high in vivo stability of the iodine label of 5-[^{125}I]IDFPdR.

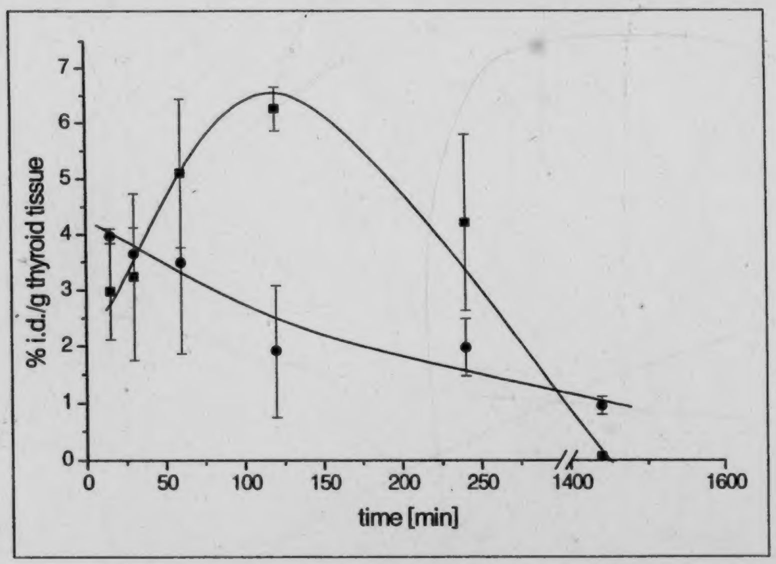

Fig. 25. Radioactivity, at preselected time points, in the thyroid of mice after i.v. bolus injection into tail vein of 5-[^{125}I]IDFPdR or *cycloSal*-5-[^{125}I]IDFPdR (■:5-[^{125}I]IDFPdR, ●: *cycloSal*-5-IDFPdR. The data are for n = 3, ± S.D..

The radioactivity from both compounds decreases over time in the kidneys, as illustrated in Figure 26. The radioactivity in kidney, after injection of *cycloSal*-5-[^{125}I]IDFPdR is slightly higher (app. 2%), relative to 5-[^{125}I]IDFPdR, during the 1440 minute time interval investigated. The observation that the radioactivity level of the *cycloSal* compound in blood is also higher than the radioactivity level of 5-[^{125}I]IDFPdR in blood suggests that this higher radioactivity level in kidneys can be explained by residual blood in the tissue. However, the radioactivity of 5-[^{125}I]IDFPdR in the bladder is higher than the radioactivity of the *cycloSal* derivative in the bladder which indicates a faster renal excretion of 5-[^{125}I]IDFPdR.

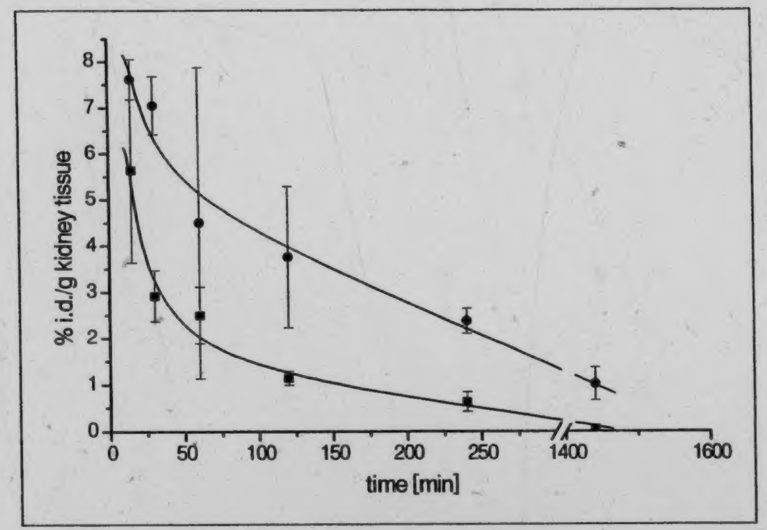

Fig. 26. Radioactivity of 5-[^{125}I]IDFPdR, and *cycloSal*-5-[^{125}I]IDFPdR in the kidney of mice after i.v. bolus into tail vein at preselected time points (■:5-[^{125}I]IDFPdR, •:*cycloSal*-5-IDFPdR). The data are for n = 3, ± S.D..

The radioactivity levels of 5-[^{125}I]IDFPdR, and its *cycloSal* derivative, also decreased over time in lung tissue which is evident from the data in Figure 27. However, the radioactivity of the *cycloSal* derivative in lung tissue is much higher than the radioactivity of 5-[^{125}I]IDFPdR. Also, the radioactivity level of the *cycloSal* derivative remains constant over a 4 hour time interval. In view of the fact that the lung has a very high circulation of blood, and the radioactivity level of the *cycloSal* derivative is high in blood, indicates this could be due to residual blood in the tissue or an absorption effect at the large surface of the alveolar membranes. Also, lung tissue is very lipoidal in nature. As *cycloSal*-5-IDFPdR is very lipophilic it might be absorbed in lung tissue and reabsorbed into blood over time. One must interpret the meaning of this curve cautiously since the standard deviation is quite high. It could also follow a normal wash out curve.

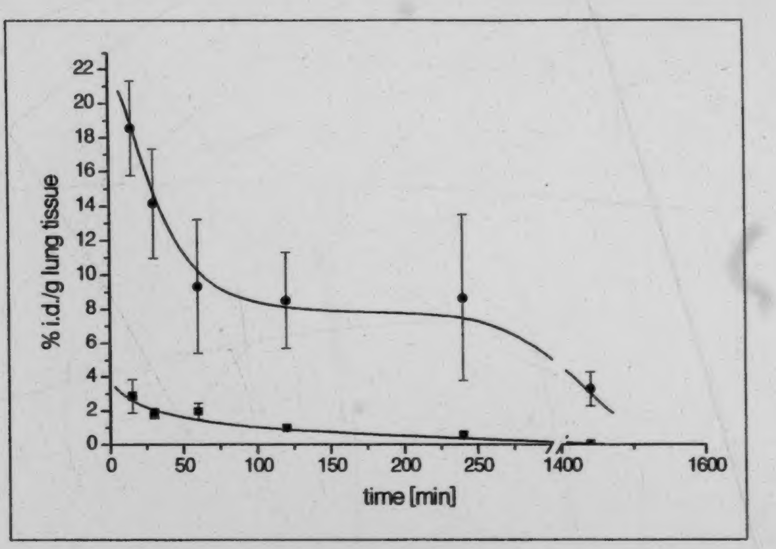

Fig. 27. Biodistribution of radioactivity, after i.v. bolus injection into tail vein of 5-[^{125}I]IDFPdR or *cycloSal*-5-[^{125}I]IDFPdR, in the lung of mice at preselected time points (■:5-[^{125}I]IDFPdR, •: *cycloSal*-5-IDFPdR). The data are for n = 3, ± S.D..

The radioactivity distribution for 5-[^{125}I]IDFPdR, and its *cycloSal* derivative, in liver with respect to time is provided in Figure 28. The radioactivity level of the *cycloSal* derivative follows the blood curve for this compound. The 5-[^{125}I]IDFPdR radioactivity indicates a delayed influx after 1 hour. This indicates that the compound is excreted more slowly from liver than it is transported into liver. However, the standard deviation of these data points is high in comparison to the measured radioactivity level. Once again the data must be considered cautiously.

The radioactivity in bile with respect to time for 5-[^{125}I]IDFPdR shows a similar course to that of the liver curve (see Figure 29) reaching its maximum level at about one hour. This observation might indicate a hepato-biliary metabolic pathway with a slow efflux from liver to bile. Once again, the large standard deviations indicate that further investigations are necessary to clarify this explanation.

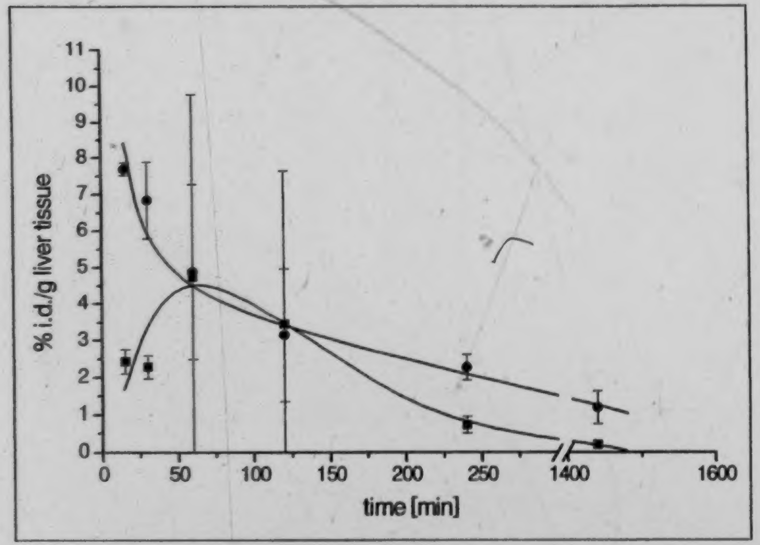

Fig. 28. Biodistribution of 5-[^{125}I]IDFPdR and *cycloSal*-5-[^{125}I]IDFPdR, in the liver of mice after i.v. bolus into tail vein at preselected time points (■:5-[^{125}I]IDFPdR, •:*cycloSal*-5-IDFPdR). The data are for n = 3, ± S.D..

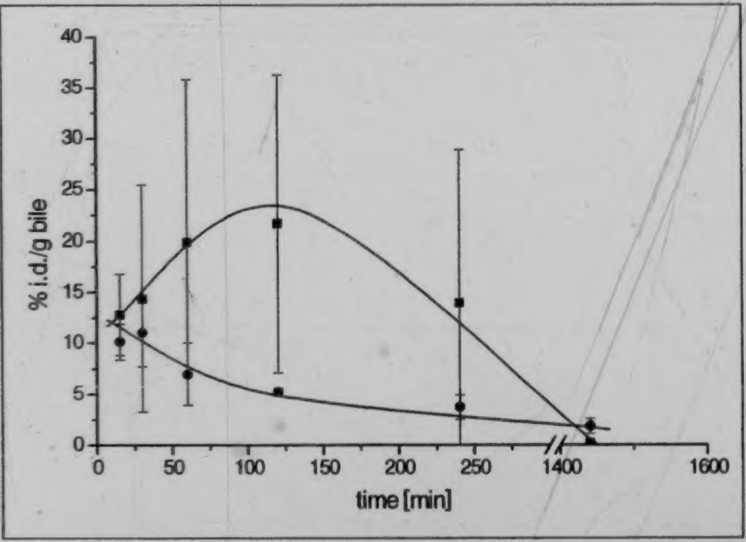

Fig. 29. Biodistribution of 5-[^{125}I]IDFPdR and *cycloSal*-5-[^{125}I]IDFPdR, in the bile of mice after i.v. bolus into tail vein at preselected time points (■:5-[^{125}I]IDFPdR, •:*cycloSal*-5-IDFPdR). The data are for n = 3; ± S.D..

Radioactivity localization, with respect to time, in tumour is shown in Figure 30. Both compounds show a low uptake after one hour. Uptake of the *cycloSal* derivative is approximately 3.5 % i.d./g tissue lower than the uptake of 5-[^{125}I]IDFPdR. 5-[^{125}I]IDFPdR uptake reaches 5 % i.d./g tissue. However, the efflux of 5-[^{125}I]IDFPdR is faster than that of *cycloSal*-5-[^{125}I]IDFPdR. Although the radioactive level for 5-[^{125}I]IDFPdR decreases to nearly zero after 24 hours, the *cycloSal* derivative is still approximately 1.5 % i.d./g tissue. Nevertheless, the tumour /blood ratio for both compounds is very low. For the *cycloSal* derivative, the ratio never exceeds 1, and for 5-[^{125}I]IDFPdR the ratio is approximately 2 at the maximum. Also the high radioactivity levels in most organs will result in a high background if these compounds were to be used for diagnostic imaging purposes.

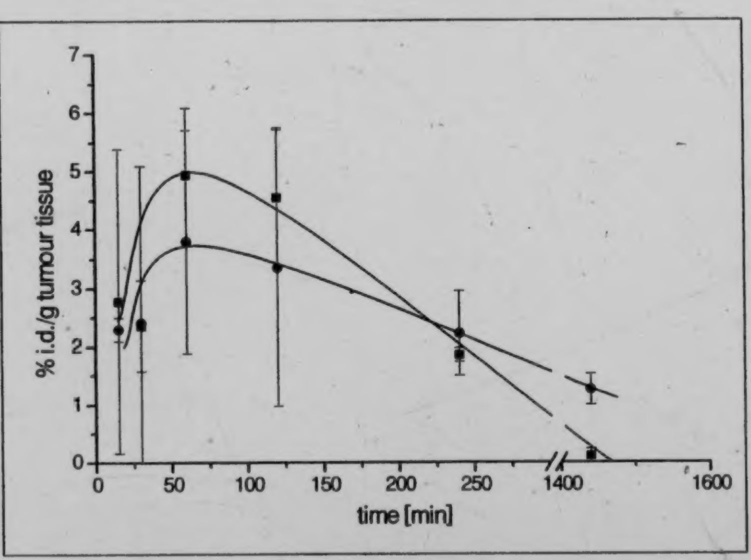

Fig. 30. Biodistribution of 5-[^{125}I]IDFPdR and *cycloSal*-5-[^{125}I]IDFPdR in the tumour of mice after i.v. bolus into tail vein at preselected time points (■:5-[^{125}I]IDFPdR, •: *cycloSal*-5-IDFPdR). The data are for n = 3, ± S.D..

9. Gamma camera images of 5-IDFPdR in vivo

9.1 Materials and methods

9.1.1 Tracer production for imaging studies with 5-[^{123}I]IDFPdR

For gamma camera imaging, 5-IDFPdR was labelled with ^{123}I$^-$. In this iodine exchange labelling reaction, the precursor (0.99 mg) was dissolved in 1 mL of methanol. , This solution (100 μL) was added to 100 μL $CuSO_4$ solution [0.36 mM] in water, and 100 μL $(NH_4)_2SO_4$ buffer [3.6 mM] in water. At this time, 40 MBq [^{123}I]iodide in 20 μL NaOH were added, the reaction vial was closed, and a syringe filled with activated carbon was attached for ventilation. The reaction mixture was then heated at 120 °C for 1 hour. The product was subsequently purified via the C-18 cartridge method described in Chapter 5.1.1. The product was dried and reconstituted in 1 mL of isotonic NaCl solution.

9.1.2 Application of the tracer for imaging studies with 5-[^{123}I]IDFdR

Two male Sprague Dawley rats (Health Sciences Laboratory Animal Services) were anaesthetised with ketamine (90 mg/kg) and xylaxine (10 mg/kg) i.p. and positioned posterior for gamma camera imaging. The animals were handled in accordance with guidelines established by the Canadian Council of Animal Care. The experimental and surgical protocols were approved by the University of Alberta Health Sciences Animal Welfare and Policy Committee. Handling the animals was performed by Mrs. Aihua Zhou. The labelled compound was injected into the tail vein of the animals. One rat, having a body weight of 250 g, was injected with 3.9 MBq of the labelled compound. The other animal, having a body weight of 600 g, was injected with a dose of 3.6 MBq. The first 20 minutes a dynamic scan was performed with 32 frames à 30 seconds. Then static images were acquired after 30, 70, 100 and 130 minutes for rat #1, and after 30, 60, 90 and 120 minutes for rat #2. The rats stayed anaesthetised during the total imaging procedure.

9.2 Results and discussion

The dynamic scan and the first static image obtained for rat #1 (weight 250 g) are shown in Figure 31. Three additional static images are shown in Figure 32. During the dynamic scan the influx of 5-[^{123}I]IDFPdR can be seen. In frame one the tail is still visible while the compound is starting to distribute through the body. However, almost from the beginning accumulation in the region of the intestine is visible. The first static image shows a strong accumulation in the middle part and on the left side of the image, most likely the stomach, intestine and bladder of the rat. Furthermore, there is a very small dark spot on the right side of the image in the neck region of the animal, most likely the thyroid. The whole body background radioactivity is still quite high. In later static images the background radioactivity decreases while radioactivity accumulation in stomach increases. Also, radioactivity accumulation in the bladder remains high during the whole imaging process. Accumulation of radioactivity in the thyroid of the animal remains very low during the entire imaging procedure although it looks like radioactivity accumulation is increasing slightly towards the end of the imaging procedure. The dynamic scan and the first static image of the second rat (600 g) are shown in Figure 33. Three additional static images are shown in Figure 34. Once again, the dynamic frames show a similar influx of the compound throughout the body of the rat. Here, similar to the first animal, activity accumulates in the middle part of the body of the rat which increases throughout the entire imaging procedure. Also, a small accumulation of radioactivity on the right side of the image can be seen in the first static scan. However, activity accumulation in the bladder (left side of the image) was not observed. This latter observation could be due to different reasons:

1. Rat #2 may have emptied its urinary bladder more completely than rat #1 which would explain the failure to detect urinary bladder radioactivity in rat #2.
2. Rat #2 was much bigger (600 g) than rat #1 (250 g), yet rat #2 received the same amount of compound, which means a lower dose per g. The dose for rat #1 was 2.6 times higher than for rat #2. The liver of rat #2 was bigger than the liver of rat #1. Therefore, rat #2 should be able to metabolise higher amounts of drug than the liver of rat #1. One metabolic pathway that occurs in liver is deiodination. Some of the free iodide accumulates in thyroid or stomach, the rest is excreted via the kidneys. If the dose in rat #2 was so low that its liver could metabolise most of the compound by first pass metabolism there may not have been any remaining labelled compound to be excreted via kidneys into the bladder.
3. Rat #1 was younger than rat #2 which could result in different extents of metabolism. An older animal has more enzymatic activity in liver than a younger animal. Therefore, more of the compound may be metabolised in liver and less is excreted via the kidneys.
4. A minimal dysfunction or infection of the kidneys, which can not be detected easily, could result in a totally altered metabolic profile such that no radioactivity is excreted renally.
5. A parasitic infection of the animal could also alter the metabolic profile.

Background radioactivity in the rat body decreased over time while the radioactivity in the stomach increased with time. The radioactivity level in thyroid seems to be constant during the static scans. The strong accumulation of radioactivity in the stomach of the rats coincides with the data obtained from a mouse biodistribution study, which also showed high accumulation of radioactivity in the stomach. Radioactivity accumulation in stomach might be due to free iodide arising from deiodination of the labelled compound. Radioactivity accumulation in intestine during the early static images may be due to the hepato-biliary metabolism. In this regard, the labelled compound passes through liver into bile, and then from bile into the upper part of the intestine where it can be reabsorbed. The high accumulation of radioactivity in the bile of mice was not seen in images obtained using rats. This difference is due to the fact that the rat has no gall bladder. Consequently, the high background stomach radioactivity will most certainly make it impossible to see the bile with a gamma-camera.

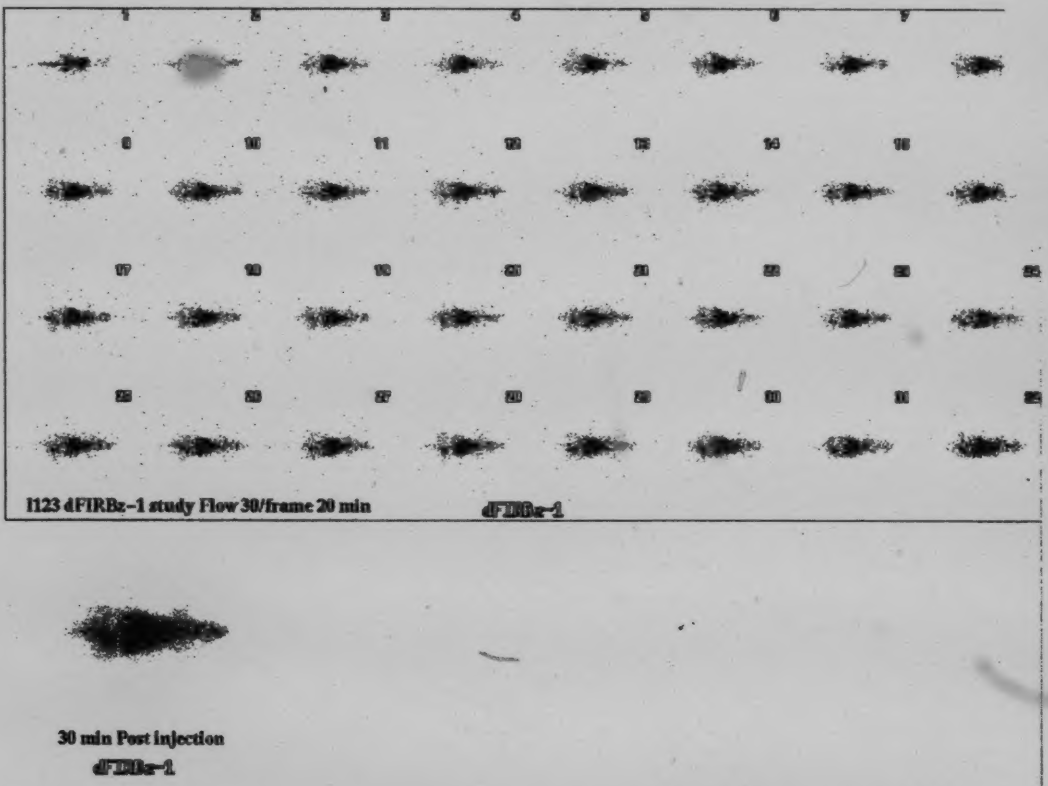

Fig. 31. Dynamic and first static scans of rat #1, dosed with 3.9 MBq 5-[^{123}I]IDFPdR via tail vein injection. Counting time for each dynamic frame was 30 seconds.

The slight radioactivity accumulation in the thyroid of both animals might be due to free iodide. In the pharmacokinetic studies it was shown that approximately 7 % of the labelled compound is degraded in plasma releasing radioactive iodide which would accumulate in thyroid. The high radioactivity accumulation in the bladder of rat

#1 is also consistent with the results obtained from the biodistribution and pharmacokinetic studies. In the pharmacokinetic study, 56 % of the administered radioactivity was excreted in the urine of the animals collected over 24 hours.

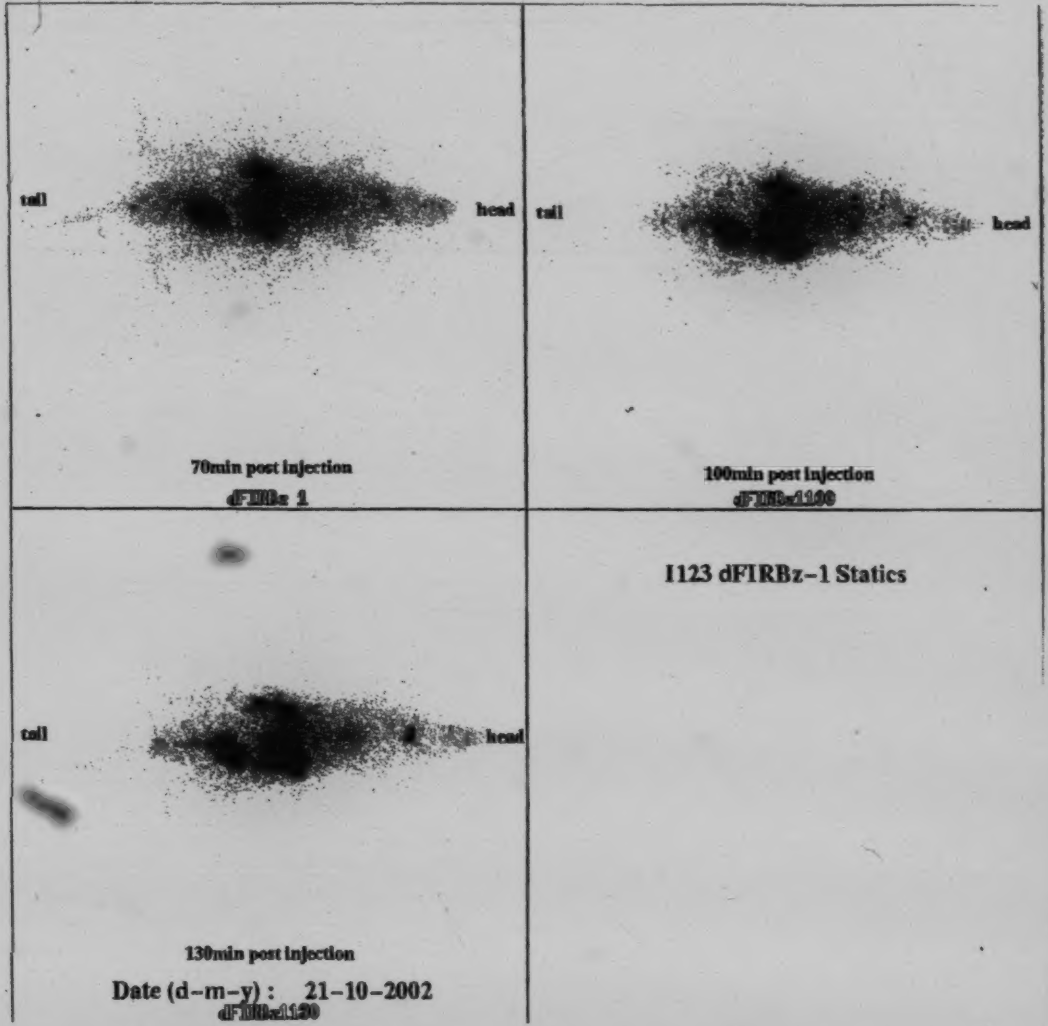
tail
head
70min post injection
dFIRBz 1
tail
head
100min post injection
I123 dFIRBz-1 Statics
tail
head
130min post injection
Date (d-m-y) : 21-10-2002

Fig. 32. Three static scans of rat #1, dosed with 3.9 MBq 5-[^{123}I]IDFPdR via tail vein injection. The images were taken 70, 100 and 130 minutes after dosing.

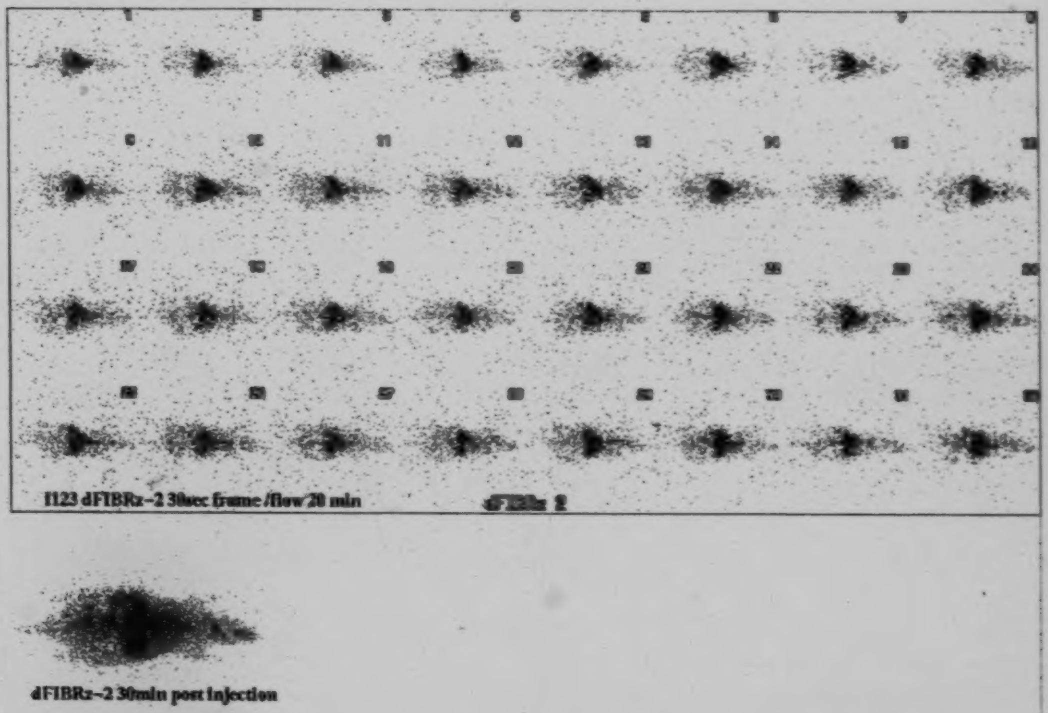
I123 dFIBRz-2 30sec frame/flow 20 min
dFIBRz-2 30min post injection

Fig. 33. Dynamic and first static scans of rat #2, dosed with 3.6 MBq 5-[^{123}I]IDFPdR via tail vein injection. Counting time for each dynamic frame was 30 seconds.

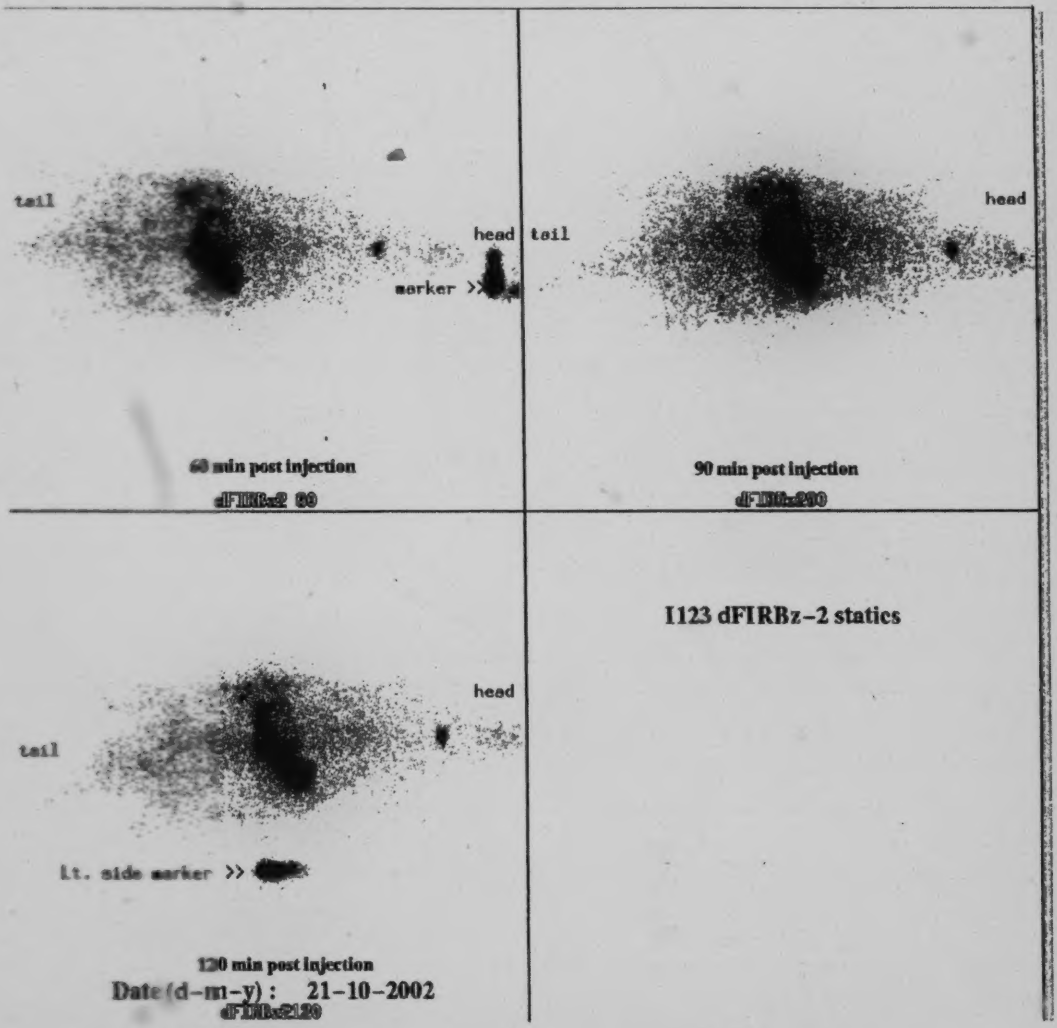
tail
head
marker >>
tail
head
60 min post injection
90 min post injection
I123 dFIRBz-2 statics
head
tail
Lt. side marker >>
120 min post injection
Date (d-m-y) : 21-10-2002

Fig. 34. Three static scans of rat #2, dosed with 3.9 MBq 5-[^{123}I]IDFPdR via tail vein injection. The images were taken 70, 100 and 130 minutes after dosing.

To get reliable imaging results, a larger number of animals that are the same weight and age should be scanned.

10. General discussion and conclusions

The first experiments and investigations regarding a stable production of ^{124}I have been established. The beam current dependency for ^{124}I production showed that it is possible to produce 60 MBq ^{124}I within one hour with a beam current of 10 μA. This beam and irradiation time was satisfactory for the preparation of sufficient 5-IDFPdR for the initial studies described in this thesis. Longer beam times or higher currents will provide an increase in radioactivity. However, further investigations are necessary to determine the optimum parameters for producing ^{124}I. At this time, it is clear that irradiation times over one hour will produce sufficient activities of ^{124}I for use in human diagnostic studies.

The synthesis of the unlabelled 5-IDFPdR could be performed in acceptable yields to perform the labelling experiments and first biological evaluations. The labelling step could be performed using an isotope exchange procedure. Optimisation of this exchange labelling procedure resulted in development of the following exchange reaction parameters: radiochemical yields up to 85 % were achieved after a one hour reaction time with a reaction temperature of 140 °C. The amount of unlabelled precursor needed for the iodine-exchange reaction was determined to be 0.5 μmol (0.17 mg). pH dependency studies showed that larger amounts of NaOH decreased the radiochemical yield even down to 0 %. This decrease in radiochemical yield could be due to polymerisation, or degradation, of the sugar moiety of 5-IDFPdR. It is known that sugar molecules exist not only as ring structures but also as an open chain structure in protic solvents. Sugar chain structures can polymerise under basic conditions. However, the equilibrium between ring, and chain, structures highly favours the ring structure since only approximately 2 % of sugar molecules exist in chain structures. Most sugar molecules can polymerise under strong basic conditions, and therefore be removed from the labelling reaction. Alternatively, if the pH is too low (acidic), formation of gaseous HI or I_2 can occur which will preclude the iodine from participating in the iodine-exchange labelling reaction resulting in a decrease in the radiochemical yield. Since pH is an important parameter, it is necessary to buffer the labelling reaction appropriately. A buffer to NaOH ratio of 0.75 provided a radiochemical yield of 61.2 %. Furthermore, it was possible to determine the activation energy of the system 5-IDFPdR/^{123}I. The calculated activation energy (100 kJ/mol) lies in the usual range of such iodination reactions when compared with literature data. For example, the labelling of p-IBG (2-*O*-(*p*-iodobenzyl)-D-glucose) has an activation energy of 79.9 kJ/mol. [69]

The biological evaluation of 5-IDFPdR showed a fast blood clearance. The plasma level of 5-IDFPdR decreased in the first 5 minutes after i.v. bolus injection to a level below 1 % of the injected dose. 56.3 % of the radioactivity was present in urine collected over 24 hours. Analysis of the urine showed that only approximately 2 % of this radioactivity was due to unchanged 5-IDFPdR. The pharmacokinetic parameters for 5-IDFPdR are strongly dose dependent. This dependency is true for most radiopharmaceuticals since a lower injected dose parallels an expected increase in the volume of distribution. A comparison of literature data with the data obtained in this study showed a decrease in clearance of 38.9 % when the dose was reduced from 53.4 mg/kg to 46.8 µg/kg. At the same time, the distribution volume increased 2.8-fold. The elimination half life for the lower dose was higher by a factor of 3.4 compared to the higher dose. Most of the injected radioactivity was recovered in the urine (56 %) of which ≤ 1% was unchanged 5-IDFPdR. Clearance of radioactivity from blood was fast. However, the amount of unchanged 5-IDFPdR increased in blood at approximately 100 minutes post-administration even though it had almost disappeared completely prior to the 100-minute time point. This data suggests there is a second operative metabolic pathway occurring for 5-IDFPdR. This pathway could involve liver metabolism, uptake into bile, and then passage into the intestine where it is possible that 5-IDFPdR is reabsorbed into blood. To clarify this possibility, a bile examination would be necessary. This study, which was performed using the higher dose of 53.4 mg/kg in rats, showed that the intact compound and the glucuronid metabolite could be detected in bile which supports the theory of the hepato-biliary pathway.[70] *cycloSal*-5-IDFPdR exhibited a slow blood clearance over time. After 5 minutes approximately 4% of the injected dose was still in plasma, and even after 24 hours 0.5 % radioactivity of the injected dose could be detected. HPLC analyses of plasma samples showed that this *cycloSal* compound was completely degraded in blood within the first five minutes. However, a small amount of unchanged *cycloSal*-5-IDFPdR reappeared after 2 hours. This observation is indicative of either absorption/desorption processes in fatty tissues or to a second metabolic pathway as is the case with 5-IDFPdR. About 25 % of the radioactivity present in the injected dose was recovered in urine collected over 24 hours. The proportion of unchanged *cycloSal*-5-IDFPdR in urine was below 10%.

Biodistribution studies with 5-IDFPdR and *cycloSal*-5-IDFPdR were performed in tumour bearing mice. A conclusive evaluation showed that most of 5-IDFPdR was present in the bladder, bile and stomach. The tumour to blood ratio reached its maximum of 2.6 after 1 hour which is a relatively low ratio. A tumour to blood ratio in the 7-10 range in mice is required to be a successful diagnostic tool in humans as the distribution volume in humans is much larger than in mice. In addition, the high background accumulation in the stomach, intestine and liver makes it difficult to use 5-IDFPdR as a diagnostic tool especially if the tumour is located near or in the region of these organs. However, the data acquired in this study supports the theory of a hepato-biliary metabolism that was postulated from the pharmacokinetic data. The *cycloSal* derivative accumulated primarily in blood (~17%), lung (~19%), bile (~11%) and bladder (~ 15%). The tumour to blood ratio never exceeded 1 which indicates that *cycloSal*-5-IDFPdR is not a useful tumour imaging agent.

The gamma camera images obtained after administration of 5-IDFPdR to rats represent preliminary experiments. In this regard, the small number of only two animals, which were scanned, provide only preliminary images that illustrate the in vivo distribution of 5-IDFPdR. The fact that the animals were anaesthetised during the imaging procedure make it difficult to compare the information in these images with the data from pharmacokinetic studies as the anesthetic may alter the biodistribution in the imaging studies. However, the accumulation of radioactivity in intestine of both animals that were imaged support the theory of hepato-biliary metabolism. The high accumulation in stomach might be due to iodide as of 5-IDFPdR is deiodinated in blood and in liver. This deiodination process is consistent with primary metabolism of 5-IDFPdR occurring in liver. The localization of radioactivity in the thyroid of the two animals used in the imaging studies is likely due to iodide.

References

1) Hevesy G.: Absorption and translocation of lead by plants. A contribution to the application of the method of radioactive indicators in the investigation of the change of substance in plants, Biochem. J. 17, 439-445 (1923)

2) Stöcklin G.: Spezielle Syntheseverfahren mit kurzlebigen Radionukliden und Qualitätskontrolle. In "Handbuch der Medizinischen Radiologie" Band XV/1B, Springer Verlag, Berlin, (1988)

3) Antony M.S.: Straßburger Nuklidkarte. AGECOM, Selestat, France (1992)

4) Phelps E., Mazziotta J.C., Schelbert H.R.: PET and autoradiography. Raven Press, New York (1986)

5) Machulla H.-J.: Clinical applications of positron emitting radiopharmaceuticals, in Textbook of Radiopharmacy, Theory and Practice, Charles B. Sampson, Gordon and Breach Science Publishers OPA (1999)

6) Wienhard K., Wagner R., Heiss W.-D.: PET - Grundlagen und Anwendungen der Positronen-Emissions-Tomographie, Springer Verlag Berlin, Heidelberg (1989)

7) Seevers R.H., Counsell R.E.: Radiation techniques for small organic molecules. Chem. Rev. 82, 575-90 (1982)

8) Doran D.M., Spar I.L.: Oxidative iodine monochloride iodination technique. J. Immunol Methods 39,155-163 (1980)

9) Lambrecht R.M., Mantescu C., Redvanly C., Wolf A.P.: Preparation of high-purity carrier free 123 I-iodine monochloride as iodination reagent for synthesis of radiopharmaceuticals. IV. J. Nucl. Med. 13 (4), 266-273 (1972)

10) Tisliar U., Kloster G., Ritzl F., Stöcklin G.: Accumulation of radioiodinated L-α-methyltyrosin in pancreas of mice: Concise Communication. J. Nucl. Med. 20, 973-6 (1979)

11) Trivedi M.A., Carnochan P.: An improved synthetic procedure for L-3-iodo-α-methyl tyrosine suitable for preparation in kit form. J. Label. Compd. Radiopharm. 33, 61-4 (1993)

12) Kawai K., Fujibayashi Y., Saji H., Konishi J., Yokoyama A.: A strategy for the study of cerebral amino acid transport using iodine-123-labeled amino acid radiopharmaceutical: 3-iodo-alpha-methyl-L-tyrosine. J. Nucl. Med. 32 (5), 819-824 (1991)

13) Langen K., Roosen N., Coenen H.H., Kuikka J.T., Kuwert T., Herzog H., Stöcklin G., Feinendegen L.E.: Brain and brain tumour uptake of L-3-[123I]iodo-alpha-methyl tyrosine: competition with natural L-amino acids. J. Nucl. Med. 32 (6), 1225-1229 (1991)

14) Krummeich C., Holschbach M., Stöcklin G.: Direct n.c.a. electrophilic radioiodination of tyrosin analogues; Their in vivo stability and brain-uptake in mice. Appl. Radiat. Isot. 45, 929-35 (1994)

15) Stöcklin G.: Emissions-Computertomographie mit kurzlebigen Zyklotron-produzierten Radiopharmaka. Aus Handbuch der Medizinischen Radiologie, Band XV/1B, Springer Verlag Berlin, Heidelberg, New York (1988)

16) Coenen H.H., Morelein S.M., Stöcklin G.: No-carrier-added-radiohalogenation methods with heavy halogens. Radiochim. Acta 34, 47-68 (1983)

17) Palmer M.: Basic mechanisms of radiolabelling, in Textbook of Radiopharmacy, Theory and Practice, Charles B. Sampson, Gordon and Breach Science Publishers OPA (1999)

18) Adam M.J., Ponce Y.Z., Berry J.M., Hoy K.: Synthesis and preliminary evaluation of L-6-iododopa as a potential SPECT brain imaging agent. J. Label. Compd. Radiopharm. 28, 155-66 (1990)

19) Mangner Th.J., Wu J.-l., Wieland D.M.: Solid-phase exchange radioiodination of aryl iodides. Facilitation by ammonium sulfate. J. Org. Chem. 47, 1484-8 (1982)

20) Bacon R.G.R., Hill H.A.O.: Copper promotes reactions in aromatic chemistry. Q. Rev. Chem. Soc. 19, 95 (1965)

21) Bacon R.G.R., Hill H.A.O.: Metal ions and complexes in organic reactions. Part I: Substitution reactions between aryl halides and cuprous salts in organic solvents. J. Chem. Soc., 1097 (1964)

22) Lindley J.: Copper assisted nucleophilic substitution of aryl halogen. Tetrahedron 40, 1433-56 (1984)

23) Tjuvajev J.C., Finn R., Watanabe K., Joshi R., Oku T., Kennedy J., Beattie B., Koutcher J., Carsons S., Blasberg R.G.: Noninvasive imaging of herpes virus thymidine kinase gene transfer and expression: a potential method for monitoring clinical gene theraphy. Cancer Res. 56 (18), 4087-4095 (1996)

24) Degreve B., Andrej G., Izquierdo M., Piette J., Morin K., Knaus E.E., Wiebe L.I., Basrah I., Walker R.T., De Clercq E., Balzarini J.: Varicella-zoster virus

thymidine kinase gene and antiherpetic pyrimidine nucleoside analogs in a combined gene/chemotherapy treatment for cancer. Gene Therapy, 4 (10), 1107-1114 (1997)

25) Nanda D., de Jong M., Vogels R., Havenga M., Driesse M., Bakker W., Bijester M., Avezaat C., Cox P., Morin K., Naimi E., Knaus E.E., Wiebe L.I., Smitt P.S.: Imaging expression of adenoviral HSV1-tk suicide gene transfer using the nucleoside analogue FIRU. European Journal of Nuclear Medicine and Molecular Imaging 29 (7), 939-47 (2002

26) Wiebe L.I., Knaus E.E., Morin K.W.: Radiolabeled pyrimidine nucleosides to monitor the expression of HSV-1 thymidine kinase in gene therapy. Nucleosides & Nucleotides 18 (4 & 5) 1065-66 (1999)

27) Shaw T., MacPhee D.G.: Rapid and complete degradation of thymidine by human peripheral blood platelets: implications for genotoxicity assays. Mutation Res. 163, 75-80 (1986)

28) Shields A.F., Lim K., Grierson J., Link J., Krohn K.A.: Utilization of labeled thymidine in DNA synthesis: studies for PET. J.Nucl. Med. 31, 337-342 (1990)

29) Goethals P., Lameire N, Eijkeren M.V., Kesteloot D., Thierens H., Dams R.: [Methyl-carbon-11]thymidine for in vivo measurement of cell proliferation. J. Nucl. Med. 37, 1048-1052 (1996)

30) Lu L., Samuelsson L., Bergström M., Sato K., Fasth K.-J., Långström B.: Rat studies comparing ^{11}C-FMAU, ^{18}F-FLT, and ^{76}Br-BFU as proliferation markers. J. Nucl. Med., 43 (12) 1688-1698 (2002)

31) Shields A.F., Grierson J.R., Dohmen B.M., Machulla H.-J., Stayanoff J.C., Lawhorn-Craws J.M., Obradovich J.E., Muzik O., Mangner T.J.: Imaging proliferation in vivo with [F-18]FLT and positron emission tomography. Nat. Med. 4, 1334-1336 (1998)

32) Schweitzer B.A., Kool E.T.: Aromatic nonpolar nucleosides as hydrophobic isosteres of pyrimidine and purine nucleosides. J. Org. Chem. 59, 7238-7242 (1994)

33) Schweitzer B.A., Kool E.T.: Hydrophobic, non-hydrogen-bonding bases and base pairs in DNA. J. Am. Chem. Soc. 117 (7), 1863-1872 (1995)

34) Moran S., Ren R.X.-F., Rumney S., Kool E.T.: Difluorotoluene, a nonpolar isostere for thymine, codes specifically and efficiently for adenine in DNA replication. J. Am. Chem. Soc. 119, 2056-2057 (1997)

35) Moran S., Ren R.X.-F., Kool E.T.: A thymidine triphosphate shape analog lacking Watson-Crick pairing ability is replicated with high sequence selectivity. Proc. Natl. Acad. Sci. 94, 10506-10511 (1997)

36) Majer V., Kupsch H.: Grundlagen der Kernchemie, Carl Hanser Verlag, München, (1982)

37) Martin J.A., Lambert R.W., Merrett J.H., Parkes K.E.B., Thomas G.J., Baker S.J., Bushnell D.J., Cansfield J.E., Dunsdon S.J., Freeman A.C., Hopkins R.A., Johns I.R., Keech E., Simmonite H., Walmsley A., Wong Kai-In P., Holland M.: Nucleoside analogues as highly potent and selective inhibitors of Herpes Simplex Virus Thymidine Kinase. Bioorg. Med. Chem. Lett. 11, 1655-1658 (2001)

38) Hohn A., Coenen H.H., Qaim S.M.: Excitation functions of ^{120}Te (d, xn) ^{121,120m,g}I reactions from threshold up to 13.5 MeV: comparative studies on the production of ^{120g}I, Appl. Radiat. Isot., 52, 923-925 (2000)

39) Hohn A., Scholten B., Coenen H.H., Qaim S.M.: Excitation functions of (p,xn) reactions on highly enriched ^{122}Te: Relevance to the production of ^{120g}I, Appl. Radiat. Isot., 49, 93-98, (1997)

40) Sudār S., Hohn A., Qaim S.M.: Nuclear model calculations on proton and deuteron induced reactions on ^{122}Te and ^{120}Te with particular reference to the formation of the isomeric states ^{120m,g}I, Appl. Radiat. Isot. 52, 4, 937-941, (2000)

41) Kondo K., Lambrecht R.M., Wolf A.P.: Iodine-123 production for radiopharmaceuticals-XX; excitation functions of the ^{124}Te(p,2n)^{123}I and ^{124}Te(p,n)^{124}I reactions and the effect of target enrichment on radionuclidic purity, Int. J. Appl. Radiat. Isot., 28, 395-401 (1977)

42) Qaim S.M.: Recent developments in the production fluorine-18, bromine-75,-76,-77 and iodine-123, Appl. Radiat. Isot. 37, 8, 803-810 (1986)

43) Bechtold V., Schweickert H.: Modern gas-target technology for the production of high quality radiopharmaceuticals, Conf. 890560 Abstract

44) Fusco M.A., Peek N.F., Jungermann J.A., Zielinski F.W., DeNardo S.J., DeNardo G.L.: Cyclotron production of carrier-free ^{123}I using the reaction ^{127}I (p, 5n) ^{123}Xe, Strahlentherapie Sonderbände 72, 367-375, (1972)

45) Livingood J.J., Seaborg G.T.: Radioactive isotopes of iodine, Phys. Rev. 54, 775 (1938)

46) Van den Bosch R., De Goeij J.M., Van der Heide J.J.A., Tertoolen J.F.W., Theelen H.J.M., Zegers C.: A new approach to target chemistry for the iodine-123 production via the ^{124}Te(p,2n) reaction, Int. J. Appl. Radiat. Isot. 28, 255 (1977)

47) Barall R.C., Beaver J.E., Hupf H.B., Rubio F.F.: Production of Curie quantities of high purity I-123 with 15 MeV protons, Eur. J. Nucl. Med. 6, 415 (1981)

48) Palmer D.W., Rao S.A.: Quantitation of iodine-124. Contamination in iodine-123 radiopharmaceuticals: Charakterisation of a second dose calibrator, J. Nucl. Med. 29, 1302 (1988)

49) Larson D.W., Pentlow K.S., Volkow N.D., Wolf A.., Finn R.D., Lambrecht R.M., Graham M.C., Di Resta G., Bendriem B., Daghighian F.: PET scanning of iodine-124-3F9 as an approach to tumor dosimetry during treatment planning for radioimmunotherapy in a child with neuroblastoma; J. Nucl. Med. 33, 2020 (1992)

50) Bakir M.A., Eccles S., Babich J.W., Aftab N., Styles J., Dean C.J., Lambrecht R.M., Ott R.J., Eccles S.A., Styles J.M.: C-erB2 protein overexpression in breast cancer as a target for PET using iodine-124-labelled monoclonal antibodies, J. Nucl. Med. 33, 2154 (1992)

51) Daghighian F., Pentlow K.S., Larson S.M., Graham M.C., Di Resta G., Yeh S.D., Macapinlac H., Finn R.D., Lambrecht R.M., Arbit E., Cheung N.K.: Development of a method to measure kinetics of radiolabelled monoclonal antibody in human tumor with applications to microdosimetry: positron emission tomography studies of iodine-124 labelled 3F8 monoclonal antibody in glioma, Eur. J. Nucl. Med. 20, 402 (1993)

52) Crawford D.C., Flower M.A., Pratt B.E., Hill C., Zweit J., McCready V.R., Harmer C.L.: Thyroid volume measurement in thyrotoxic patients: Comparison between ultrasonography and iodine-124 positron emission tomography, Eur. J. Nucl. Med. 24, 1470 (1997)

53) Scholten B., Kovács Z., Tárkányi F., Qaim S.M.: Excitation functions of ^{124}Te(p,xn) ^{124,123}I reactions from 6 to 31 MeV with special reference to the production of ^{124}I at a small cyclotron, Appl. Radiat. Isot. 46 (4), 255-59 (1994)

54) Sharma H.L., Zweit J., Downey S., Smith A.M., Smith A.G.: Production of ^{124}I for positron emission tomography, J. Labelled Compd. Radiopharm. 26, 165 (1989)

55) Lambrecht R.M., Sajjad M., Qureshi M.A., Al-Yanbawi S.J.: Production of iodine-124, J. Radioanal. Nucl. Chem., Letters 127, 2, 1988, 143-150

56) Firouzbakht M.L., Schlyer D.J., Finn R.D., Laguzzi G., Wolf A.P.: Iodine-124 production: Excitation functions for the ^{124}Te(d,2n)^{124}I and ^{124}Te(d,3n)^{123}I reactions from 7 to 24 MeV, Nucl. Instrum. Methods Phys. Res. B79, 909 (1993)

57) Hohn A.: Kernchemische Untersuchungen zur Produktion der medizinisch relevanten längerlebigen Positronenstrahler Iod-120 und Iod-124, Dissertation am Institut für Nuklearchemie, Forschungszentrum Jülich (2000)

58) Zweit J., Bakir M.A., Ott R.J., Sharma H.L., Cox M., Goodall R.: Excitation functions of proton induced reactions on natural tellurium: Production of no-carrier added ^{124}I for PET applications, Proc. IV Int. Workshop on Targetry and Target Chemistry, Villingen, Switzerland, 76 (1991)

59) Clem R.G., Lambrecht R.M.: Enriched ^{124}Te targets for the production of ^{124}I and ^{123}I, Nucl. Instrum. Methods Phys. Res., A303, 115 (1991)

60) Weinreich R., Knust E.J.: Quality assurance of iodine-124 produced via the nuclear reaction ^{124}Te(d,2n)^{124}I, J. Radioanalyt. Nucl. Chem. Lett. 213, 18 (2000)

61) Knust E.J., Dutschka K., Weinreich R.: Preparation of ^{124}I solutions after thermodistillation of irradiated ^{124}TeO$_2$ targets, Appl. Radiat. Isot. 52, 181-84 (2000)

62) Sheh Y., Koziorowski J., Balatoni J., Lom C., Dahl J.R., Finn R.D.: Low energy cyclotron production and chemical separation of "no carrier added" iodine-124 from a reusable, enriched tellurium-124 dioxide/ aluminium oxide solid solution target. Radiochim. Acta 88, 169-173 (2000)

63) Bresesti M., Bresesti Del Turco A.M., Neumann H., Orvini E.: The thermal neutron capture cross-section and resonance capture integral of ^{125}I, J. Inorg. Nucl. Chem 26, 1625-1631, (1964)

64) Helus F.: Radionuclides Production, Vol. I, CRC Press Inc., Boca Raton, Florida, (1983)

65) Finn R.D., Sheh Y., Bui V., Larson S.M., Schlyer D.: Refinements with targetry to overcome accelerator energy constraints. Nucl. Instr. and Meth. in Phys. Res. B99, 814-816 (1995)

66) Firouzbakht M.L., Schlyer D.J., Wolf A.P.: The yield of I-124 from different

target materials in the ^{124}Te(d,2n)^{124}I reaction and an improved recovery method for Te-124. J. Lab. Comp. Radiopharm. 35, 257-259 (1994)

67) Qaim S.M., Hohn A., Bastian Th., El-Azoney K.M., Blessing G., Spellerberg S., Scholten B., Coenen H.H.: Some optimisation studies relevant to the production of high-purity ^{124}I and ^{120g}I at a small-sized cyclotron. Appl. Radiat. Isot. 58, 69-78 (2003)

68) Wang Z.-X, Duan W., Wiebe L.I., Balzarini J., De Clercq E., Knaus E.E.: Synthesis of 1-(2-deoxy-β-D-ribofuranosyl)-2,4-difluoro-5-substituted -benzene thymidine mimics, some related α-anomers; and their evaluation as antiviral and anticancer agents. Nucleosides, Nucleotides & Nucleic Acids 20 (1 & 2), 11-40 (2001)

69) Stahlschmidt A.: Untersuchungen zur aromatischen Radioiodierung im Hinblick auf die Herstellung von Radiopharmaka. Diplomarbeit Gesamthochschule Essen (1990)

70) Khalili P., Naimi E., Knaus E.E., Wiebe L.I.: Pharmacokinetics and metabolism of the novel synthetic C-nucleoside, 1-(2-deoxy-β-D-ribofuranosyl)-2,4-difluoro-5-iodobenzene, a potential mimic of 5-iodo-2'-deoxyuridine. Biopharm. Drug Dispos. 23, 105-113 (2002)

71) Gerlowski L.E., Jain R.K.: Physiologically based pharmacokinetic modeling: principles and applications. J. Pharm. Sci. 72, 1103-1126 (1983)

72) Forth W., Henschler D., Rummel W., Starke K.: Allgemeine und spezielle Pharmakologie und Toxikologie. Wissenschaftsverlag Mannheim/ Leipzig/ Wien/ Zürich (1992)

73) Page R.D., Woods P.J., Cunningham R.A., Davison T., Davis N.J., James A.N., Livingston K., Sellin P.J., Shotter A.C.: Alpha radioactivity above ^{100}Sn including the decay of ^{108}I, Physical Review C, 49, No 6, 3312-3315 (1994)

74) Faestermann T., Gillizer A., Hartel K., Kienle P.: Two new proton activities: ^{109}I and ^{113}Cs; At. Masses Fundam. Constants, Proc. Int. Conf. 7th, 177-183, (1984)

75 Yu C.-H., Galindo-Uribarri A., Paul S.D., Carpenter M.P., Davids C. N., Janssens R.V. F., Lister C.J., Seweryniak D., Uusitalo J., MacDonald B.D.: Spectroscopy of the proton emitter ^{109}I, Physical Review C, 59 (4), R 1834-R 1838 (1999)

76) Paul E.S., Woods P.J., Davinson T., Page R.D., Sellin P.J., Beausang C.W., Clark R.M., Cunningham R.A., Forbes S.A., Fossan D.B., Gizon A., Gizon J.,

Hauschild K., Hibbert I.M., James A.N., LaFosse D.R., Lazarus I., Schnare H., Simpson J., Wadsworth R., Waring M.P.: In-beam γ-ray spectroscopy above 100Sn using the new technique of recoil decay tagging, Physical review C, 51 (1), 78-87 (1995)

77) Roeckl E., Kirchner R., Klepper O., Nnyman G., Reisdorf W., Schardt D., Wien K., Fass R., Mattsson S.: A new island of α-emission: α-decay energies and widths of neutron deficient tellurium, iodine and xenon isotopes, Physics Letters, 78B (4), 393-396, (1978)

78) Kirchner R., Klepper O., Nyman G., Reisdorf W., Roeckl E., Schardt D., Kaffrell N., Peuser p., Schneeweiss K.: New neutron-deficient tellurium, iodine and xenon isotopes produced by reactions of 290 MeV ^{58}Ni and ^{63}Cu targets, Physics Letters,70B (2), 150-154, (1977)

79) Paul E.S., Starosta K., Boston A.J., Chiara C.J., Devlin M., Dorvaux O., Fossan D.B., Greenlees P.T., Helariutta K., Jones P., Julin R., Juutinen S., Kankaanpä H., Kettunen H., LaFosse D.R., Lane G.J., Lee I.Y., Macchiavelli A.O., Muikku M., Nieminen P., Rahkila P., Sarantites D.G., Scraggs H.C., Sears J.M., Semple A.T., Smith J.F., Stezowski O.: High-spin study of ^{111}I, Physical Review C, 61, No 6, 064320-1ff (2000)

80) Reinhold J., Friese J., Körner H.-J., Schneider R., Zeitelhack K.: Projectile fragmen-tation of ^{129}Xe at Elab= 790A MeV, Physical Review C, 58, No 1, 247-253 (1998)

81) Heine F., Faestermann T., Gillitzer A., Homolka J., Koepf M., Wagner W.: Proton and alpha radioactivity of very neutron deficient tellurium, iodine, xenon and cesium isotopes, studied after electrostatic separation. Zeitschrift für Physik A: Hadrons and Nuclei 340 (2), 225-226, (1991).

82) Waring M.P., Paul E.S., Beausang C.W., Clark R.M., Cunningham R.A., Davinson T., Forbes S.A., Fossan D.B., Gale S.J., Gizon A., Gizon J., Hauschild K., Hibbert I.M., James A.N., Jones P.M., Joyce M.J., LaFosse D.R., Page R.D., Ragnarsson I., Schnare H., Sellin P.J., Simpson J., Vaska P., Wadsworth R., Woods P.J.: Intruder bands in (Z=53) ^{113}I: Band termination interpretation, Physical Review C, 51 (5), 2427-2437, (1995)

83) Paul E.S., Beausang C.W., Forbes S.A., Gale S.J., James A.N., Jones P. M., Joyce M.J., Clark R.M., Hauschild K., Hibbert I.M., Wadsworth R., Cunningham R.A., Simpson J., Davinson T., Page R.D., Sellin P.J., Woods P.J.,

Fossan D.B., LaFosse D.R., Schnare H., Waring M.P., Gizon A., Gizon J.: Deformed intruder band in 113I, Physical Review C, 48 (2), R490-R493, (1993)

84) Paul E.S., Andrews H.R., Drake T.E., DeGraaf J., Janzen V.P., Pilotte S., Radford D.C., Ward D.: High-spin states in doubly odd ^{114}I, Physical Review C, 52 (3), 1691-1693, (1995)

85) Paul E.S., Andrews H.R., Janzen V.P., Radford D.C., Ward D., Drake T.E., DeGraaf J., Pilotte S., Ragnarsson I.: Multiple band structures at high angular momentum in ^{115}I: Towards unfavored band termination, Physical Review C, 50 (2), 741-745, (1994)

86) Hansen P.G., Hornshøj P., Nielsen H.L., Wilsky K., Kugler H., Astner G., Hagebø E., Hudis J., Kjelberg A., Münnich F., Patzelt P., Alpstein M., Andersson G., Appelqvist A., Bengtsson B., Naumann R.A., Nielsen O.B., Beck E., Foucher R., Husson J.P., Jastrzębski J., Johnson A., Alstad J., Jahnsen T., Pappas A.C., Tunaal T., Henck R., Siffert P., Rudstam G.: Decay characteristics of short-lived radio-nuclides studied by on-line isotope separator techniques, Physics Letters, 28B (6), 415-419, (1969)

87) Piel W.F., Chowdhury P., Garg U., Quader M.A., Stwertka P.M., Vajda S., Fossan D.B.: Collective structures in the odd-Z transitional nuclei ^{115,117}I and ^{121,123}Sb, Physical Review C, 31 (2), 456-464, (1985)

88) Giezon A., Genevey J., Gizon J., Barci V., P ochocki A., Batsch T., Żylicz J., Charvet A., Marguier G.: In beam spectroscopy and cross-section studies for the ^{106}Cd + ^{12}C reaction, Z. Phys. A. 302, 79-87, (1981)

89) Quader M.A., Piel W.F., Vajda S., Watson III W.A., Yang F.C., Fossan D.B.: Proton-hole-induced bands in odd-odd ^{116,118,120,122}I nuclides, Physical Review C, 30 (5), 1772-1775, (1984)

90) Gowdy G.M., Xenoulis A.C., Wood J.L., Baker K.R., Fink R.W., Weil J.L., Kkern B.D., Hofstetter K.J., Spejewski E.H., Mlekodaj R.L., Carter H.K., Schmidt-Ott W.D., Lin J., Bingham C.R., Riedinger L.L., Zganjar E.F., Sastry K.S.R., Ramayya A.V., Hamilton J.H.: On-line mass separator investigation of the new isotope 2.9-sec ^{116}I, Physical Review C, 13 (4), 1601-1608, (1976)

91) Wu C.Y., Satteson M., Wang K., Cline D., Gove H.E., Hanna S.S., Hass M., Ibbotson R., Ramayya A.V., Isomers in iodine nuclei, Physical Review C, 41 (4), 1600-1605, (1990)

92) Spejewski E.H., Hopke P.K., Loeser F.W.: Level sructure of Te^{116,118,120,122},

Physical Review, 186 (4), 1270-1279, (1969)

93) Paul E.S., Waring M.P., Clark R.M., Forbes S.A., Fossan D.B., Hughes J.R., LaFosse D.R., Liang Y., Ma R., Vaska P., Wadsworth R.: Delayed neutron alignment in ^{117}I, Physical Review C, 45 (6), R2531-R2535 (1992)

94) Lee R.S., Hamilton J.H., Ramayya A.V., de Lima A.P., Sastry D.L., Sastry K.S.R., Spejewski E.H., Mlekodaj R.L., Carter H.K. Schmidt-Ott W.-D., Lin J., Bingham C.R., Riedinger L.L., Zganjar E.F., Weil J.L., Kern B.D., Xenoulis A.C., Fink R.W., Sun X.-J., Guo J.-S., Cho C.-C., Pan Z.-Y., Guo Y.-X.: Decays of $^{117}\mathrm{Xe} \longrightarrow {}^{117}\mathrm{I} \longrightarrow {}^{117}\mathrm{Te}$, Physical Reviews C, 32 (1), 277-287 (1985)

95) Ladenbauer-Bellis I.M., Bakhru H., Luzzati A.: Decay study of I^{117} and I^{119}, Physical Review, 187 (4), 1739-1744 (1969)

96) Fossan D.B., Gai M., Gaigalas A.K., Gordon D.M., Shroy R.E.: Deformed 9/2+ proton-hole states in odd-A I nuclei, Physical Review C, 15 (5), 1732-1737 (1977)

97) Ohkubo Y., Porile N.T., Orth C.J., Liu L.C.: Excitation functions of the ^{127}I (π, πxn) reactions in the region of the (3,3) resonance, Physical Review C, 27 (3), 1146-1161 (1983)

98) Paul E.S., Fossan D.B., Hauschild K., Hibbert I.M., Schnare H., Sears J.M., Thorslund I., Wadsworth R., Wilson A.N., Wilson J.N.: Yrast bands in ^{117}I and $^{116-118}$Xe: Anomalus quasiparticle alignment frequencies and band termination, Physical Review C, 51 (6), R2857-R2861 (1995)

99) Kudo H., Moody K.J., Seaborg G.T.: Mass distributions in the reaction of 240 MeV ^{12}C with ^{197}Au, Physical Review C 30 (5), 1561-1572 (1984)

100) Michael H., Rosezin H., Apelt H., Blessing G., Knieper J., Qaim S.M.: Some technical improvements in the production of ^{123}I via the ^{124}Te(p,2n)^{123}I reaction at a compact Cyclotron, Int. J. Appl. Radiat. Isot. 32, 581-587 (1981)

101) Lederer: Table of Isotopes, seventh edition, John Wiley and Sons, Inc. 1978

102) Laughlin J.S., Tilbury R.S., Dahl J.R.: The cyclotron: Source of short lived radionuclides and positron emitters for medicine, Recent Advances in Nuclear Medicine 3, 39-62 (1971)

103) Kronrad L., Sara V.: Recent state in the production of sodium[^{125}I]iodide in the nuclear research institute- Problems and perspectives, Nucleon 4, 17-20 (1992)

104) Dickens J.K., McConnell J.W., Yields of fission products produced by thermal-neutron fission of ^{245}Cm, Physical Review C, 23 (1), 331-350 (1981)

105) Alfassi Z.B.: A simple method for preparation of high specific activity ^{128}I. Journal of Radioanalytical and Nuclear Chemistry, 83 (2), 187-190 (1984)

106) Katoh T., Nakamura S., Harada H., Ogata Y.: Measurement of thermal neutron capture cross section and resonance integral of the reaction ^{127}I(n,γ)^{128}I. Journal of Nuclear Science and Technology 36 (3), 223-231 (1999)

107) Wahl A.C.: Nuclear-charge distribution in fission: Cumulative yields of short-lived krypton and xenon isotopes from thermal-neutron fission of ^{235}U: J. Inorg. Nucl. Chem. 6, 263-277 (1958)

108) Studier M.H., Postmus C., Mech J., Walters R.R., Sloth E.N.: The use of ^{129}I as an isotopic tracer and its determination along with normal ^{127}I by neutron activation – The isolation of iodine from a variety of materials, J. Inorg. Nucl. Chem. 24, 755- 761 (1962)

109) Nakamura S., Harada H., Measurement of thermal neutron capture cross section and resonance integral of the^{129}I (n,γ) ^{130}I reaction, Journal of Nuclear Science and Technology, 33 (4), 283-289 (1996)

110) Lieser K.H.: Einführung in die Kernchemie, Verlag Chemie, Weinheim, 1980

111) Bögle W., Bächmann K., Matschoss V.: Separation of nuclear reaction products in the gas phase – III, J. Inorg. Nucl. Chem., 37, 1557-1561 (1975)

112) Kratz K.-L., Lauppe W., Herrmann G.: Gamma-ray emission from short-lived bromine and iodine isotopes, Inorg. Nucl. Chem. Letters, 11, 331-339 (1975)

113) Khalili P., Naimi E., Sun W.-Y., Knaus E.E., Wiebe L.I.: Dose-dependent pharmaco-kinetics of 1-(2-deoxy-β-D-ribofuranosyl)-2,4-difluoro-5-iodobenzene: A potential mimic of 5-iodo-2'-deoxyuridine. Biopharm. Drug Dispos., 24 (9), 385-95 (2003).

Appendix A: Quality and vendors of chemicals used in the studies described.

acetyl chloride	Merck p.a.
aluminium oxide	Aldrich >99%
Ammonium chloride	Merck p.a.
Ammonium sulphate	Merck p.a.
boron trifluoride diethyloxide	Aldrich p. redistilled
cadmium chloride	Fluka p.a.
chlorobenzoyl chloride	Fluka >99%
copper sulphate	Merck p.a.
2-deoxyribose	Fluka >95%
dichloromethane	Merck for chromatography
1,3-difluorobenzene	Aldrich 99%
dimethyl ether	Merck for chromatography
DMPH, 1,3-Dimethyltetrahydro-2(1*H*)-pyrimidone	Aldrich, 98%
ethyl acetate	Merck for chromatography
Hexane	Merck for chromatography
Iodine	Merck p.a.
N-iodosuccinimide	Aldrich 95%
Magnesium	Merck >99%
Methanol	Merck for chromatography
Nitroethane	Fluka 99%
phosphorus pentoxide	Merck p.a.
Pyridine	Fluka
sodium bisulphite	Merck p.a.
sodium hydrogen carbonate	Merck p.a.
sodium hydrogen sulphite	Merck p.a.
sodium methoxide	Lancaster
sodium sulphate	Fluka >99%
sulphuric acid	Merck 100%
tellurium dioxide	Chemotrade 99.8%
trifluoroacetic acid	Acros 99%

Appendix B: Tables

Table 6: **^{124}I radioactivity recovered in 4 mM NaOH from a 300 mg target after 10 minutes irradiation with different beam currents**

Current [μA]	Radioactivity X_1 [MBq]	Radioactivity X_2 [MBq]	Radioactivity X_3 [MBq]	Mean [MBq]	S.D.
5	3361	2411	2587	2786	505
7	2556	3556	3358	3157	529
10	5324	4693	6102	5373	706
13	7070	7188	7568	7275	260

Table 7: **Production yield of ^{124}I with a 300 mg target after 10 minutes irradiation with different beam currents**

Current [μA]	Yield X_1	Yield X_2	Yield X_3	Mean	S.D.
5	4033	2893	3104	3343	606
7	2191	3048	2878	2706	454
10	3194	2816	3661	3224	423
13	3263	3318	3493	3358	120

Table 8: **Temperature dependency of the reaction of [^{123}I]I^{-} with 5-IDFPdR with a reaction time of 2 hours**

Temperature [°C]	RCY X_1 [%]	RCY X_2 [%]	RCY X_3 [%]	Mean [%]	S.D.
60	2.3	2.5	2.5	2.4	0.2
80	9.8	10.2	12.5	10.8	1.5
85	27.6	29.1	26.5	27.7	1.3
90	52.6	53.5	--	53	0.6
95	68.9	68.12	63.3	66.8	3.1
100	76.4	80.2	63	73.2	9.0
120	69.1	80.4	80	76.5	6.4
160	77.8	67.5	84.3	76.5	8.5

Table 9: Dependency of the reaction of [^{123}I]I$^-$ with 5-IDFPdR on the amount of 5-IDFPdR, reaction time was 2 hours, reaction temperature 120°C

amount [µmol]	RCY X_1 [%]	RCY X_2 [%]	RCY X_3 [%]	RCY X_4 [%]	RCY X_5 [%]	RCY X_6 [%]	RCY X_7 [%]	RCY X_8 [%]	RCY X_9 [%]	mean [%]	S.D.
0.0195	20	18.9	28.0	29.9	31.3	30.1	29.9	23.9	19.0	25.8	4.8
0.039	31.9	31.9	40.3	23.3	24.8	20.1	33.4	28.5	29.3	29.3	5.7
0.098	38.5	30.8	54.6	31.2	35.3	35.2	42.0	47.5	60.4	41.7	9.3
0.195	57.5	59.5	59.8	45.5	46.6	60.6	50.4	44.74	43.5	52.0	6.5
0.29	56.1	56.1	57.6	51.6	55.0	45.7	76.1	78.2	75.6	61.3	10.7
0.39	53.6	56.2	53.9	43.6	64.4	72.1	63.8	57.0	63.1	58.6	7.4
0.78	59.2	59.1	62.2	71.6	71.0	73.0	60.9	58.3	62.9	64.2	5.3
1.17	70.8	68.6	69.9	65.9	64.6	65.6	59.7	59.9	58.1	64.8	4.2
1.56	61.7	62.1	63.9	75.6	74.4	76.7	68.1	69.4	69.6	69.1	5.1
1.95	66.8	67.2	67.6	62.3	61.7	63.6	66.2	65.1	64.7	65.0	1.9
2.34	69.8	69.0	69.4	70.1	67.8	71.2	69.5	68.4	68.7	69.3	0.9
2.73	56.6	62.6	62.5	60.3	69.2	68.1	64.3	63.0	66.7	63.7	3.5
3.12	67.1	66.0	64.1	66.4	65.7	66.0	66.5	66.4	66.4	66.1	0.8

Table 10: Dependency of the reaction of [^{123}I]I$^-$ with 5-IDFPdR on the mass of sodium hydroxide, reaction time was 2 hours, reaction temperature was 120°C

Mass of NaOH [µg]	RCY X_1 [%]	RCY X_2 [%]	RCY X_3 [%]	RCY X_4 [%]	Mean [%]	S.D.
3.2	55.0	57.0	--	--	56.0	1.4
5.2	63.3	51.5	51.1	55.0	55.2	5.6
9.2	56.3	51.4	--	--	53.9	3.5
11.2	64.6	63.6	--	--	64.1	0.8
19.2	60.4	62.1	--	--	61.2	1.2
27.2	39.8	37.4	--	--	38.6	1.8
35.2	24.2	23.9	--	--	24.1	0.2
43.2	1.1	2.3	--	--	1.7	0.9

Table 11: Time dependency of the reaction of [^{123}I]I$^-$ with 5-IDFPdR at a temperature of 85°C

Time [min]	RCY X_1 [%]	RCY X_2 [%]	RCY X_3 [%]	Mean [%]	S.D.
1	0.5	0.9	0.7	0.7	0.2
5	2.3	2.0	2.6	2.3	0.3
10	10.5	9.5	11.0	10.3	0.8
15	13.6	14.9	12.5	13.7	1.2
30	17.4	15.9	18.9	17.4	1.5
60	22.4	21.0	21.6	21.7	0.7
120	27.6	29.1	26.5	27.7	1.3

Table 12: Time dependency of the reaction of [^{123}I]I$^-$ with 5-IDFPdR at a temperature of 120°C

Time [min]	RCY X_1 [%]	RCY X_2 [%]	RCY X_3 [%]	RCY X_4 [%]	Mean [%]	S.D.
1	1.5	1.0	1.7	--	1.8	0.5
5	10.4	8.5	9.0	--	9.0	0.6
10	17.3	16.8	17.7	--	28.6	0.7
15	29.5	31.2	28.8	--	41.6	0.8
30	57.7	56.5	58.2	--	54.1	1.3
60	59.5	58.0	57.5	--	70.9	3.6
120	62.0	68.9	63.3	68.1	80.2	0.3

Table 13: Time dependency of the reaction of [^{123}I]I$^-$ with 5-IDFPdR at a temperature of 140°C

Time [min]	RCY X_1 [%]	RCY X_2 [%]	RCY X_3 [%]	RCY X_4 [%]	RCY X_5 [%]	RCY X_6 [%]	RCY X_7 [%]	RCY X_8 [%]	RCY X_9 [%]	Mean [%]	S.D.
1	2.0	1.8	1.7	1.5	2.4	2.0	2.5	2.0	1.3	2.0	0.5
5	19.2	19.9	24.4	18.7	14.6	17.5	20.6	15.9	18.5	18.5	3.0
10	45.1	42.1	43.0	42.3	30.4	48.8	44.5	47.1	45.6	43.2	5.3
15	89.5	84.5	74.8	80.0	82.2	88.6	83.3	--	--	83.3	5.5
30	91.7	91.3	89.8	90.9	94.3	89.3	92.7	--	--	91.8	1.5
60	94.4	93.5	94.0	90.9	94.3	89.3	92.7	--	--	92.7	2.1
120	93.0	91.7	93.5	93.1	90.3	91.0	--	--	--	92.1	1.3

Table 14: Values for calculating the rate constant for the synthesis of 5-[^{123}I]IDFPdR at a temperature of 85°C

time [min]	Y [%]	Y/100	1-Y/100	ln (1-Y/100)
1	0.7	0.007	0.993	-0.007
5	2.3	0.023	0.977	-0.023
10	10.3	0.103	0.897	-0.109
15	13.7	0.137	0.863	-0.147
30	17.4	0.174	0.826	-0.191
60	21.7	0.217	0.783	-0.244

Table 15: Values for calculating the rate constant for the synthesis of 5-[^{123}I]IDFPdR at a temperature of 120°C

time [min]	Y [%]	Y/100	1-Y/100	ln (1-Y/100)
1	1.8	0.02	0.98	-0.02
5	9.0	0.09	0.91	-0.09
10	28.6	0.29	0.71	-0.34
15	41.6	0.42	0.58	-0.54
30	54.1	0.54	0.46	-0.78
60	70.9	0.71	0.29	-1.23

Table 16: Values for calculating the rate constant for the synthesis of 5-[^{123}I]IDFPdR at a temperature of 140°C

time [min]	Y [%]	Y/100	1-Y/100	ln (1-Y/100)
1	2.0	0.02	0.98	-0.02
5	18.5	0.185	0.82	-0.20
10	43.2	0.432	0.57	-0.57
15	83.3	0.833	0.17	-1.77
30	91.8	0.918	0.082	-2.50

Table 17: Values for calculating the activation energy for the synthesis of 5-$[^{123}I]$IDFPdR

T [K]	$1/T*10^{-3}$	k	ln k
368.15	2.72	0.001	-6.83
393.15	2.54	0.01	-5.33
413.15	2.42	0.04	-3.22

Table 18: Total radioactivity measured in 1 mL of plasma and its percentage applied to the injected dose of 5-IDFPdR into each rat

	Radioactivity [cpm]/mL plasma			Radioactivity [% i.d./mL plasma]				
Time [min]	rat 1	rat 2	rat 3	rat 1	rat 2	rat 3	Mean	S.D.
1	435191	736419	416326	1.7	2.3	1.4	1.8	0.5
3	--	267494	255056	--	0.9	0.7	0.8	0.2
5	219427	223194	221550	0.4	0.8	0.4	0.5	0.2
7	--	259066	232242	--	0.4	0.3	0.3	0.0
10	186418	265689	210852	0.1	0.4	0.2	0.2	0.2
12	--	237197	222491	--	0.5	0.2	0.3	0.2
15	184060	234829	216148	0.1	0.1	0.1	0.1	0.0
30	156467	182579	174033	0.1	0.2	0.3	0.2	0.1
45	125469	177845	161729	0.1	0.2	0.3	0.2	0.1
60	116999	169514	146113	0.0	0.1	0.3	0.1	0.1
90	113855	171406	112707	0.1	0.1	0.2	0.1	0.1
120	99621	151056	119141	0.2	0.1	0.2	0.2	0.0
150	92199	--	--	0.3	--	--	--	--
180	94032	145469	98604	0.3	0.3	0.0	0.2	0.2
1440		20181	18008	--	0.1	0.1	0.1	0.0

Table 19: Total radioactivity measured in 1 mL of plasma and its percentage applied to the injected dose of the *cycloSal* derivative into each rat

	Radioactivity [cpm]/mL plasma			Radioactivity [% i.d./mL plasma]				
Time [min]	rat 1	rat 2	rat 3	rat 1	rat 2	rat 3	Mean	S.D.
1	2211292	1304386	2411951	9.2	5.5	12.1	8.9	3.3
3	1025716	843949	1087368	4.3	3.5	5.5	4.4	1.0
5	891007	819054	988218	3.7	3.4	5.0	4.0	0.8
7	954421	829628	942895	4.0	3.5	4.7	4.1	0.6
10	850623	877862	830157	3.6	3.7	4.2	3.8	0.3
12	814866	723141	1036422	3.4	3.0	5.2	3.9	1.2
15	842305	837641	963660	3.5	3.5	4.8	4.0	0.8
30	786253	813271	1039604	3.3	3.4	5.2	4.0	1.1
45	791782	769409	942858	3.3	3.2	4.7	3.8	0.9
60	728806	695332	693141	3.0	2.9	3.5	3.1	0.3
90	674371	689967	865554	2.8	2.9	4.4	3.4	0.9
120	651765	683383	754423	2.7	2.9	3.8	3.1	0.6
180	523759	593723	634498	2.2	2.5	3.2	2.6	0.5
240	519142	539629	552416	2.2	2.3	2.8	2.4	0.3
360	235628	405323	414056	1.0	1.7	2.1	1.6	0.6
1440	149373	66764	157494	0.6	0.3	0.8	0.6	0.3

Table 20: **Radioactivity [cpm] of 5-IDFPdR in 1 mL plasma and its percentile contribution to each fraction analysed on HPLC following injection of 5-[^{125}I]IDFPdR into rats via catheter.**

	Radioactivity [cpm]/mL plasma			Radioactivity [% i.d./mL plasma]				
Time [min]	rat 1	rat 2	rat 3	rat 1	rat 2	rat 3	Mean	S.D.
1	322291	488634	303486	87.4	79.5	80.0	82.3	4.5
3	--	202453	158147	--	56.2	57.8	57.0	1.7
5	68375	164608	89867	36.79	48.1	39.4	41.4	5.9
7	--	76236	66142	--	28.3	30.6	29.5	1.6
10	19419	87771	48695	12.30	29.8	24.3	22.2	9.0
12	--	99919	41707	--	30.4	19.9	25.1	7.4
15	14374	25449	31032	9.22	10.8	15.5	11.9	3.3
30	17555	32319	56258	13.3	17.6	22.1	17.7	4.4
45	22367	41818	67498	21.1	19.5	24.9	21.8	2.8
60	2958	11032	54447	3.0	7.8	27.3	12.7	12.9
90	14845	16973	34837	15.4	11.4	24.0	16.9	6.4
120	38847	25557	38444	46.0	15.4	27.0	29.5	15.5
150	54659	--	--	70.0	--	--	--	--
180	54222	66522	3767	68.1	45.7	3.8	39.2	32.6
1440	--	16308	13793		80.8	76.6	78.7	3.0

Table 21: Radioactivity [cpm] of unchanged *cycloSal* compound in 1 mL plasma and its percentile contribution to each fraction analysed on HPLC, following injection of *cyclo*Sal-5-[^{125}I]IDFPdR into rats via catheter.

	Radioactivity [cpm]/mL plasma			Radioactivity [% i.d./mL plasma]				
Time [min]	rat 1	rat 2	rat 3	rat 1	rat 2	rat 3	Mean	S.D.
1	791	0	706348	0.0	0	30.6	10.2	17.6
3	0	0	927017	0	0	53.3	17.8	30.8
5	0	0	0	0	0	0	0	0
7	0	0	0	0	0	0	0	0
10	0	0	9006	0	0	1.0	0.3	0.6
12	0	0	0	0	0	0	0	0
15	0	0	0	0	0	0	0	0
30	0	0	0	0	0	0	0	0
45	0	0	0	0	0	0	0	0
60	0	0	0	0	0	0	0	0
90	0	0	0	0	0	0	0	0
120			0	3.5	0	0	1.2	2.0
180	26344	0	0	6.6	0	0	2.19	3.79
240	47612	0	0	8.6	0	0	2.9	5.0
360	75081	0	8758	18.1	0	3.6	7.2	9.6
1440	37145	0	18929	23.6	0	12.1	11.9	11.8

Table 22: Radioactivity [cpm] of metabolites from 5-IDFPdR in 1 mL plasma and their percentile contribution to each fraction analysed on HPLC following injection of 5-[^{125}I]IDFPdR into rats via catheter.

	Radioactivity [cpm]/mL plasma			Radioactivity [% i.d./mL plasma]				
Time [min]	Rat 1	rat 2	rat 3	rat 1	rat 2	rat 3	Mean	S.D.
1	46341	126235	76138	12.6	20.5	20.1	17.7	4.5
3	--	157846	115291	--	43.8	42.2	43.0	1.2
5	117493	177716	137984	63.3	51.9	60.6	58.6	5.9
7	--	192823	149984	--	71.67	69.40	70.54	1.61
10	138488	206803	151364	87.7	70.2	75.7	77.9	9.0
12	--	229064	168284	--	69.6	80.1	74.9	7.4
15	141536	170713	168938	90.8	87.0	84.5	87.4	3.2
30	114981	150868	198355	86.8	82.4	77.9	82.3	4.4
45	83913	172578	203645	79.0	80.5	75.1	78.2	2.8
60	96147	129985	145009	97.0	92.2	72.7	87.3	12.9
90	81597	132127	110621	84.6	88.6	76.1	83.1	6.4
120	45538	140159	103716	54.0	84.6	73.0	70.5	15.5
150	23440	--	--	30.0	--	--	--	--
180	25429	78947	94838	31.9	54.3	96.2	60.2	33.5
1440	--	3873	4215	--	19.2	23.4	24.8	6.5

Table 23: Radioactivity [cpm] of metabolites from *cycloSal* derivative in 1 mL plasma and their percentile contribution to each fraction analysed on HPLC after injection of *cyclo*Sal-5-[^{125}I]IDFPdR into rats via catheter.

	Radioactivity [cpm]/mL plasma			Radioactivity [% i.d./mL plasma]				
Time [min]	Rat 1	rat 2	rat 3	rat 1	rat 2	rat 3	Mean	S.D.
1	2411159	1304386	1604699	100	100	69.4	89.8	17.6
3	1087368	843949	812452	100	100	46.7	82.2	30.8
5	988218	819054	931202	100	100	100	100	0
7	942895	829628	997477	100	100	100	100	0
10	830157	877862	879989	100	100	99	99.7	0.6
12	1036422	723141	851626	100	100	100	100	0
15	963660	837641	880303	100	100	100	100	0
30	1039604	813271	821722	100	100	100	100	0
45	942858	769409	827501	100	100	100	100	0
60	693141	695332	761684	100	100	100	100	0
90	865554	689967	704793	100	100	100	100	0
120	728079	683383	681167	96.5	100	100	98.8	2.0
180	592836	593723	547387	93.4	100	100	97.8	3.8
240	504804	539629	542562	91.4	100	100	97.1	5.0
360	338975	405323	237499	81.9	100	96.4	92.8	9.6
1440	120348	66764	137183	76.4	100	87.9	88.1	11.8

Table 24: In vivo biodistribution of 5-[^{125}I]IDFdR in mice following i. v. injection via tail vein, expressed as % I.D./g organ.

Organs	15 min	30 min	1 hr	2 hr	4 hr	24 hr
Blood	4.77	2.70	2.29	1.33	0.78	0.04
Lung	2.86	1.85	1.98	0.99	0.55	0.04
Bile	12.82	14.39	19.89	21.73	13.97	0.26
Liver	2.43	2.28	4.73	3.45	0.73	0.20
Spleen	2.00	0.85	0.84	0.64	0.35	0.03
Stomach	9.20	6.57	13.01	6.90	4.77	0.06
Intestine	3.09	2.51	3.22	1.99	1.34	0.03
Kidney	5.64	2.92	2.50	1.15	0.63	0.05
Bladder	28.17	23.61	16.03	16.81	1.85	0.05
Thyroid	2.97	3.24	5.10	6.26	4.21	0.07
Tumor	2.78	2.36	4.94	4.55	1.86	0.11
Tail	4.22	1.98	0.69	0.52	0.46	0.19
Carcass	1.33	0.97	0.98	0.71	0.46	0.12

Table 25: In vivo biodistribution of 5-[^{125}I]IDFdR in mice following i. v. injection into tail vein, expressed as % I.D./total organ.

Organs	15 min	30 min	1 hr	2 hr	4 hr	24 hr
Blood	8.57	5.07	3.80	2.43	1.39	0.08
Lung	0.52	0.28	0.33	0.14	0.09	0.01
Bile	0.31	0.18	0.42	0.27	0.18	0.00
Liver	2.95	2.86	2.18	1.31	0.88	0.24
Spleen	0.35	0.14	0.13	0.09	0.06	0.01
Stomach	1.76	1.61	2.65	2.11	1.00	0.02
Intestine	7.45	6.37	8.30	4.78	3.21	0.09
Kidney	2.65	1.34	1.00	0.50	0.28	0.02
Bladder	0.66	0.50	0.20	0.29	0.04	0.00
Thyroid	0.53	0.55	0.75	0.93	0.65	0.01
Tumor	1.97	2.27	2.25	3.50	1.60	0.03
Tail	2.08	0.98	0.31	0.24	0.21	0.09
Carcass	20.99	15.53	14.23	10.69	7.06	1.74

Table 26: In vivo biodistribution of 5-[^{125}I]IDFdR in mice following i. v. injection into tail vein, expressed as organ/blood ratio.

Organs	15 min	30 min	1 hr	2 hr	4 hr	24 hr
Blood	1.00	1.00	1.00	1.00	1.00	1.00
Lungs	0.62	0.69	0.86	0.74	0.70	0.92
Bile	2.76	5.63	8.06	16.74	17.04	6.21
Liver	0.56	0.85	1.91	2.35	0.95	4.77
Spleen	0.42	0.32	0.35	0.48	0.44	0.81
Stomach	1.91	2.50	5.67	5.35	5.94	1.33
Intestine	0.67	0.94	1.44	1.48	1.74	0.82
Kidney	1.21	1.08	1.09	0.87	0.81	1.31
Bladder	5.80	8.62	6.99	12.87	2.34	1.23
Thyroid	0.64	1.17	2.22	4.76	5.35	1.65
Tumor	0.55	0.87	2.18	3.49	2.63	2.22
Tail	0.94	0.75	0.31	0.41	0.68	4.43
Carcass	0.28	0.36	0.43	0.55	0.58	2.89

Table 27: In vivo biodistribution of *cyclo*Sal-5-[^{125}I]IDFdR in mice following i. v. injection into tail vein, expressed as % I.D./g organ.

Organs	15 min	30 min	1 hr	2 hr	4 hr	24 hr
Blood	16.53	12.97	10.82	10.28	6.34	2.60
Lungs	18.55	14.15	9.32	8.50	8.64	3.30
Bile	10.16	11.08	6.98	5.27	3.77	1.92
Liver	7.70	6.84	4.88	3.15	2.27	1.19
Spleen	2.66	1.73	1.48	1.34	0.89	0.47
Stomach	2.44	3.59	4.36	2.11	1.73	0.39
Intestine	1.52	1.59	1.64	1.19	0.89	0.35
Kidney	7.62	7.06	4.51	3.76	2.37	1.02
Bladder	14.28	7.75	5.26	3.51	2.68	1.37
Thyroid	3.97	3.65	3.49	1.92	1.98	0.96
Tumor	2.30	2.41	3.80	3.35	2.23	1.27
Tail	5.85	5.64	4.42	3.67	5.38	1.01
Carcass	1.37	1.43	1.19	0.95	0.63	0.49

Table 28: In vivo biodistribution of *cyclo*Sal-5-[^{125}I]IDFdR in mice following i. v. injection into tail vein, expressed as % I.D./total organ.

Organs	15 min	30 min	1 hr	2 hr	4 hr	24 hr
Blood	29.65	24.19	18.93	17.24	10.36	4.81
Lungs	2.33	2.20	1.63	1.40	1.57	0.46
Bile	0.09	0.17	0.11	0.12	0.07	0.03
Liver	8.97	8.59	5.78	3.77	2.74	1.70
Spleen	0.29	0.27	0.19	0.17	0.10	0.08
Stomach	0.78	0.91	0.92	0.46	0.47	0.12
Intestine	4.13	3.98	3.91	2.90	2.09	1.01
Kidney	3.42	3.29	2.41	1.57	0.95	0.68
Bladder	0.16	0.16	0.14	0.05	0.05	0.03
Thyroid	0.61	0.64	0.53	0.30	0.31	0.16
Tumor	0.78	1.33	2.15	1.54	0.93	0.57
Tail	2.68	2.65	2.02	1.72	2.34	0.47
Carcass	21.44	22.69	17.91	13.78	8.83	7.50

Table 29: In vivo biodistribution of *cyclo*Sal-5-[^{125}I]IDFdR in mice following i. v. injection into tail vein, expressed as organ/blood ratio.

Organs	15 min	30 min	1 hr	2 hr	4 hr	24 hr
Blood	1.00	1.00	1.00	1.00	1.00	1.00
Lungs	1.12	1.10	0.84	0.85	1.32	1.26
Bile	0.61	0.85	0.63	0.52	0.59	0.74
Liver	0.47	0.53	0.44	0.30	0.36	0.45
Spleen	0.16	0.14	0.13	0.13	0.14	0.18
Stomach	0.15	0.28	0.37	0.20	0.27	0.16
Intestine	0.09	0.12	0.15	0.12	0.14	0.13
Kidney	0.46	0.55	0.39	0.36	0.38	0.42
Bladder	0.87	0.59	0.49	0.33	0.43	0.54
Thyroid	0.24	0.29	0.31	0.18	0.31	0.37
Tumor	0.14	0.20	0.34	0.32	0.35	0.49
Tail	0.35	0.43	0.41	0.37	0.82	0.38
Carcass	0.08	0.11	0.11	0.09	0.10	0.19

Table 30: **Evaluation of two to three ROIs of the static gamma camera pictures acquired using two male Sprague Dawley rats dosed with 5-[^{123}I]DFPdR after 70 minutes for rat #1 and after 60 minutes for rat #2**

	rat #1 after 70 minutes			rat #2 after 60 minutes	
	bladder	stomach	thyroid	stomach	thyroid
Radioactivity [counts]	4650	5226	460	9257	498
Size of ROI [pixel]	230	176	34	331	40
Average/pixel	20.22	29.69	13.53	27.97	12.[illegible]
S.D.	7.614	7.766	4.962	13.182	5.875

Table 31: **Evaluation of two to three ROIs of the static gamma camera pictures taken in two male Sprague Dawley rats dosed with 5-[^{123}I]DFPdR after 100 minutes for rat #1 and after 90 minutes for rat #2**

	rat #1 after 100 minutes			rat #2 after 90 minutes	
	bladder	stomach	thyroid	stomach	thyroid
radioactivity [counts]	5997	8585	437	10608	597
Size of ROI [pixel]	230	176	34	331	40
Average/pixel	26.07	48.78	12.85	32.05	14.93
S.D.	10.367	15.227	4.446	14.908	7.543

Table 32: Evaluation of two to three ROIs of the static gamma camera pictures taken in two male Sprague Dawley rats dosed with 5-[^{123}I]DFPdR after 130 minutes for rat #1 and after 120 minutes for rat #2

	rat #1 after 130 minutes			rat #2 after 120 minutes	
	bladder	stomach	thyroid	stomach	thyroid
radioactivity [counts]	6182	9168	526	10012	637
Size of ROI [pixel]	230	176	34	331	40
Average/pixel	26.88	52.09	15.47	30.25	15.93
S.D.	9.5	17.652	4.788	16.022	5.53

Appendix C: Detailed production parameters for producing iodine isotopes

Detailed information on nuclear reactions, production parameters, cross sections, purification and physical characteristics:

Production of Iodine-108:[73]

Nuclear reaction:

^{54}Fe (^{58}Ni,p3n) ^{108}I

cross section:

effective cross section σ ~500nb

Production parameters:

5 particle nA beam of 255 MeV ^{58}Ni for 15.5h and a 3 particle nA beam of 240 MeV ^{58}Ni for 21.5h.

Characteristics:

$T_{1/2\,a}$: 36±6 ms

α 3947± 5 keV

Purification:

The isotope is purified and identified via fragment mass analyser

Use:

For basic research.

Production of Iodine-109:

Nuclear reaction:

^{54}Fe (^{58}Ni, p2n) ^{109}I [74,75,76]

cross section:

effective cross section estimation: σ: 40μb [74]

estimation of production cross section: 16 ± 4 μb [75]

Production parameters:

Pulsed ^{58}Ni beam of 250 MeV from the Munich MP tandem-linear accelerator onto a ^{54}Fe target with a pulsing period of 6.4 μs. [74]

A ^{58}Ni beam of 220 MeV at the ATLAS superconducting linear accelerator at the Argonne National Laboratory was used on an isotopically enriched ^{54}Fe foil of 500 μg/cm^2. [75]

A ^{58}Ni beam of 240 MeV at the Daresbury tandem Van de Graaff accelarator was used to bombard a 500 μg/cm^2 self supporting ^{54}Fe target with a beam current of 3-4 particle nA for 21 hours. As the energy is not optimal for this nuclear reaction the ^{109}I was produced only with a very low cross section of 3 μb as an impurity. [76]

Characteristics:

$T_{1/2\,a}$: 14μs [74]

P: 0.811 MeV

$T_{1/2}$: 100μs [75]

P:0.829 ± 0.004 MeV

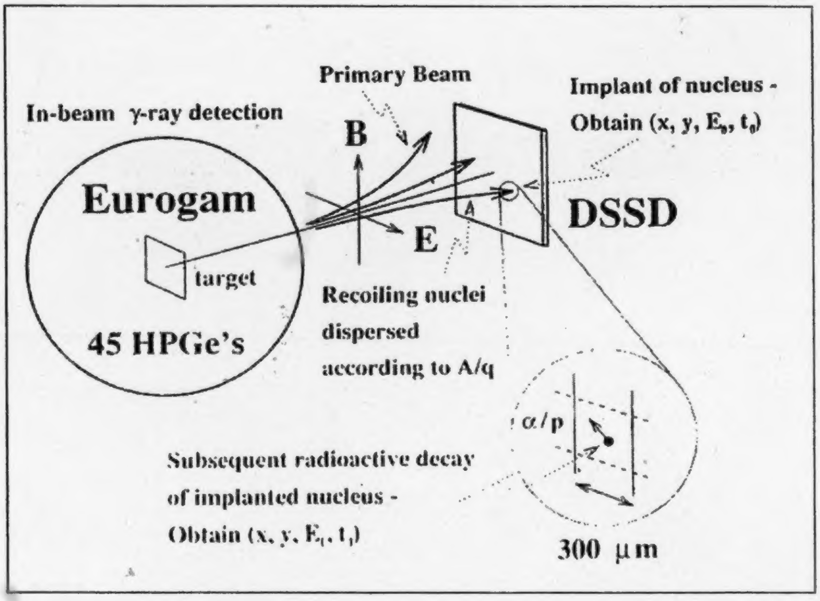
Primary Beam
In-beam γ-ray detection
Implant of nucleus - Obtain (x, y, E$_0$, t$_0$)
B
Eurogam
DSSD
E
A
target
Recoiling nuclei dispersed according to A/q
45 HPGe's
α/p
Subsequent radioactive decay of implanted nucleus - Obtain (x, y, E$_1$, t$_1$)
300 μm

Fig. 35. Schematic diagram showing the principle of recoil decay tagging. Prompt γ rays are recorded by Eurogam. Recoiling evaporation residues pass through a velocity filter with crossed electric (E) and magnetic (B) fields (Daresbury Recoil Separator) and are there dispersed according to their mass-to-charge ratio (A/q) before being implanted into the double sided silicon strip detector (DSSD) at position (x,y) at time t_0 with energy E_0. Within the same pixel (x,y) subsequent charged-particle radioactivity (decay at time t1 with energy E1) can be correlated with the initial implantation. [76]

Purification:

The isotope will be purified for identification only by a recoil mass separator or a fragment mass analyser. The detection and identification will be performed by implanting the evaporation residues into silicon detectors. A scheme of such a detector developed by the Edinburgh group, a double –sided silicon strip detector is shown in figure 35.

Use:

Product is used for measurement and fundamental physic research purposes (nuclear masses and nuclear structure very far from the valley of β-stability).

Production of Iodine-110:

Nuclear reaction:

^{58}Ni (^{58}Ni, αpn) ^{110}I [77]

Characteristics:

$T_{1/2\,a}$: 650± 20ms [73]

$T_{1/2\,a}$: 690 ms [78]

p: 2500-6000 keV

α: 3392 keV

Production parameters:

A 5 MeV/u ^{58}Ni beam from the UNILAC at GSI was used to bombard a 4mg/cm^2 ^{58}Ni target. [77]

290 MeV ^{58}Ni ions were used to bombard a 3mg/cm^2 ^{58}Ni target. [78]

Purification:

The produced evaporation residues were collected by recoil in a tantalum catcher which was kept at a temperature of 2500°C inside an arc discharge ion source. The products were released, ionised and extracted. For separation they were accelerated and magnetically separated. [77,78]

Production of Iodine-111:

Nuclear Reaction:

^{58}Ni (^{58}Ni, αp)^{111}I [77, 78, 79]

Production parameters:

A thin ^{58}Ni-target foil with 600 μg/cm^2 backed by 17 mg/cm^2 ^{197}Au was bombarded with a ^{58}Ni particle beam of 210 MeV at a beam intensity of 10pnA. [79]

A 5 MeV/u ^{58}Ni beam from the UNILAC at GSI was used to bombard a 4mg/cm^2 ^{58}Ni target. [77]

290 MeV ^{58}Ni ions were used to bombard a 3mg/cm^2 ^{58}Ni target. [78]

Characteristics:

$T_{1/2\,a}$: 2.5 s [78]

γ: 266.5, 321.5, 341.2 keV

α: 3120 keV

Purification:

The produced evaporation residues were collected by recoil in a tantalum catcher which was kept at a temperature of 2500°C inside an arc discharge ion source. The products were released, ionised and extracted. For separation they were accelerated and magnetically separated. [77,78]

Use:

For basic research.

Production of Iodine-112:

Nuclear reaction:

^{58}Ni (^{58}Ni, 3pn) ^{112}I [76, 77, 78]

Production parameters:

A ^{58}Ni beam was used to bombard a 440 μg/cm2 thick ^{58}Ni target with a beam energy of 240 MeV. [76]

A 5 MeV/u ^{58}Ni beam from the UNILAC at GSI was used to bombard a 4mg/cm^2 ^{58}Ni target. [77]

290 MeV ^{58}Ni ions were used to bombard a 3mg/cm2 ^{58}Ni target. [78]

Characteristics:

$T_{1/2\,a}$: 3.4 s [77, 78]

α: 2866 keV [77]

p: 2000-5000 keV; γ: 688.9, 786.9 keV [78]

Purification:

The produced evaporation residues were collected by recoil in a tantalum catcher which was kept at a temperature of 2500°C inside an arc discharge ion source. The products were released, ionised and extracted. For separation they were accelerated and magnetically separated. [77, 78]

Use:

For basic research.

Production of Iodine-113:

Nuclear reaction:

^{58}Ni (^{60}Ni, αp) ^{113}I [79]

^{27}Al (^{129}Xe, fragmentation)^{113}I [80]

^{58}Ni (^{58}Ni, 3pγ) ^{113}I [76, 81, 82, 83]

Cross section:

Production cross section σ: (7.2 ± 8.8) μb [80]

Production parameters:

A thin ^{60}Ni-target foil with 600 μg/cm^2 backed by 17 mg/cm^2 ^{197}Au was bombarded with a ^{58}Ni particle beam of 210 MeV at a beam intensity of 10pnA. [79]

A ^{58}Ni beam was used to bombard a 440 μg/cm2 thick ^{58}Ni target with a beam energy of 240 MeV. [76, 82, 83]

290 MeV ^{58}Ni ions were used to bombard a 3mg/cm2 ^{58}Ni target. [78]

Characteristics:

$T_{1/2}$: 5.9 s [78]

γ: 55, 160, 216.4, 320.4, 351.5, 462.5, 511, 567.4, 622.4, 798.3, 802.2 keV

β^+

Purification:

The isotope will be purified for identification only by a recoil mass separator or a fragment mass analyser. The detection and identification will be performed by implanting the evaporation residues into silicon detectors. A scheme of such a detector developed by the Edinburgh group, a double –sided silicon strip detector is shown in figure 33. [76, 82, 83] The produced evaporation residues were collected by recoil in a tantalum catcher which was kept at a temperature of 2500°C inside an arc discharge ion source. The products were released, ionised and extracted. For separation they were accelerated and magnetically separated. [78]

Use:

For basic research.

Production of Iodine-114:

Nuclear reaction:

^{27}Al (^{129}Xe, fragmentation) ^{114}I [80]

^{60}Ni (^{58}Ni, 3pnγ) ^{114}I [84]

^{63}Cu (^{58}Ni,α2pn) ^{114}I [78]

Cross section:

Production cross section σ: $(4.19 \pm 4.50) * 10^{-5}$ b [80]

Production parameters:

Two self supporting foils of ^{60}Ni, thickness 480 μg/cm^{2}were bombarded with ^{58}Ni at an energy of 250 MeV. Impurities for this reaction are the formation of ^{115}I. [84]

290 MeV ^{58}Ni ions were used to bombard a 3mg/cm^2 ^{63}Cu target. [78]

Characteristics:

$T_{1/2\,a}$: 2.1 sec [78]

γ: 511, 682.6, 708.8 keV

β^+

Two isomers with two structures are shown in the decay scheme (figure 36)

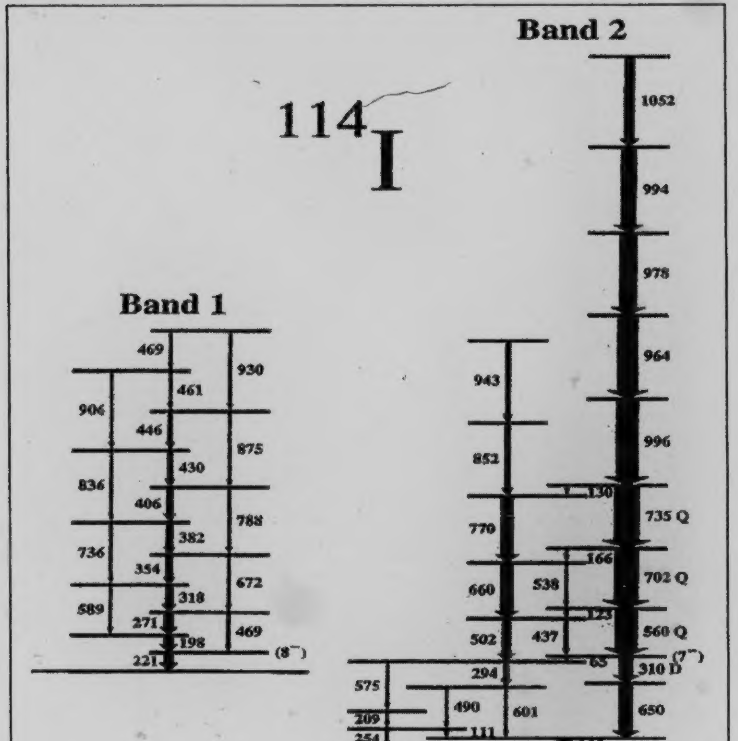

Band 2
^{114}I
1052
994
978
964
996
Band 1
469
930
461
906
446
875
430
836
406
788
382
736
354
672
318
589
271
469
198
(8⁻)
221
943
852
130
735 Q
770
166
660
538
702 Q
123
502
437
560 Q
(7⁻)
65
310 D
294
575
490
601
650
209
111
254
144
203
186
102

Fig. 36. Decay scheme of both isomers of ^{114}I.

Purification:

Purification was performed via the recoil separator at Daresbury coupled to the POLYTESSA array to record both mass and charge information. [84]

The produced evaporation residues were collected by recoil in a tantalum catcher which was kept at a temperature of 2500°C inside an arc discharge ion source. The products were released, ionised and extracted. For separation they were accelerated and magnetically separated. [78]

Use:

For basic research.

Production of Iodine-115:

Nuclear reaction:

^{129}Xe (^{27}Al, fragmentation) ^{115}I [80]

^{60}Ni (^{58}Ni, 3p) ^{115}I [85]

$CeO_2*(H_2O)_x$ (p,) Xe $\longrightarrow$ $^{115\text{-}119}I$ [86]

^{106}Cd (^{12}C,p2n) ^{115}I [87]

Cross section:

Production cross section σ: $(2.85 \pm 0.38) * 10^{-4}$ b [80]

Production parameters:

A thick $CeO_2*(H_2O)_x$ powder target was bombarded with 600 MeV protons at the Cern Synchrocyclotron. The main element which was separated was xenon. As impurities and/or decay products also ^{115}I and other iodine isotopes could be found and investigated. [86]

Two self supporting foils of ^{60}Ni, thickness 480 $\mu g/cm^2$were bombarded with ^{58}Ni at an energy of 250 MeV. [85]

A 3.5 mg/cm^2 thick ^{106}Cd target was bombarded with ^{12}C at a beam energy of 58 and 63 MeV. Possible impurities are $^{113,115}Te$ from the (^{12}C, αn) and (^{12}C, 2pn) reactions. For the investigation performed in this study these impurities were not important as their γ-rays could be excluded in the detection with a Ge(Li) detector. [87]

Characteristics:

$T_{1/2\,a}$: 1.3 ± 0.2 min [86]

β^+

Purification:

The products were purified by extraction from the target into the ion source of an isotope separator where they were ionised and magnetically separated. [86]

Use:

For basic research.

Production of Iodine-116:

Nuclear reaction:

^{129}Xe (^{27}Al, fragmentation) ^{116}I [80]

$CeO_2*(H_2O)_x$ (p,) Xe [86]

^{106}Cd (^{12}C, 2n) ^{116}Xe ⟶ ^{116}I [88]

^{106}Cd (^{12}C, pn) ^{116}I [88, 89]

^{103}Rh (^{16}O, 3n) ^{116}I [90]

^{104}Pd (^{16}O, 4n) ^{116}Xe ⟶ ^{116}I [90]

^{104}Pd (^{16}O, p3n) ^{116}I [90]

^{92}Mo (^{28}Si, 3pn) ^{116}I [91]

La (p, spallation) ^{116}I [92]

Cross section:

Production cross section σ: $(1.05 \pm 0.21) * 10^{-3}$ b [80]

Production cross section σ: 16 mb [88]

Production parameters:

A thick $CeO_2*(H_2O)_x$ powder target was bombarded with 600 MeV protons at the Cern Synchrocyclotron. The main element which was separated was xenon. As impurities and/or decay products also ^{116}I and other iodine isotopes could be found and investigated. [86]

A 4.3 mg/cm2 ^{106}Cd target with 27μm lead backing was bombarded with a ^{12}C-beam of 48, 52, 57 and 61MeV to study the excitation functions. The spectra were recorded during and between the beam bursts without separation. [88]

A self-supporting 3mg/cm^2 thick palladium foil was bombarded with a $^{16}O^{4+}$ beam of 91 MeV to produce ^{116}Xe which decays to ^{116}I with a half life time of 57 sec. To avoid the ambiguities which are a result of the ^{116}Xe-^{116}I transient equilibrium the production of ^{116}I via the ^{103}Rh (^{16}O, 3n) was also performed. Therefore a self-supporting 4 mg/cm^2 thick rhodium foil was bombarded with a $^{16}O^{4+}$-beam of 83

MeV. [90]

A self-supporting 340 μg/cm^2 thick ^{92}Mo-target was bombarded with a ^{28}Si- beam at an energy of 120 MeV. [91]

Lanthanum foils (38*16*0.25 mm) were bombarded with 3 GeV protons from the Princeton-Pennsylvania Accelerator for 1h periods. [92]

A self-supporting ^{106}Cd-target was bombarded with ^{12}C-beams at lab energies of 58 and 63 MeV. [89]

Characteristics:

$T_{1/2\,a}$: << 0.5 min [86]

β^+

γ: 104 keV

$T_{1/2\,a}$: 2.91 ± 0.15 min [90]

β^+: 1.55-3.04 MeV; 3.05-4.53 MeV; 4.55-6.05 MeV

γ: 511; 540; 679 keV

A new isomer with a half life time of 3.27 ± 0.16 μsec was found, γ: 65.4, 105, 109.6 and 114.2, 227.2 keV [91]

Purification:

The products were purified by extraction from the target into the ion source of an isotope separator where they were ionised and magnetically separated. [86]

The products were purified via an on-line isotope mass separator. [90]

The lanthanum foils were placed into the ion source of an electromagnetic isotope separator after irradiation. Into the foil placed at the separators focal plane a hole was cut at mass-116 position. The isotopes collected there were allowed to pass down a pipe where they were collected on a thin Al-foil for counting. [92]

Use:

For basic research.

Production of Iodine-117:

Nuclear reaction:

a: ^{129}Xe (^{27}Al, fragmentation) ^{117}I [80]

b: ^{94}Mo (^{27}Al, 2p2n) ^{117}I [93]

c: ^{109}Ag (^{12}C, 4n) ^{117}I [94, 95]

d: ^{114}Sn (^{6}Li, 3n) ^{117}I [94, 95] e: $CeO_2*(H_2O)_x$ (p,) Xe $\longrightarrow$ $^{115-119}I$ [86]

f: $^{112}Sn(^{12}C, \alpha p2n)\ ^{117}I$ [87]

g: $^{106}Cd\ (^{14}N, 2pn)\ ^{117}I$ [87]

h: $^{127}I\ (\pi^{\pm}, 10n)\ ^{117}I$ [97]

i: $^{90}Zr\ (^{31}P, 2p2n)\ ^{117}I$ [98]

Cross section:

Production cross section σ: $(2.45 \pm 0.24) * 10^{-3}$ b for reaction a.

Table 33: Independent production cross section in (mb) for the reaction of ^{127}I with pions having the energy of 60-350 MeV to result in ^{117}I: [97]

T_π	60 MeV		100 MeV		120 MeV		140 MeV		180 MeV		210 MeV		250 MeV		300 MeV		350 MeV	
Nuclide	σ^+	σ^-	σ^+	σ^-	σ^+	σ^-	σ^+	σ^-	σ^+	σ^-	σ^+	σ^-	σ^+	σ^-	σ^+	σ^-	σ^+	σ^-
^{117}I	5.7± 0.9		8.94 ± 1.23				8.63 ± 1.27		5.36 ± 0.25		5.38 ± 0.30	2.69 ± 0.44	4.32 ± 0.55	2.38 ± 0.43	3.37 ± 0.27	2.03 ± 0.18	3.34 ± 0.19	2.29 ± 0.56

Production parameters:

^{27}Al particles with an energy of 129 MeV were used for reaction **b** at the Stony Brook Nuclear Structure Laboratory.

For reaction **c** carbon-12 ions with an energy of 50 to 70 MeV from the Lanchow cyclotron were used on a natural silver target.

For reaction **c** carbon-12 ions with an energy of 6.8 MeV/nucleon from the Yale Heavy-Ion Accelerator were used on a natural Ag-target. For the target 1.5 mg/cm^2 of silver was evaporated on Al and bombarded for 3 min. [95]

A thick $CeO_2*(H_2O)_x$ powder target was bombarded with 600 MeV protons at the Cern Synchrocyclotron. The main element which was separated was Xenon. As impurities and/or decay products also ^{117}I and other iodine isotopes could be found and investigated. [89]

For reaction **f** carbon-12 with an energy of 86 MeV was used to bombard a 3.9 mg/cm^2 thick target of ^{112}Sn. For reaction **g** nitrogen-14 was used to bombard a 3.5 mg/cm^2 thick target of ^{106}Cd.

For reaction **d** a ^{114}Sn target was bombarded with ^6Li ions at an energy of 25-35 MeV. [96]

For reaction **h** KI pellets with a thickness of ~ 120 mg/cm2 in thin Mylar guard foils were bombarded with either protons at an energy of 500MeV or π^+ and π^- produced in the P^3 and LEP channels of the Clinton P. Anderson Meson Physics Facility (LAMPF) ranging in energy between 60 and 350 MeV and a momentum bite of 6% and 4% respectively. [97]

For reaction **i** two stacked self-supporting ^{90}Zr-foils with a thickness of 440µg/cm^2 were bombarded with a ^{31}P beam at an energy of 150 MeV provided by the Centre de Recherches Nucléaires in Strasbourg. [98]

Characteristics:

$T_{1/2\,a}$: 2.2 ± 0.05 min [94]

β^+ : 5.25 MeV

$T_{1/2}$: 2.4 ± 0.1 min [86]

β^+

γ: 158, 325, 720 and others keV

$T_{1/2}$: 2.7 ± 0.2 min [95]

β^+: 3.25 MeV ± 50 keV and 3.5 MeV ± 50 keV

γ: 274 ± 1, 325 ± 1, 599 ± 1 keV

$T_{1/2}$: 2.2 min [97]

γ: 325.9 keV

Purification:

For reaction **c** the products were transported through a 10 m long capillary by a stream of helium gas and were collected on an aluminised Mylar tape.

The products were purified by extraction from the target into the ion source of an isotope separator where they were ionised and magnetically separated. [86]

After catching the recoiling ^{117}I in an Al-catcher foil this foil was dissolved in HCl. 10 mg/mL iodide carrier was added and the iodine was extracted with CCl_4. After reextraction into water the iodide was precipitated as AgI. Natural silver gives no impurities which would interfere with ^{117}I under these conditions. [95]

Impurities (^{115,116}I, $^{114-117}$Te and ^{113,114}Sb) were not separated from the sample as a characterisation via a HPGe-detector was performed. [98]

Use:

For basic research.

Production of Iodine-118:

Nuclear reaction:

a: ^{129}Xe (^{27}Al, fragmentation) ^{118}I [80]

b: $CeO_2*(H_2O)_x$ (p,) Xe $\longrightarrow$ $^{115\text{-}119}I$ [86]

c: ^{112}Cd (^{10}B, 4n) ^{118}I [89]

d: ^{114}Sn (^{7}Li, 3n) ^{118}I [89]

e: La (p, spallation) I [92]

f: Ag (^{12}C) ^{118}I [95]

g: ^{127}I ($\pi^{\pm}$, 9n) ^{118}I [97]

h: ^{197}Au (^{12}C, f) ^{118}I [99]

Cross section:

Production cross section σ: (7.23 ± 1.57) * 10^{-3} b [80]

Production cross section from the interaction of ^{127}I with 500 MeV protons in mb: 6.77 ± 0.4 [97]

Table 34: Independent production cross section in (mb) for the reaction of ^{127}I with pions having the energy of 60-350 MeV to result in ^{118}I: [97]

T_π	60 MeV		100 MeV		120 MeV		140 MeV		180 MeV		210 MeV		250 MeV		300 MeV		350 MeV	
Nuclide	σ^+	σ^-	σ^+	σ^-	σ^+	σ^-	σ^+	σ^-	σ^+	σ^-	σ^+	σ^-	σ^+	σ^-	σ^+	σ^-	σ^+	σ^-
^{118}I	19.3 ± 4.5		13.5 ± 1.9	1.43 ± 0.33	16.1 ± 0.9		14.8 ± 0.6	2.94 ± 0.3	13.0 ± 0.8	3.7 ± 0.25	12.8 ± 0.8	4.68 ± 0.24	10.0 ± 0.6	4.05 ± 0.23	7.82 ±0.38	4.16 ± 0.22	7.24 ±0.80	2.88 ± 0.26

Production cross section for ^{118}I produced via reaction h σ: 1.79 ± 0.48 mb [99]

Production parameters:

A thick $CeO_2*(H_2O)_x$ powder target was bombarded with 600 MeV protons at the Cern Synchrocyclotron. The main element which was separated was xenon. As impurities and/or decay products also ^{118}I and other iodine isotopes could be found and investigated. [86]

A self-supporting ^{112}Cd-target was bombarded with a ^{10}B-beam at an energy of 54 MeV.

A self-supporting ^{114}Sn-target was bombarded with a ^{7}Li-beam at an energy of 34 MeV. [89]

Lanthanum foils (38*16*0.25 mm) were bombarded with 3 GeV protons from the Princeton-Pennsylvania Accelerator for 1h periods. [92]

^{118}I was produced as an impurity in the reaction of natural silver with ^{12}C-ions at an energy of 57 MeV. [95]

For reaction **g** KI pellets with a thickness of ~ 120 mg/cm2 in thin Mylar guard foils were bombarded with either protons at an energy of 500MeV or π^+ and π^- produced in the P^3 and LEP channels of the Clinton P. Anderson Meson Physics Facility (LAMPF) ranging in energy between 60 and 350 MeV and a momentum bite of 6% and 4% respectively. [97]

For reaction **h** a 5.16 mg/cm^2 thick gold foil was bombarded. [99]

Characteristics:

$T_{1/2\,a}$: 14.3 ± 0.1 min

β^+

γ: 545, 606, 1150 and others keV [86]

$T_{1/2}$: 8 min [91]

γ: 352.7, 496.4, 510.8, 523.8, 544.8, 551.8, 559.5, 600, 605.2, 614, 684.9, 711.2, 740.7, 875.6, 1116.2, 1149.9, 1257, 1285.9, 1338.4, 1349.2, 1414.9 keV [92]

β^+: 5.45 MeV [95]

Two isomers:

$T_{1/2}$: 14.3 min for ^{118}I

$T_{1/2}$: 8.5 min for ^{118m}I

γ for 118I: 605.2 keV

γ for 118mI: 599.8, 605.2 keV [97]

Purification:

The products were purified by extraction from the target into the ion source of an isotope separator where they were ionised and magnetically separated. [86]

Cross contaminations from neighbouring masses were below 1%. Produced isotopes were mainly xenon with small amounts of iodine and very small amounts of caesium. For mass numbers 118, 120 and 122 chemically pure samples were obtained by dissolving the catcher foil of the mass separator in NaOH. After acidifying the sample with HNO_3 and adding of NaI carrier the iodine was precipitated as AgI and collected on filter paper. [92]

Use:

For basic research.

Production of Iodine-119:

Nuclear reaction

^{122}Te (p, 4n) ^{119}I [39]

^{129}Xe (^{27}Al, fragmentation) ^{119}I [80]

$CeO_2*(H_2O)_x$ (p,) Xe $\longrightarrow$ $^{115\text{-}119}I$ [86]

^{109}Ag (^{12}C, 2n) ^{119}I [95]

^{116}Sn (^{6}Li, 3n) ^{119}I [96]

^{127}I ($\pi^{\pm}$, 8n) ^{119}I [97]

Cross section:

Production cross section σ: $(1.16 \pm 0.20) * 10^{-2}$ b [80]

Production cross section from the interaction of ^{127}I with 500 MeV protons in mb:
15.0 ± 0.9 [97]

Table 35: Independent production cross section in (mb) for the reaction of ^{127}I with pions having an energy of 60-350 MeV to result in ^{119}I: [97]

T_π	60 MeV		100 MeV		120 MeV		140 MeV		180 MeV		210 MeV		250 MeV		300 MeV		350 MeV	
Nuclide	σ^+	σ^-	σ^+	σ^-	σ^+	σ^-	σ^+	σ^-	σ^+	σ^-	σ^+	σ^-	σ^+	σ^-	σ^+	σ^-	σ^+	σ^-
^{119}I	38.8 ± 9.1		26.6 ± 3.6	1.04 ± 0.21	34.0 ±1.7	6.4 ± 0.4	33.0 ± 1.8	10.8 ± 0.4	32.4 ± 1.1	13.7 ± 0.6	29.6 ± 1.8	13.5 ± 0.6	22.7 ± 1.3	11.4 ± 0.5	16.8 ± 0.9	9.97 ± 0.43	14.5 ± 1.0	7.05 ± 0.57

Production parameters:

A thick $CeO_2*(H_2O)_x$ powder target was bombarded with 600 MeV protons at the Cern Synchrocyclotron. The main element which was separated was xenon. As impurities and/or decay products also ^{119}I and other iodine isotopes could be found and investigated. [86]

A 1.5mg/cm^2 thick natural silver target with Al-backing was bombarded with C-12 ions at an energy of 57 MeV from the Yale Heavy-Ion Accelerator for 15 min. [95]

A ^{116}Sn target was bombarded with ^{6}Li ions at an energy of 25-35 MeV.

For reaction **d** a ^{114}Sn target was bombarded with ^{6}Li ions at an energy of 25-35 MeV. [96]

For reaction **h** KI pellets with a thickness of ~ 120 mg/cm2 in thin Mylar guard foils were bombarded with either protons at an energy of 500MeV or π^+ and π^- produced in the P^3 and LEP channels of the Clinton P. Anderson Meson Physics Facility (LAMPF) ranging in energy between 60 and 350 MeV and a momentum bite of 6% and 4% respectively. [97]

Characteristics:

β^+

γ: 258, 320, and others keV [86]

$T_{1/2}$: 18.2 ± 0.3 min

β^+: 2.35 ± 0.1 MeV

γ: 255 ± 1 keV [95]

$T_{1/2\,a}$: 19.3 min

γ: 257.5 keV [97]

Purification:

The products were purified by extraction from the target into the ion source of an isotope separator where they were ionised and magnetically separated. [86]

After catching the recoiling ^{119}I in an Al-catcher foil this foil was dissolved in HCl. 10 mg/mL iodide carrier was added and the iodine was extracted with CCl_4. After reextraction into water the iodide was precipitated as AgI. ^{107}Ag gives ^{117}I as impurity which decreases rapidly by decay. Other impurities are $^{118,120}I$. [95]

Production of Iodine-120:

Nuclear reaction:

a) $^{127}I\ (p, 8n)\ ^{120}Xe \xrightarrow[40\ \text{min}]{\beta^+,\ EC} {}^{120g}I$ [38, 39]

b) $^{122}Te\ (p, 3n)\ ^{120g}I$ [38, 39]

c) $^{120}Te\ (p, n)\ ^{120g}I$ [38, 39]

d) $^{120}Te\ (d, 2n)\ ^{120g}I$ [38, 39]

e) $^{nat}Sb\ (\alpha, x)\ ^{120m}I$ [38, 39]

f) $^{129}Xe\ (^{27}Al, \text{fragmentation})\ ^{120}I$ [80]

g) $^{114}Cd\ (^{10}B, 4n)\ ^{120}I$ [89]

h) $^{116}Sn\ (^{7}Li, 3n)\ ^{120}I$ [89]

i) La (p, spallation) I [92]

j) $^{127}I\ (\pi^{\pm}, 7n)\ ^{120}I$ [97]

cross section:

The cross sections for the tellurium reactions are given in references [38, 39].

Production cross section σ: (1.40 ± 0.25) * 10^{-2} b [80]

Table36: Independent production cross section in (mb) for the reaction of ^{127}I with pions having an energy of 60-350 MeV to result in ^{120}I: [97]

T_π	60 MeV		100 MeV		120 MeV		140 MeV		180 MeV		210 MeV		250 MeV		300 MeV		350 MeV	
Nuclide	σ^+	σ^-	σ^+	σ^-	σ^+	σ^-	σ^+	σ^-	σ^+	σ^-	σ^+	σ^-	σ^+	σ^-	σ^+	σ^-	σ^+	σ^-
^{120}I	42.6 ± 9.9		29.1 ± 3.5	7.69 ± 0.41	39.7 ± 1.4	17.3 ± 0.8	45.7 ± 1.3	23.3 ± 0.7	46.2 ± 1.3	25.3 ± 1.0	42.0 ± 2.3	22.9 ± 0.7	30.5 ± 1.2	18.3 ± 0.8	21.9 ± 1.0	15.3 ± 0.5	18.9 ± 1.2	11.0 ± 0.8

Production parameters:

For reaction a) a NaI target was irradiated with 340 MeV protons.

For reaction b) ^{122}Te was bombarded with lower energy protons in an energy range from 30-40 MeV .

For reaction c) ^{120}Te was bombarded with protons with an energy of 9-15 MeV.

For reaction d) ^{120}Te was bombarded with deuterons with an energy of 9-14 MeV. [38, 39]

For reaction g) a self-supporting ^{114}Cd-target was bombarded with a ^{10}B-beam at an energy of 51 MeV.

For reaction h) a self-supporting ^{116}Sn-target was bombarded with a ^{7}Li-beam at an energy of 34 MeV. [89]

For reaction i) lanthanum foils (38*16*0.25 mm) were bombarded with 3 GeV protons from the Princeton-Pennsylvania Accelerator for 1h periods. [92]

For reaction j) KI pellets with a thickness of ~ 120 mg/cm2 in thin Mylar guard foils were bombarded with either protons at an energy of 500MeV or π^+ and π^- produced in the P^3 and LEP channels of the Clinton P. Anderson Meson Physics Facility (LAMPF) ranging in energy between 60 and 350 MeV and a momentum bite of 6% and 4% respectively. [97]

Characteristics:

Main γ: 511, 560.3, 601, 640.6 keV [92]

Two isomers:

$T_{1/2\,a}$: 1.35 h for ^{120}I

$T_{1/2\,a}$: 53 min for ^{120m}I

γ for ^{120}I: 560.4 keV

γ for ^{120m}I: 560.4, 614.7 keV. [97]

Purification:

Cross contaminations from neighbouring masses were below 1%. Produced isotopes were mainly xenon with small amounts of iodine and very small amounts of caesium. For mass numbers 118, 120 and 122 chemically pure samples were obtained by dissolving the catcher foil of the mass separator in NaOH. After acidifying the sample with HNO_3 and adding of NaI carrier the iodine was precipitated as AgI and collected on filter paper. A small amount of ^{121}I as cross contamination was found. [92]

For reactions b),c) and d) a purification was not performed prior to identification. Thus the impurities could be determined. Reaction b) gives high levels of ^{120m}I and ^{121}I impurities and a little bit of ^{119}I while reaction c) gives only ^{120m}I as impurity and reaction d) gives ^{120m}I and ^{121}I as impurities. [38]

Use:

As tracer for PET (diagnostic).

Production of Iodine-121:

^{120}Te (d, n) ^{121}I [4]

^{122}Te (p,2n) ^{121}I [4]

^{129}Xe (^{27}Al, fragmentation) ^{121}I [80]

^{116}Cd (^{11}B, 6n) ^{121}I [91]

^{118}Sn (^{6}Li, 3n) ^{121}I [96]

^{127}I ($\pi^{\pm}$, 6n) ^{121}I [97]

cross section:

Production cross section σ: $(2.07 \pm 0.17) * 10^{-2}$ b [80]

Production cross section from the interaction of ^{127}I with 500 MeV protons in mb: 27.2 ± 2.3 [97]

Table 37: Independent production cross section in (mb) for the reaction of ^{127}I with pions having an energy of 60-350 MeV to result in ^{121}I: [97]

T_π	60 MeV		100 MeV		120 MeV		140 MeV		180 MeV		210 MeV		250 MeV		300 MeV		350 MeV	
Nuclide	σ^+	σ^-	σ^+	σ^-	σ^+	σ^-	σ^+	σ^-	σ^+	σ^-	σ^+	σ^-	σ^+	σ^-	σ^+	σ^-	σ^+	σ^-
^{121}I	35.9 ± 12.9	<3.3 ± 1.1	32.8 ± 6.4	32.9 ± 1.7		52.1 ± 2.4	61.0 ± 7.8	53.7 ± 1.4	59.4 ± 4.3	47.1 ± 1.8	56.6 ± 5.0	39.9 ± 1.3	41.2 ± 3.8	30.3 ± 1.2	26.8 ± 2.0	24.6 ± 0.7	23.6 ± 2.9	17.8 ± 1.3

Production parameters:

A self-supporting 740μg/cm^2 thick ^{116}Cd-target was bombarded with a ^{11}B-beam of 65 MeV energy. [91]

A ^{118}Sn target was bombarded with ^{6}Li ions at an energy of 25-35 MeV. [96]

For the reaction of iodine with pions KI pellets with a thickness of ~ 120 mg/cm2 in thin Mylar guard foils were bombarded with either protons at an energy of 500MeV or π^+ and π^- produced in the P^3 and LEP channels of the Clinton P. Anderson Meson Physics Facility (LAMPF) ranging in energy between 60 and 350 MeV and a momentum bite of 6% and 4% respectively. [97]

Characteristics:

A second isomer in ^{121}I was found with a half life of:

$T_{1/2\,a}$: 16 ± 1.4 μsec

γ: 135, 301.6, 315.4, 329.2, 359.1, 379.2, 405.2, 434.6 keV [91]

$T_{1/2\,a}$: 2.12 h

γ: 212.5 keV [97]

Purification:

Purification was performed via a recoil mass separator. [91]

Production of Iodine-122:

Nuclear reaction:

$^{122}Xe \longrightarrow {}^{122}I$

^{129}Xe (^{27}Al, fragmentation) ^{122}I [80]

^{116}Cd (^{11}B, 5n) ^{122}I [91]

^{116}Cd (^{10}B, 4n) ^{122}I [89]

^{118}Sn (^{7}Li, 3n) ^{122}I [89]

La (p, spallation) I [92]

^{127}I ($\pi^{\pm}$, 5n) ^{122}I [97]

Cross section:

Production cross section σ: (1.93 ± 0.16) * 10^{-2} b [80]

Production cross section from the interaction of ^{127}I with 500 MeV protons in mb: 16.8 ± 2.8 [97]

Table 38: Independent production cross section in (mb) for the reaction of ^{127}I with pions having an energy of 60-350 MeV to result in ^{122}I: [97]

T_π	60 MeV		100 MeV		120 MeV		140 MeV		180 MeV		210 MeV		250 MeV		300 MeV		350 MeV	
Nuclide	σ^+	σ^-	σ^+	σ^-	σ^+	σ^-	σ^+	σ^-	σ^+	σ^-	σ^+	σ^-	σ^+	σ^-	σ^+	σ^-	σ^+	σ^-
^{122}I	23.6 ± 5.0		42.6 ± 10.2	59.7 ± 16.1			64.5 ± 14.6	59.4 ± 14.1	49.2 ± 7.9	49.5 ± 8.0	39.4 ± 8.9	43.4 ± 9.8	29.6 ± 6.7	33.0 ± 7.5	24.6 ± 5.6	20.8 ± 4.8	22.1 ± 5.2	20.8 ± 4.8

Production parameters:

^{122}I is a generator produced isotope. The ^{122}Xe/^{122}I generator is prepared from mixed radioxenons (^{122}Xe, ^{123}Xe and ^{125}Xe) from by products of ^{127}I (p,5n) ^{123}Xe production of high purity ^{123}I. The generator is used 24 h after the end of cyclotron bombardment, permitting ^{123}Xe to decay to less than 1% of the total radioxenon activity. The impurity of ^{125}I was low because the time of taking out ^{122}I was kept low.

A self-supporting 740µg/cm^2 thick ^{116}Cd-target was bombarded with a ^{11}B-beam of 65 MeV energy. [91]

A self-supporting ^{116}Cd-target was bombarded with a ^{10}B-beam at an energy of 51 MeV.

A self-supporting ^{118}Sn-target was bombarded with a ^{7}Li-beam at an energy of 34 MeV. [89]

Lanthanum foils (38*16*0.25 mm) were bombarded with 3 GeV protons from the Princeton-Pennsylvania Accelerator for 1h periods. [92]

For the reaction of iodine with pions KI pellets with a thickness of ~ 120 mg/cm2 in thin Mylar guard foils were bombarded with either protons at an energy of 500MeV or π^+ and π^- produced in the P^3 and LEP channels of the Clinton P. Anderson Meson Physics Facility (LAMPF) ranging in energy between 60 and 350 MeV and a momentum bite of 6% and 4% respectively. [97]

Characteristics:

$T_{1/2\,a}$: 3.6 min

β^+: 77%

γ

ε

second isomer was found:

$T_{1/2\,a}$: 80 ± 8 μsec for the new isomer

γ : 32.5, 51.5, 61.9, 95, 160.1, 188 keV [91]

$T_{1/2}$: 3.5 min

Main γ: 511.3, 564.2, 692.9, 793.1 keV [92]

$T_{1/2\,a}$: 3.6 min

γ: 564.0 keV [97]

Purification:

Here not necessary as the generator gives pure iodine.

Purification was performed via a recoil mass separator. [91]

Cross contaminations from neighbouring masses were below 1%. Produced isotopes were manly xenon with small amounts of iodine and very small amounts of caesium. For mass numbers 118, 120 and 122 chemically pure samples were obtained by dissolving the catcher foil of the mass separator in NaOH. After acidifying the sample with HNO_3 and adding of NaI carrier the iodine was precipitated as AgI and collected on filter paper. A moderately large amount of ^{121}I and a small amount of ^{123}I was found as cross contamination. [92]

Use:

For labelling of PET diagnostics (especially aromatic compounds).

Production of Iodine-123:

Possible target materials: Tellurium, telluriumdioxide, antimony and xenon

Nuclear reactions:

$^{124}Te(p,2n)^{123}I$ [41, 42, 64]

$^{123}Te(p,n)^{123}I$ [41, 100]

$^{122}Te(d,n)^{123}I$ [41, 42, 64]

$^{121}Sb(\alpha,2n)^{123}Sb$ [41, 101, 102]

$^{124}Xe(p, 2n)^{123}Cs \longrightarrow {}^{123}Te \longrightarrow {}^{123}I$ [42, 43]

$^{124}\mathrm{Xe(p,pn)}^{123}\mathrm{Xe} \longrightarrow {}^{123}\mathrm{I}$ [42]

$^{127}\mathrm{I(p,5n)}\ ^{123}\mathrm{Xe} \longrightarrow {}^{123}\mathrm{I}$ [42, 44]

$^{122}\mathrm{Te}\ (^{4}\mathrm{He, 3n})\ ^{123}\mathrm{Xe} \longrightarrow {}^{123}\mathrm{I}$ [102]

$^{129}\mathrm{Xe}\ (^{27}\mathrm{Al}$, fragmentation) $^{123}\mathrm{I}$ [80]

$^{120}\mathrm{Sn}\ (^{6}\mathrm{Li, 3n})\ ^{123}\mathrm{I}$ [96]

$^{127}\mathrm{I}\ (\pi^{\pm}, 4\mathrm{n})\ ^{123}\mathrm{I}$ [97]

Cross section:

cross section σ: 1barn for $^{124}\mathrm{Te(p,2n)}$ reaction

cross section σ: 450mbarn for $^{123}\mathrm{Te(p,n)}$ reaction [41]

Production cross section σ: $(2.43 \pm 0.15) * 10^{-2}$ b for the fragmentation reaction [80]

Production cross section from the interaction of $^{127}\mathrm{I}$ with 500 MeV protons in mb: 41.2 ± 2.5 [97]

Table 39: Independent production cross section in (mb) for the reaction of $^{127}\mathrm{I}$ with pions having an energy of 60-350 MeV to result in $^{123}\mathrm{I}$: [97]

T_π	60 MeV		100 MeV		120 MeV		140 MeV		180 MeV		210 MeV		250 MeV		300 MeV		350 MeV	
Nuclide	σ^+	σ^-	σ^+	σ^-	σ^+	σ^-	σ^+	σ^-	σ^+	σ^-	σ^+	σ^-	σ^+	σ^-	σ^+	σ^-	σ^+	σ^-
$^{123}\mathrm{I}$	31.4 ± 6.9	52.4 ± 31.1	58.5 ± 9.9	104.8 ± 6.2			83.4 ± 5.2	96.5 ± 3.1	64.9 ± 3.0	74.2 ± 2.3	55.9 ± 2.4	58.6 ± 2.1	46.0 ±2.4	49.2 ± 1.6	29.6 ± 2.4	44.9 ± 1.5	29.8 ± 1.7	34.9 ± 1.8

Production parameters:

Irradiation of $^{124}\mathrm{Te}$ with protons which have an energy of 25-30 MeV. Impurity of 1% to 4% $^{124}\mathrm{I}$. Target material is usually $\mathrm{TeO_2}$, target thickness is approximately 80-256 mg/cm^2. Irradiating times are usually 3h with a current of 10 μA. [41]

Highly enriched Xenon-124 gas is bombarded with 30 MeV protons. The target is operated at a pressure of 14 bar and beam currents up to 50 μA. The production yield for $^{123}\mathrm{I}$ is 370 MBq/μAh. Natural xenon contains only 0.1 % of $^{124}\mathrm{Xe}$, therefore an enrichment is necessary which is quite expensive. [42, 43]

Iodine is irradiated with protons of an energy of 50-80 MeV, is therefore only possible with high energy cyclotrons. Target material is usually NaI, KI, $\mathrm{I_2}$ or $\mathrm{CH_2I_2}$. The produced xenon gas is extracted with helium and is then frozen out. [42, 44]

A $^{120}\mathrm{Sn}$ target was bombarded with $^{6}\mathrm{Li}$ ions at an energy of 25-35 MeV. [96]

For the reaction of iodine with pions KI pellets with a thickness of ~ 120 mg/cm2 in thin Mylar guard foils were bombarded with either protons at an energy of 500MeV or π^+ and π^- produced in the P^3 and LEP channels of the Clinton P. Anderson Meson Physics Facility (LAMPF) ranging in energy between 60 and 350 MeV and a momentum bite of 6% and 4% respectively. [97]

Characteristics:

$T_{1/2\,a}$: 13.14 h

ε: 100%

γ: 159keV 86%

$T_{1/2}$: 13.04 h

γ: 159.0 keV [97]

Purification:

Sublimation of the iodine from metal targets and trapping of the iodide in sodium hydroxide, extraction with helium for the iodine targets.

The xenon gas is pumped over an ion exchange column and the trapped iodine is washed down with 0.02 N NaOH.

Use:

As tracer for SPECT or γ-camera.

Production of Iodine-124:

Nuclear reactions:

$^{124}Te(d,2n)^{124}I$ [55, 60]

$^{124}Te(p,n)^{124}I$ [55]

$^{121}Sb(\alpha,n)^{124}I$ [55]

^{129}Xe (^{27}Al, fragmentation) ^{124}I [80]

^{127}I ($\pi^{\pm}$, 3n) ^{124}I [97]

Cross section:

Production cross section σ: $(2.23 \pm 0.14) * 10^{-2}$ b [80]

Production cross section from the interaction of ^{127}I with 500 MeV protons in mb: 33.7 ± 2.8 [97]

Table 40: Independent production cross section in (mb) for the reaction of ^{127}I with pions having an energy of 60-350 MeV to result in ^{124}I: [97]

T_π	60 MeV		100 MeV		120 MeV		140 MeV		180 MeV		210 MeV		250 MeV		300 MeV		350 MeV	
Nuclide	σ^+	σ^-	σ^+	σ^-	σ^+	σ^-	σ^+	σ^-	σ^+	σ^-	σ^+	σ^-	σ^+	σ^-	σ^+	σ^-	σ^+	σ^-
^{124}I	27.2 ± 4.2	103.9 ± 23.0	61.9 ± 8.8	112.5 ± 11.2			68.0 ± 6.5	88.1 ± 7.6	57.9 ±3.7	76.9 ± 6.5	48.5 ± 4.1	61.9 ± 5.7	40.4 ± 3.6	51.3 ± 4.4	30.9 ± 2.3	49.3 ± 4.3	30.7 ± 2.0	39.3 ± 3.8

Production parameters:

Target: 130-160 mg of 95 % isotopically enriched ^{124}Te that was electrodeposited onto a 16.15 cm^2 area of electroplated Ni on a Cu plate.

Irradiation: deuteron beam of 15 MeV energy, 6 h irradiation of 80-85 μA

Cyclotron: CS-30. [55, 60]

For the proton reaction with tellurium usually a thin layer of highly enriched (up to 99%) $^{124}TeO^2$ mixed with 6% Al_2O_3 is electroplated onto a platinum/iridium backing. This target plate is placed into a target chamber at an angle of 10-15 degrees. This will increase the efficient beam length in the target material and increase the yield. The target is then bombarded with protons of an energy of 8-12 MeV to keep the amount of ^{123}I low.

For the reaction of iodine with pions KI pellets with a thickness of ~ 120 mg/cm2 in thin Mylar guard foils were bombarded with either protons at an energy of 500MeV or π^+ and π^- produced in the P^3 and LEP channels of the Clinton P. Anderson Meson Physics Facility (LAMPF) ranging in energy between 60 and 350 MeV and a momentum bite of 6% and 4% respectively. [97]

Characteristics:

$T_{1/2\,a}$: 4.18 d

β^+ : 2.13 MeV, 1.53 MeV.... 25%

ε

γ: 603 keV, 1691 keV, 723 keV [55]

$T_{1/2}$: 4.2 d

γ: 602.7, 27.3 keV [97]

Purification:

1) Target is dissolved in a mixture of 1 mL 5 M NaOH, 2 mL of 30% H_2O_2 and deionised water. Transferring of the solution onto 250 mg aluminium powder. Heating of the solution until the reaction was complete and all H_2O_2 was decomposed. Te^{+IV} was reduced to Te° by aluminium. Excess aluminium was precipitated with carbon dioxide gas that was bubbling through the solution. The volume of the solution was reduced by heating it gently and afterwards bubbling carbon dioxide through it again. The final solution was used as stock solution for labelling procedures.
2) The iodine is sublimated at 740°C from the target material and trapped in 100 µl 0.02M NaOH

Use:

As tracer for PET (diagnostic).

Production of I-125:

Nuclear reaction:

$$^{124}Xe(n,\gamma)^{125}Xe \xrightarrow{E.C} {}^{125}I \ [63, 103]$$

$^{122}Sn\ (^{6}Li,3n)\ ^{125}I$ [96]

$^{127}I\ (\pi^{\pm}, 2n)\ ^{125}I$ [97]

$^{123}Sb(\alpha,2n)\ ^{125}I$ [101]

Cross section:

Production cross section from the interaction of ^{127}I with 500 MeV protons in mb: 90.2 ± 8.9 [97]

Table 41: Independent production cross section in (mb) for the reaction of ^{127}I with pions having an energy of 60-350 MeV to result in ^{125}I: [97]

T_π	60 MeV		100 MeV		120 MeV		140 MeV		180 MeV		210 MeV		250 MeV		300 MeV		350 MeV	
Nuclide	σ^+	σ^-	σ^+	σ^-	σ^+	σ^-	σ^+	σ^-	σ^+	σ^-	σ^+	σ^-	σ^+	σ^-	σ^+	σ^-	σ^+	σ^-
^{125}I	71.5 ± 16.0	215.5 ± 86.8	97.8 ± 17.1	192.7 ± 31.6			80.6 ± 9.2	168.6 ± 20.3	83.3 ± 9.4	127.4 ± 18.8	94.1 ± 11.7	139.0 ± 18.1	69.3 ± 7.9	94.5 ± 13.5	59.7 ± 7.2	71.6 ±16.9	71.3 ± 9.4	50.6 ± 14.3

Production parameters:

A ^{122}Sn target was bombarded with ^{6}Li ions at an energy of 25-35 MeV. [96]

For the reaction of iodine with pions KI pellets with a thickness of ~ 120 mg/cm2 in thin Mylar guard foils were bombarded with either protons at an energy of 500MeV or π^{+} and π^{-} produced in the P^{3} and LEP channels of the Clinton P. Anderson Meson Physics Facility (LAMPF) ranging in energy between 60 and 350 MeV and a momentum bite of 6% and 4% respectively. [97]

For the reaction of xenon gas a high pressure gas target with enriched ^{124}Xe is irradiated with thermal neutrons in a reactor or natural XeF_2 is irradiated with thermal neutrons. [103]

Characteristics:

$T_{1/2\,s}$: 59.4 d

ε from K and L

γ: 35.5 keV

$T_{1/2}$: 60.2 d

γ: 27.3 keV [97]

Purification:

Purification is performed either by dry distillation or via chemical processes.

Use:

As tracer element in biology, for therapy in nuclear medicine and for in vitro diagnostics.

Production of Iodine-126:

Nuclear reactions:

$^{125}I(n,\gamma)^{126}I$

$^{127}I(n,2n)^{126}I$ [77]

$^{127}I\ (\pi^{\pm}, n)\ ^{126}I$ [97]

cross section:

for the reaction $^{125}I(n,\gamma)^{126}I$ [77]

effective cross section $\underset{\wedge}{\sigma}$: 991±100 barns

thermal cross section σ_0 : 894±90 barns

Production cross section from the interaction of ^{127}I with 500 MeV protons in mb: 59.4 ± 3.6 [97]

Table 42: Independent production cross section in (mb) for the reaction of ^{127}I with pions having an energy of 60-350 MeV to result in ^{126}I: [97]

T_π	60 MeV		100 MeV		120 MeV		140 MeV		180 MeV		210 MeV		250 MeV		300 MeV		350 MeV	
Nuclide	σ^+	σ^-	σ^+	σ^-	σ^+	σ^-	σ^+	σ^-	σ^+	σ^-	σ^+	σ^-	σ^+	σ^-	σ^+	σ^-	σ^+	σ^-
^{126}I	57.3 ± 6.2	152.9 ± 31.0	59.0 ± 6.0	128.2 ± 9.4			62.8 ± 4.4	133.0 ± 8.5	70.5 ± 3.8	145.9 ± 9.3	68.6 ± 4.4	132.9 ± 9.1	65.0 ± 4.4	110.7 ± 7.2	54.3 ± 3.3	105.0 ± 6.8	53.9 ± 2.6	82.3 ± 5.9

Production parameters:

For the reaction of iodine with pions KI pellets with a thickness of ~ 120 mg/cm2 in thin Mylar guard foils were bombarded with either protons at an energy of 500MeV or π^+ and π^- produced in the P^3 and LEP channels of the Clinton P. Anderson Meson Physics Facility (LAMPF) ranging in energy between 60 and 350 MeV and a momentum bite of 6% and 4% respectively. [97]

For the activation reaction a solution of sodium [^{125}I] iodide is evaporated onto a thin disk of aluminium which is rolled up and sealed into silica ampoules. The ampoules are then irradiated in a reactor. [77]

Characteristics:

$T_{1/2\,a}$: 13.6 d

isomere:

ε, β+: 1.1 MeV...

γ: 666 keV...

ground state:

β-: 0.9 MeV...

γ: 389 keV...

$T_{1/2\,a}$: 13.0 d

γ: 388.6, 666.3, 27.3 keV [63]

Use:

For basic research.

Production of Iodine-127:

Nuclear reaction:

^{126}Te(n, γ)^{127m}Te$\rightarrow$^{127}Te$\rightarrow$^{127}I, 1)I.U.; 109 d 2) β^-; 9,4 h

^{235}U (n_{th},f) ^{127}I [104]

^{124}Sn (^{6}Li, 3n) ^{127}I [96]

production parameters:

A ^{124}Sn target was bombarded with ^{6}Li ions at an energy of 25-35 MeV. [96]

Characteristics:

Stable isotope

Production of Iodine-128:

Nuclear reaction:

^{127}I(n, γ) ^{128}I [105, 106]

^{235}U (n_{th},f) ^{128}I [107]

Production parameters:

Potassium iodide or methyl iodide are irradiated with neutrons from an Am-Be source with a neutron flux of ~5*10^7 n/sec for 15 min. The potassium iodide is in a plastic cylindrical vessel. The yield was 1-2 µCi. [105] Irradiation of an ^{127}I/^{129}I solution from Amersham, filled into polyethylen capsule, in a Triga Mark-II research reactor with a thermal neutron flux of 4.6X 10^{11} n/(cm^2*sec). [106] Electroplated 235U and uranyl stearate were irradiated in the Los Alamos Homogeneous reactor with a thermal neutron flux of 5X10^{11}/(cm^2*sec). [107]

Characteristics:

$T_{1/2\,a}$: 25 min

ε, β^+, γ: 743 keV

β^-: 2.12MeV, 1.67 MeV

γ: 443keV, 527 keV, 969 keV 86%

Purification:

Mostly Szilard-Chalmers reactions. Iodine-127 is used in the form of a salt or as methyliodide and irradiated with neutrons. Through the nuclear reaction the produced new iodine-128 nucleus is set free from the compound because of its high energy. [36,105]

Use:

^{128}I was used in medicine in 1934, 1935 and 1936. After that it was replaced by ^{131}I because of its short half life. [36]

Production of Iodine-129:

Nuclear reaction:

$^{127}I\ (n,\gamma)\ ^{128}I\ (n,\gamma)\ ^{129}I$ [108]

$^{235}U\ (n_{th},f)\ ^{129}I$ [104]

$^{128}Te(n,\gamma)^{129m}Te \rightarrow ^{129}Te \rightarrow ^{129}I$, 1)I.T.; 34 d 2) β^-; γ; 69 min

Characteristics:

$T_{1/2\,a}$: $1.7*10^7$ years [108]

$T_{1/2\,a}$: $1.6*10^7$ a

β^-: 0.15 MeV

γ: 40 keV, e^-

Purification:

High energetic neutrons will produce ^{126}I as an impurity. This can be avoided or drastically decreased by choosing a well moderated neutron flux. Other isotopic impurities will decay faster than ^{129}I and will be cleared from it thereby. Purification from non isotopic tracer is performed mostly by ignition of the sample to be purified in a stream of oxygen, trapping of the iodine in a diluted solution of sulphuric acid , carrying the iodide on a precipitate of silver chloride, decomposing the silver chloride by heating it with aluminium metal in vacuum and distilling the iodine into a quartz tube. [108]

Use:

As a standard for radioactive measuring devices, in waste management and as tracer in biological experiments. [41, 108] Through activation by neutrons I-130 is formed and can be measured easily. The activation is necessary because of the low specific radioactivity of ^{129}I.

Production of Iodine-130:

Nuclear reaction:

$^{129}I\ (n,\gamma)\ ^{130m,g}I$ [41, 108, 109]

Cross section:

$\sigma_0\,{}^{130m}I$: 17.8 ± 0.7

$\sigma_0\,{}^{130g}I$: 12.5 ±0.5

$\sigma_{0\ both}$: 30.3 ± 1.2

Production parameters:

The targets consisted of either a ^{129}I –solution which was poured into a polyethylene capsule which was then placed into a Cd-capsule or a diluted ^{129}I-solution which was irradiated only in a polyethylene capsule. The Cd-capsule was used to reduce the thermal neutron flux at the target capsule. The capsules were placed into the reflector surrounding the reactor core at the TRIGA MARK-II reactor at Rikkyo University. The targets were irradiated for 10 min at a flux of 4.6*1011 n/(cm^2*s). [41]

Characteristics:

Two isomers: ^{130m}I and ^{130g}I

$T_{1/2\,a}$: 8.78 min ^{130m}I

$T_{1/2\,a}$: 12.34 h ^{130g}I

γ (^{130m}I): 536, 586, 1614 keV

γ (^{130g}I): 418, 536, 586, 668, 739, 1157 keV [41]

Use:

For basic research.

Production of I-131:

Nuclear reactions:

$$^{130}Te(n,\gamma)^{131m}Te \xrightarrow[30\ h]{I.T.} {}^{131}Te \xrightarrow[25\ min]{\beta-,\ \gamma} {}^{131}I\ [64, 110]$$

$^{235}U(n_{th},f)\ ^{131}I$ [64, 110]

$^{245}Cm\ (n_{th},f)\ ^{131}I$ [104]

$^{252}Cf\ (n_{th},f)\ ^{131}I$ [111]

Production parameters:

For the tellurium reactions either an enriched elemental ^{130}Te or an natural TeO_2 target are bombarded with thermal neutrons in a reactor. For the fission reactions either a $^{235}U/Al$ alloy or the other elements are bombarded with thermal neutrons in a reactor.

Characteristics:

$T_{1/2}$: 8.067 d

β^- : 0.61 MeV, 0.34 MeV

γ: 354 keV, 637 keV, 284 keV

$T_{1/2\,a}$: 8.05 d [96]

Purification:

1) The irradiated tellurium will be oxidised with dichromate and sulphuric acid. Tellurian acid [$Te(OH)_6$ or H_6TeO_6] is formed as well as ^{131}I-iodate ($^{131}IO_3^-$). Afterwards the excess of the oxidising agents and the iodate can be reduced by the addition of oxalic acid. Via this process [^{131}]I-iodine is formed again which can be distilled into a solution of sodium carbonate, saturated with sulphur dioxide. Repeated oxidation with potassium permanganate, reduction and distillation of the iodine will give a product which can be used for medical applications.
2) Irradiated tellurium dioxide will be dissolved in 10% aqueous sodium hydroxide solution which then will be acidified with sulfuric acid. The iodide will be oxidised with iron(III)sulphate to iodine which can be distilled into a solution of sodium carbonate. Further purification is prepared as in 1).
3) Irradiated tellurium dioxide will be heated to 750°C in a stream of nitrogen. The iodine will sublimate into a solution of sodium hydroxide where it will be trapped. [36]
4) The uranium/aluminium target which is used for the nuclear fission reaction will be stored for a short time period after bombardment to give other short living nuclides which are build simultaneously time to decay. These nuclides are for example ^{90}Kr, ^{143}Ba and their daughters with half lives of 32 s and 20 s respectively. Then the target is dissolved in a 4.5 M sodium hydroxide solution. Aluminium hydroxide will precipitate. A couple of not desired radionuclides will coprecipitate. After vacuum filtration the solution will be acidified with sulphuric acid and the iodine will be recovered from it by distillation into a solution of sodium carbonate, saturated with sodium sulphite. Redistillation will further purify the iodine. Another possibility to recover the iodine from the acidic solution would be an absorption process on a platinum sponge with following desorption step in 0.3M sodium hydroxide solution.

   The iodine from the fission process will contain ^{127}I and ^{129}I which cannot be separated from the ^{131}I. [64]

A separation of the complex mixture of the elements after the fission reaction was performed with oxygen in the gas phase. Therefor the fission products were stopped in a fast nitrogen stream and swept to an inlet where oxygen was added. The separation was then performed by adsorption chromatography in a transfer tube (Pyrex) and adsorption of volatile compounds in a trap. [111]

Use:

As isotope for tumour therapy.

Production of Iodine-132:

Nuclear reaction:

^{245}Cm (n_{th},f) ^{132}I [104]

$^{132}\text{Te} \longrightarrow {}^{132}\text{I}$

^{252}Cf (n_{th},f) ^{132}I [111]

Characteristics:

$T_{1/2\,a}$: 2.4 h [111]

Purification:

A separation of the complex mixture of the elements after the fission reaction was performed with oxygen in the gas phase. Therefor the fission products were stopped in a fast nitrogen stream and swept to an inlet where oxygen was added. The separation was then performed by adsorption chromatography in a transfer tube (Pyrex) and adsorption of volatile compounds in a trap. [111]

Use:

For basic research.

Production of Iodine-133:

Nuclear reaction:

^{245}Cm (n_{th},f) ^{133}I [104]

^{252}Cf (n_{th},f) ^{133}I [111]

Characteristics:

$T_{1/2\,a}$: 20.8 h [111]

Purification:

A separation of the complex mixture of the elements after the fission reaction was performed with oxygen in the gas phase. Therefor the fission products were stopped in a fast nitrogen stream and swept to an inlet where oxygen was added. The separation was then performed by adsorption chromatography in a transfer tube (Pyrex) and adsorption of volatile compounds in a trap. [111]

Use:

For basic research.

Production of Iodine-134:

Nuclear reaction:

^{245}Cm (n_{th},f) ^{134}I [104]

^{252}Cf (n_{th},f) ^{134}I [111]

Characteristics:

Two isomers

$T_{1/2\,a}$: 52m

$T_{1/2\,a}$: 3.7 m [111]

Purification:

A separation of the complex mixture of the elements after the fission reaction was performed with oxygen in the gas phase. Therefor the fission products were stopped in a fast nitrogen stream and swept to an inlet where oxygen was added. The separation was then performed by adsorption chromatography in a transfer tube (Pyrex) and adsorption of volatile compounds in a trap. [111]

Use:

For basic research.

Production of I-135

Nuclear fission products:

U(n_{th},f) ^{135}Te → ^{135}I (n,γ)^{136}I, 1) β^-; 2 min [110]

^{245}Cm (n_{th},f) ^{135}I [104]

^{252}Cf (n_{th},f) ^{135}I [111]

Characteristics:

$T_{1/2\,a}$: 6.7 h [111]

$T_{1/2\,a}$: 6.7 h

β^-: 1.5, 0.9 MeV

γ: 1260, 1132, 527 keV

Purification:

Melting process or extraction with CCl_4 [110]

A separation of the complex mixture of the elements after the fission reaction was performed with oxygen in the gas phase. Therefor the fission products were stopped in a fast nitrogen stream and swept to an inlet where oxygen was added. The separation was then performed by adsorption chromatography in a transfer tube (Pyrex) and adsorption of volatile compounds in a trap. [111]

Use:

For basic research.

Production of Iodine-136:

Nuclear reactions:

Fission product in uranium ores (natural occurrence)

^{235}U (n$_{th}$,f) ^{136}I

^{245}Cm (n$_{th}$,f) ^{136}I [104]

^{252}Cf (n$_{th}$,f) ^{136}I [111]

^{135}I (n,γ)^{136}I

Characteristics:

$T_{1/2\,a}$: 46 sec	$T_{1/2}$: 1.39 m
β^-: 5.3, 5.9 MeV	β^-: 4.3, 5.6 MeV
γ: 1313, 381, 197* keV	γ: 1313, 1321, 2290 keV
$T_{1/2\,a}$: 44 sec [96]	$T_{1/2}$: 83 sec [96]

Use:

For basic research.

Production of Iodine-137:

Nuclear reactions:

^{235}U (n$_{th}$, f) ^{137}I [112]

^{245}Cm (n$_{th}$,f) ^{137}I [104]

^{252}Cf (n$_{th}$,f) ^{137}I [111]

Production parameters:

Thermal neutron bursts of 30 msec FWHM with a flux of 1015 n*cm-2 were used for the irradiation of ^{235}U at the Mainz Triga reactor.

Characteristics:

$T_{1/2\,a}$: 24.2 ± 0.5 sec

$T_{1/2\,a}$: 24 sec [111]

Purification:

The products were purified by an automatic gas-phase separation procedure as methyl-halides. [112]

A separation of the complex mixture of the elements after the fission reaction was performed with oxygen in the gas phase. Therefore the fission products were stopped in a fast nitrogen stream and swept to an inlet where oxygen was added. The separation was then performed by adsorption chromatography in a transfer tube (Pyrex) and adsorption of volatile compounds in a trap. [111]

Use:

For basic research.

Production of Iodine-138:

Nuclear reaction:

^{235}U (n_{th}, f) ^{138}I [112]

^{252}Cf (n_{th},f) ^{138}I [111]

Production parameters:

Thermal neutron bursts of 30 msec FWHM with a flux of 1015 n*cm-2 were used for the irradiation of ^{235}U at the Mainz Triga reactor.

Characteristics:

$T_{1/2\,a}$: 6.33 ± 0.08 sec

$T_{1/2\,a}$: 6 sec [111]

Purification:

The products were purified by an automatic gas-phase separation procedure as methyl-halides. [112]

A separation of the complex mixture of the elements after the fission reaction was performed with oxygen in the gas phase. Therefore the fission products were stopped in a fast nitrogen stream and swept to an inlet where oxygen was added. The separation was then performed by adsorption chromatography in a transfer tube (Pyrex) and adsorption of volatile compounds in a trap. [111]

Use:

For basic research.

Production of Iodine-139:

Nuclear reaction:

^{235}U (n$_{th}$, f) ^{139}I [112]

^{252}Cf (n$_{th}$,f) ^{139}I [111]

Production parameters:

Thermal neutron bursts of 30 msec FWHM with a flux of 1015 n*cm-2 were used for the irradiation of ^{235}U at the Mainz Triga reactor. [112]

Characteristics:

$T_{1/2\,a}$: 2.42 ± 0.27 sec [112]

$T_{1/2\,a}$: 2.7 sec [111]

Purification:

The products were purified by an automatic gas-phase separation procedure as methyl-halides. [112]

A separation of the complex mixture of the elements after the fission reaction was performed with oxygen in the gas phase. Therefor the fission products were stopped in a fast nitrogen stream and swept to an inlet where oxygen was added. The separation was then performed by adsorption chromatography in a transfer tube (Pyrex) and adsorption of volatile compounds in a trap. [111]

Use:

For basic research.

Production of Iodine-140:

Nuclear reaction:

^{235}U (n$_{th}$, f) ^{140}I [112]

Production parameters:

Thermal neutron bursts of 30 msec FWHM with a flux of 1015 n*cm-2 were used for the irradiation of ^{235}U at the Mainz Triga reactor.

Characteristics:

$T_{1/2\,a}$: 0.87 ± 0.04 sec

Purification:

The products were purified by an automatic gas-phase separation procedure as methyl-halides.

Use:

For basic research.

Production of Iodine-141:

Nuclear reaction:

^{235}U (n_{th}, f) ^{141}I [112]

Production parameters:

Thermal neutron bursts of 30 msec FWHM with a flux of 1015 n*cm-2 were used for the irradiation of ^{235}U at the Mainz Triga reactor.

Characteristics:

$T_{1/2\,a}$: 0.45 ± 0.10 sec

Purification:

The products were purified by an automatic gas-phase separation procedure as methyl-halides.

Use:

For basic research.

Production of Iodine-142:

Nuclear reaction:

Thermal fission reaction

Characteristics:

$T_{1/2\,a}$: 0.2 sec [112]

Use:

For basic research.

Production of Iodine-143:

Nuclear reaction:

Thermal fission reaction.